1969

Low-lying levels in some spherical and rotational nuclides by Coulomb excitation and radiative capture of thermal neutrons

Donald Allan McClure

Department: Physics

Argonne Physics Division
Informal Report PHY-1969E
August 1969

LOW-LYING LEVELS IN SOME SPHERICAL AND ROTATIONAL NUCLIDES BY COULOMB EXCITATION AND RADIATIVE CAPTURE OF THERMAL NEUTRONS

by

Donald A. McClure

Argonne National Laboratory, Argonne, Illinois 60439

The facilities of Argonne National Laboratory are owned by the United States Government. Under the terms of a contract (W-31-109-Eng-38) between the U. S. Atomic Energy Commission, Argonne Universities Association and The University of Chicago, the University employs the staff and operates the Laboratory in accordance with policies and programs formulated, approved and reviewed by the Association.

MEMBERS OF ARGONNE UNIVERSITIES ASSOCIATION

The University of Arizona
Carnegie-Mellon University
Case Western Reserve University
The University of Chicago
University of Cincinnati
Illinois Institute of Technology
University of Illinois
Indiana University
Iowa State University
The University of Iowa
Kansas State University
The University of Kansas
Loyola University
Marquette University
Michigan State University
The University of Michigan
University of Minnesota
University of Missouri
Northwestern University
University of Notre Dame
The Ohio State University
Ohio University
The Pennsylvania State University
Purdue University
Saint Louis University
Southern Illinois University
University of Texas
Washington University
Wayne State University
The University of Wisconsin

LOW-LYING LEVELS IN SOME SPHERICAL AND ROTATIONAL NUCLIDES BY COULOMB EXCITATION AND RADIATIVE CAPTURE OF THERMAL NEUTRONS

by

DONALD A. McCLURE (1942)

A DISSERTATION

Presented to the Faculty of the Graduate School of the

UNIVERSITY OF MISSOURI - ROLLA

In Partial Fulfillment of the Requirements for the Degree

DOCTOR OF PHILOSOPHY

in

PHYSICS

1969

W. P. Pratt
Advisor

Grant D. Gunn

James Paul Wesley

J. M. Zenor

W. H. Robertson

ABSTRACT

The work presented in this dissertation was performed in order to obtain additional information on the level schemes and decay properties of several nuclei in an attempt to explain the observations in terms of an applicable nuclear model. Various nuclear models are discussed in Section II. A general review from the classical point of view of the Coulomb excitation reaction is discussed in Section III and the thermal-neutron-capture reaction is outlined in Section IV.

The experimental equipment and procedure is discussed in Section V in which the ramper method of energy determination is outlined. This method allows the measurement of γ-ray energies to an accuracy of ≈ 0.1 keV in many cases and therefore increases the chances for an unambiguous placement of the γ ray in a level scheme. A method for the accurate determination of the analyzing system dead time is also presented. The exclusive use of Ge(Li) detectors is made in both singles and coincidence γ-ray studies.

A series of measurements on the singles and coincidence γ-ray spectra as well as the conversion electron spectra following the decay of ^{66}Ge is presented in Section VI. This nucleus decays primarily by allowed beta transitions permitting the determination of the quantum mechanical parameters of many of the states in ^{66}Ga. This nuclide is expected to exhibit excited states being primarily single-particle in nature. The shell model structure of these states could lead to the occurrence of forbidden M1 transitions and indeed the first excited state of ^{66}Ga does exhibit a retarded M1 transition as reflected in its 21 nsec lifetime.

Measurements of the de-excitation γ rays following Coulomb excitation of the low-lying levels in ^{105}Pd are presented in Section VII. Attempts to describe this nucleus in terms of Nilsson orbitals have been largely unsuccessful. A description of the low-lying levels in terms of the core-excitation model is presented. The agreement

between the experimental observations and the predictions of the core-excitation model is somewhat less than satisfying. However, accurate $B(E2)\uparrow$ transition probabilities are presented which may be compared to a more extensive theoretical treatment.

Section VIII discusses the thermal-neutron-capture reaction $^{186}W(n,\gamma)^{187}W$. Both high-energy and low-energy γ rays have been observed using both singles and coincidence γ-ray spectroscopic techniques in an attempt to construct an unambiguous level scheme. The resulting low-lying energy levels are discussed in terms of the Nilsson model including the Coriolis band mixing terms. Evidence is presented for the existence of Coriolis mixed states built on the $[512]\frac{3}{2}^-$, and $[510]\frac{1}{2}^-$ intrinsic states. The results of the model-predicted energy level sequence and γ-ray branching ratios are discussed.

PREFACE

The research described in this dissertation was performed at and supported by the Physics Division of Argonne National Laboratory while the author was the holder of an AUA-ANL Predoctoral Fellowship. The author wishes to thank Dr. H. Q. Fuller, Chairman of the Physics Department at the University of Missouri at Rolla for encouraging his application as an AUA-ANL Fellow.

The author wishes to express sincere gratitude to Dr. H. H. Bolotin of the Physics Division at Argonne National Laboratory for his help, direction, and encouragement during the course of these investigations. Mr. C. H. Batson has also been of considerable help in the taking and analysis of much of the data.

The author is indebted to the members of the Physics Division at Argonne for their assistance, particularly to the staff of the Tandem Van de Graaff, the graphic arts and editorial sections, and to the staff members at the Argonne CP-5 research reactor and the Argonne 60-in. cyclotron. Mr. M. G. Strauss and R. W. Bannon of the Electronics Division have been of invaluable aid and the author is especially grateful to Mrs. K. M. Pemble, Mrs. N. A. Smith, and Miss Pat Sniegowski for the typing of the manuscript.

TABLE OF CONTENTS

LIST OF ILLUSTRATIONS

Page

Figures

LIST OF TABLES

I. INTRODUCTION

The motivating force behind the study of nuclear physics is a desire to understand the "first principles" involved in the interaction between nucleons and to predict the behavior of the atomic nucleus from a theory based upon these principles. Unfortunately, the interaction laws are complicated and our understanding of them increases very slowly. In order to make even slow progress, the problem demands simplification. A variety of grossly simplifying assumptions are made at this point concerning the many-body nucleon interaction. Each set of assumptions results in a "nuclear model" which is applicable only in the region of the periodic table where the basic assumptions of the model have some validity.

The experimental nuclear physicist observes only certain limited properties of nuclei. In each experimental situation a particular model is expected to provide a useful description. The results of experimental probing (which may be likened to trying to find the composition and shape of a frying pan buried in a hay stack using only a 22 calibre rifle) serve to indicate the limits of applicability of a given model. Such probing suggests ways in which a model could be altered to provide a wider range of applicability and might shed some light on the transitions between models which are applicable in different regions of the periodic table. Ultimately, it is hoped, of course, that one model will result which will predict all of the interesting nuclear properties.

Experiment and theory are complementary in this attempt to describe the nucleus. The experiment points up the properties of nuclei as specifically as possible. This provides a test of the merit of a certain model in its ability to correlate experimental results, hopefully in a simple and elegant manner, which in turn may suggest new and more crucial experiments. Neither phase of this process would be complete in itself.

Chapter II of this dissertation will present very briefly several of the models which are expected to be valid for certain nuclei in the medium to heavy weight mass region. This discussion is by no means original and is meant only as a review of the aspects of nuclear models which are used in an attempt to explain the experimental data of Chapters VI, VII, and VIII. Chapters III and IV discuss the theory behind two reaction processes which are used to populate the low-lying energy levels in the nuclei of interest, in particular, Coulomb excitation and the (n,γ) reaction.

Chapter V explains the experimental procedures employed to collect the data. Both singles and coincidence γ-ray spectroscopic techniques were employed with the exclusive use of Ge(Li) detectors. The use of high-resolution Ge(Li) detectors in each arm of the coincidence system enabled unambiguous coincidence gates to be set on close lying γ-ray peaks as well as the clear separation of peaks appearing in the coincidence spectra. Such unambiguous separation is not possible with the use of a lower-resolution NaI(Tl) crystal. Two-parameter coincidence spectra (1024 channels each) were stored on magnetic tape in a 1024×1024 channel array. Coincidence spectra corresponding to individual γ-ray peaks could be separated at a later time with the use of an associated read-search station.

An improved method for the determination of γ-ray energies was employed which is based on the use of a highly linear voltage ramp generator which is used to trace out the differential nonlinearity of the entire analyzing system (excluding the detector).

A method for the accurate determination of the dead time associated with the entire analyzing system was developed and utilized. The method is based on the injection of a pulser peak into the preamplifier at a rate which is proportional to the source strength. The number of pulses injected can then be compared to the number which are analyzed to find the ratio of experimental time to live time. The

error associated with this method is at least as good as that associated with the counting statistics.

II. NUCLEAR MODELS

A. Introduction

H. J. Lipkin has remarked[1] that ". . . an important interaction in the many-body problem is that between the particles and the physicists who are trying to solve the problem; an important characteristic of the physicists is that we cannot solve the three-body problem, and can solve the two-body problem only because it reduces readily to two one-body problems, the only type we really can solve." It is our inability to handle the many-body problem coupled with the fact that the properties of the nuclear interaction laws are not well known which forces us to make some very drastic simplifying assumptions concerning the interaction of nucleons contained in a nucleus. Each set of assumptions results in a different nuclear model, each model usually having a very restricted number of nuclei to which it can be successfully applied.

In the following sections several of the more widely applicable models will be discussed in an attempt to provide a background for the experimental studies to be discussed later. Section B describes the single-particle model and shell structure. Section C discusses the pairing interaction which results in the observed energy gap between the ground state and the lowest single-particle state in even-even nuclei. Section D is a review of collective motions and the Nilsson model of intrinsic states. Section E describes the core-excitation model of Lawson and Uretsky.

B. The Single-Particle Model

In the 1930's it was suggested that the force on a nucleon within a nucleus could be described in terms of a potential field which might be produced by an average of the individual internucleon

forces.[2] This suggestion was largely ignored until the late 1940's when a large number of measurements of spins and magnetic moments of nuclei had accumulated and it was noted that anomalies in several nuclear parameters appeared at the so-called magic numbers. In 1949 two independent groups published papers describing the nuclear shell model which was more successful in explaining empirical data.[3—6]

The model is based on the assumption that each nucleon within a nucleus "sees" a central potential field which results from an average of the forces exerted by all the other nucleons. The orbital angular momentum is a constant of the motion for a central potential. For each value of the orbital quantum number ℓ there is a series of energy levels which are distinguished by the quantum number n (n equaling the number of nodes in the radial wave function). The energy levels are labeled according to the notation of the atomic spectroscopists so the state of lowest energy with $\ell = 0$ is called the 1s state, etc.

The spacing of the energy levels is a function of the potential which is used, but it was discovered that a "realistic" (see Ref. 7, p. 147) potential would not produce energy gaps in the level structure at the so-called magic numbers. In order to obtain the observed energy gaps at the magic numbers it was necessary to assume that, in addition to the static potential already discussed, each nucleon also experienced a potential proportional to $\bar{\ell} \cdot \bar{s}$, where $\bar{s}$ is the intrinsic spin of the nucleon. The net potential may then be written as

$$V = V_s + V_{\ell s}, \tag{B1}$$

where

$$V_{\ell s} = - V(r)\, \bar{\ell} \cdot \bar{s} = - V(r)\, (\bar{r} \times \bar{p}) \cdot \bar{s}. \tag{B2}$$

This potential produces nucleon orbitals for which ℓ is no longer a constant of the motion and only the total angular momentum $\bar{j}$ ($\bar{j} = \bar{\ell} \pm \bar{s}$)

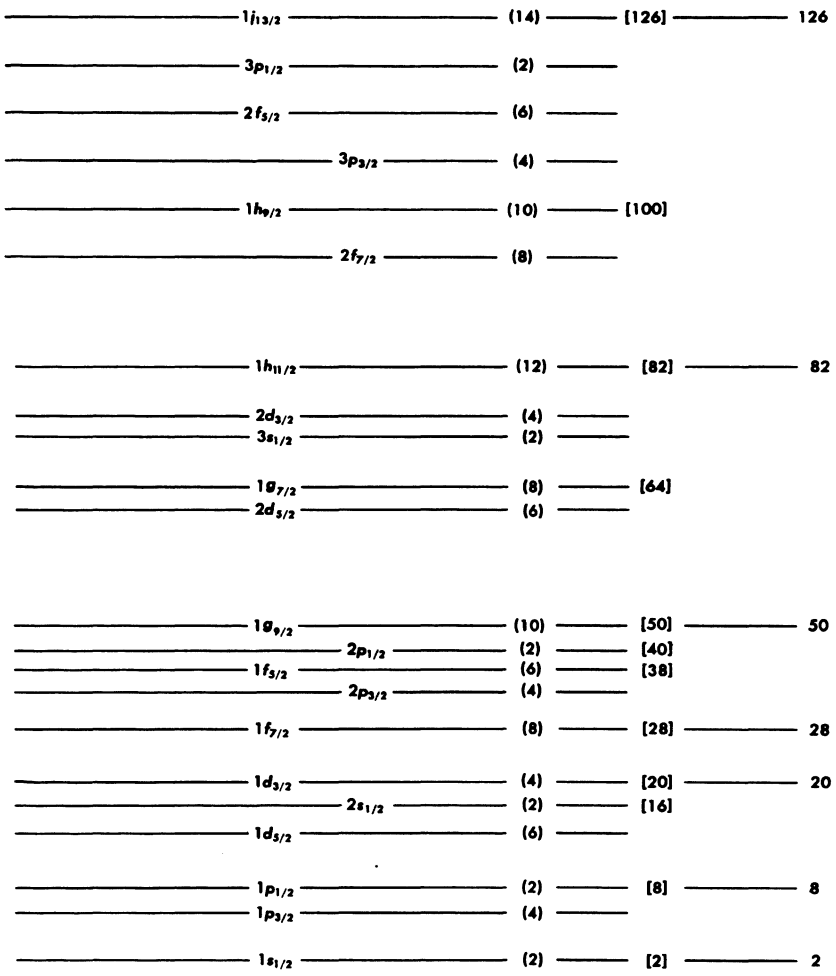

Fig. 1. The energy levels of the first 126 neutrons in the simple shell model. (From Ref. 7.)

remains a good quantum number in the sense of Condon and Shortly (Chap. VIII).[8] Taking V(r) in Eq. (B1) as being positive produces a sequence of energy levels in which the state with $j = \ell + \frac{1}{2}$ has a lower energy than the state with $j = \ell - \frac{1}{2}$ (see Fig. 1). Not only are the magic numbers described accurately, but a large number of ground-state nuclear spins are successfully predicted using this model.

In the model as so far considered all of the states which can be formed by k particles with the same (n, ℓ, j) have the same energy. This degeneracy is removed by considering an interaction between the particles which is strong enough to remove the degeneracies but not so strong that j ceases to be a good quantum number. This interaction is assumed to be of the type which acts between nucleons in vacuo

(see Ref. 7, Chap. V). Due to the short range of this interaction, the force between nucleons in different shells is assumed to be much smaller than the force between nucleons within the same shell and, therefore, the angular momentum coupling within a shell is not upset by interaction with intershell nucleons. The following spin predictions result. In even-even nuclei, i.e., even N and even Z (where N is the neutron number and Z the proton number) the total spin (J) is predicted to be zero. For an even-Z, odd-N nucleus the protons still couple to $J = 0$ and the neutrons to $J = j_n$, the j value of the neutron shell which is filling. Similarly for an odd-Z, even-N nucleus $J = j_p$. For an odd-odd nucleus an ambiguity exists due to the fact that the angular momenta may couple to any J satisfying the triangular rule ($|j_n - j_p| \leq J \leq j_n + j_p$). The Nordheim rules[9] aid in the prediction of the energy sequence of these levels. Defining Nordheim's number as $N = j_p - \ell_p + j_n - \ell_n = \Sigma_p + \Sigma_n$ the following rules result. For $N = 0$ the state with $J = |j_n - j_p|$ will be lower in energy. For $N = \pm 1$ either the state $J = |j_p - j_n|$ or $J = j_p + j_n$ will be lowest in energy.

Of course the wave function of an actual nucleus is not exactly that of the single-particle model. A single state in a real nucleus may be a mixture of several single-particle states. Therefore, the wave function for a nucleus which contains k nucleons (ψ_k) is taken to be an anti-symmetric product of a complete set of orthogonal single-particle states for each nucleon. The single-particle states are those of any reasonable potential [usually the states which result from the use of the harmonic oscillator potential for V_s in Eq. (B1)] and products are formed in terms of either the L-S or j-j coupling schemes.[10] Let us call these single-particle wave functions ϕ_i. The energy matrix is then set up $(\phi_i|H|\phi_i)$, where H is the Hamiltonian of the system. This matrix is then diagonalized to produce the energy eigenvalues E_k of the actual system with corresponding eigenvectors

a_{ik}, where the actual wave function is given by $\psi_k = \Sigma_i a_{ik} \phi_i$. Of course the accuracy with which the set ϕ_i corresponds to ψ_k determines the number of steps necessary to bring about diagonalization of the Hamiltonian matrix. If ψ_k conforms closely to ϕ_i, then only a few a_{ik} will be non-zero.

Once the eigenvectors are known, then in principle any matrix elements O_{km} of an operator corresponding to any observable (O) of a transition between two states ψ_k and ψ_m can be determined

$$O_{km} = (\psi_k | O | \psi_m) = \sum_{\mu\nu} a^*_{\mu k} a_{\nu m} (\phi_\mu | O | \phi_\nu) . \tag{B3}$$

Letting

$$O'_{\mu\nu} = (\phi_\mu | O | \phi_\nu) \tag{B4}$$

and thinking of a and O as matrices, it is found that

$$O = a^H O' a . \tag{B5}$$

Thus the matrix elements of an operator may be found using the set of simpler single-particle functions and the eigenvector matrix serves to transform this value into the quantity observed in the actual nucleus.

C. The Pairing Interaction

There is one further short range component of the nucleon-nucleon interaction which manifests itself as an energy gap observed between the ground state and the first excited particle state in even-even nuclei. It has been suggested that this gap is the result of an additional attractive force existing between nucleons contained in the same shell model state. The energy necessary to break this attraction would cause such a gap.

Let $|\nu\rangle$ represent the wave function of a particle state except for the sign of the angular-momentum component. Let $|\nu\bar{\nu}\rangle$ represent

a pair of particles in the same state, one with positive m the other with negative m. We shall call this a conjugate pair. The empirical evidence suggests that a stronger force exists between conjugate pairs than between any other two particles. We now have the following model: a self-consistent potential field having nuclear state $|\nu\rangle$ with a force G between conjugate pairs which has non-zero matrix elements only for $\langle \nu_2 \bar{\nu}_2 | G | \nu_1 \bar{\nu}_1 \rangle$.

Let us first consider the case of two identical particles restricted to move in a particular single-particle j orbital and experiencing a δ interaction[11]

$$V = V_0 \, \delta (\bar{r}_1 - \bar{r}_2) . \tag{C1}$$

This results in a ground-state wave function

$$\begin{aligned} \psi_{I=0}(1,2) &= \sum_m \langle \nu \bar{\nu} | 00 \rangle \, \psi_\nu(1) \, \psi_{\bar{\nu}}(2) \\ &= (2j+1)^{-1/2} \sum \psi_\nu(1)(-1)^{j-m} \psi_{\bar{\nu}}(2) \end{aligned} \tag{C2}$$

and predicts a depression of the energy of the I=0 ground state as shown in Fig. 2.

The pairing interaction[12] is a simplification of the δ force which preserves the gross features of this force but allows a simpler mathematical treatment. Using second-quantization notation where a_ν^+ and a_ν are the creation and annihilation operators for a particle in the shell-model state $|\nu\rangle = |jm\rangle$. We then have the total wave function of a spherical shell-model state expressed as

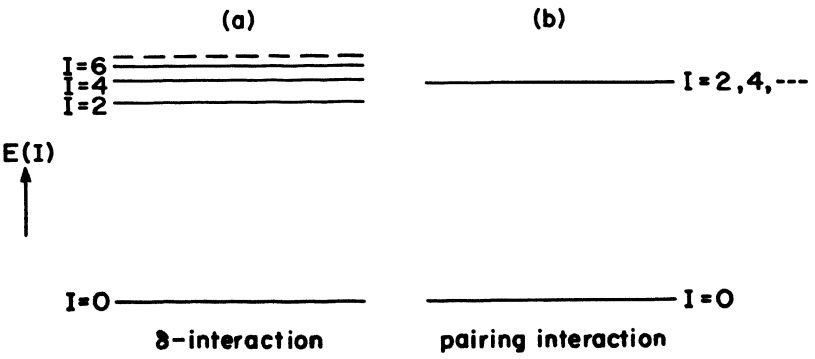

Fig. 2. Spectra resulting from two identical particles in a degenerate shell-model orbital (j, ℓ) under the influence of a δ force and a pairing force, respectively.

$$\psi_\nu \equiv a_\nu^+ |0\rangle, \tag{C3}$$

where $|0\rangle$ represents the particle vacuum. The creation and annihilation operators for the state $|\bar{\nu}\rangle = |j - m\rangle$ are $a_{\bar{\nu}}^+$ and $a_{\bar{\nu}}$, respectively, and the two-particle wave function can be expressed in terms of these four operators. The Pauli or antisymmetric "anticommutation" rules are used

$$\begin{aligned} &\{a_{\nu_1}^+, a_{\nu_2}^+\} = 0, \quad (j_1 = j_2), \\ &\{a_{\bar{\nu}_1}, a_{\bar{\nu}_2}\} = 0, \quad (j_1 = j_2), \\ &\{a_{\nu_1}^+, a_{\nu_2}\} = \delta_{m_1 m_2} \delta_{j_1 j_2}. \end{aligned} \tag{C4}$$

The pairing force is expressed as

$$V_{pair} = -G \sum a_\nu^+ a_{\bar{\nu}}^+ a_{\bar{\nu}'} a_{\nu'}, \quad (j = j'), \tag{C5}$$

and represents a scattering of two particles. If the restriction that the particles must be in the same j shell is removed, the calculation is kept amenable by assuming constant matrix elements between two or three oscillator shells and matrix elements equal to zero outside of these shells.

$$\langle \nu_2 \bar{\nu}_2 | V_{pair} | \nu_1 \bar{\nu}_1 \rangle = \begin{cases} -G & \text{"in" shells} \\ 0 & \text{"out"} \end{cases} \tag{C6}$$

Even with this restriction the calculations are tedious. However, an excellent solution for the wave function of the ground state exists which is based on the superconductor problem solved by Bardeen, Cooper, and Schrieffer.[13] This solution was adapted to nuclear physics by Bohr, Mottelson, and Pines.[14] In this adaptation the ground-state wave function becomes

$$\phi_0^{BCS} = \prod_\nu (U_\nu + V_\nu a_\nu^+ a_{\bar{\nu}}^+) |0\rangle, \tag{C7}$$

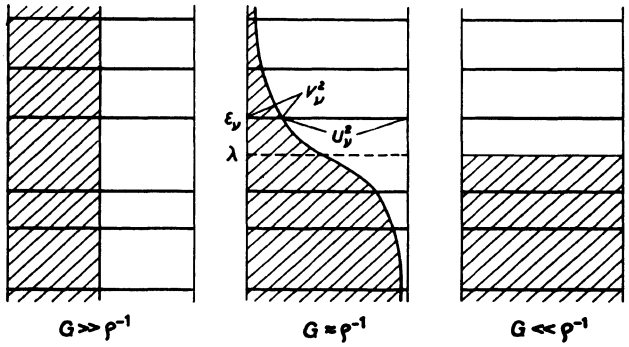

Fig. 3. Populations V_ν^2 of pairs over single-particle levels ϵ_ν for different ratios of pairing strength to average distance between single-particle levels. Note in the middle diagram the position of λ, the fermi surface. (From Ref. 11.)

where U_ν and V_ν represent the probability that a state is occupied and unoccupied, respectively. Thus we have

$$U_\nu^2 + V_\nu^2 = 1 \tag{C8}$$

and

$$2 \sum_\nu V_\nu^2 = n, \tag{C9}$$

where n is the total number of particles.

Figure 3 represents the populations of the states for different values of the ratio of the pairing strength G to the average level spacing ρ^{-1}. The probability of occupation is given by

$$V_\nu^2 = \tfrac{1}{2} [1 - (\epsilon_\nu - \lambda)/E_\nu], \tag{C10}$$

where $E_\nu = \sqrt{(\epsilon_\nu - \lambda)^2 + \Delta^2}$ (the terms are defined in Fig. 3) and

$$\Delta = G \sum_\nu U_\nu V_\nu ; \tag{C11}$$

2Δ represents the energy gap between the ground state and first excited particle state in an even-even nucleus.

Excited states are discussed in terms of the quasi-particle concept. The ground state discussed above and expressed in Eq. (C7) is assumed to be the quasi-particle vacuum $|\tilde{0}\rangle$. Excitations are expressed in terms of the quasi-particle operators

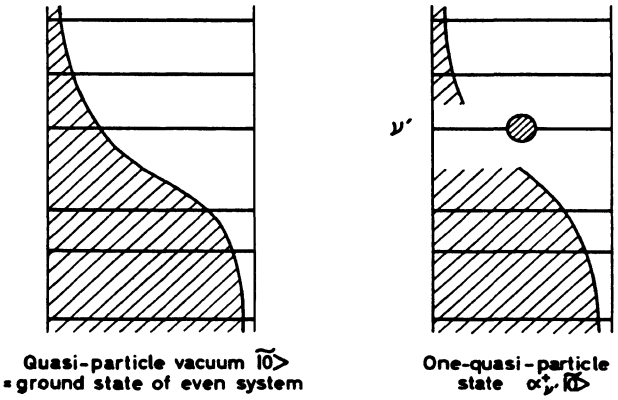

Fig. 4. Schematic illustration of the "vacuum" state and the one-quasi-particle state associated with orbital ν'. (From Ref. 11.)

$$a_{\nu}^{+} = U_{\nu} a_{\nu}^{+} + V_{\nu} a_{\bar{\nu}}, \qquad a_{\bar{\nu}}^{+} = U_{\nu} a_{\bar{\nu}}^{+} + V_{\nu} a_{\nu} . \tag{C12}$$

Figure 4 represents the quasi-particle vacuum and a one-quasi-particle state. The quasi-particle is associated with one and only one single-particle state and represents a change in occupation brought about in that shell model orbit. Far above the fermi surface a quasi-particle has the properties of a particle and far below the fermi surface, a hole. One-quasi-particle states occur as the ground states and excited states of odd systems. In even-even systems the excitations are two-quasi-particle states $a_{\nu_1}^{+} a_{\nu_2}^{+} |\tilde{0}\rangle$.

It should be noted that the concepts discussed above for spherical nuclei may be adapted for deformed nuclei.

D. Collective Motion and the Nilsson Model

1. Introduction.

So far we have been concerned with the short-range nucleon-nucleon interaction. Empirical evidence seems to indicate that there may be long-range effects of the nuclear potential which leads to a correlated motion of the nucleons within an average potential well. The potential for the two-particle interaction between nucleons within

this well can be expanded in terms of central coordinates

$$V(\bar{r}_1 - \bar{r}_2) = \sum_\ell U_\ell (r_1, r_2) P_\ell (\cos \theta_{12}), \qquad \text{(D1)}$$

where $\bar{r}$ is measured from the center of mass and θ_{12} is the angle between $\bar{r}_1$ and $\bar{r}_2$. It has been proposed that the isotropic part ($\ell = 0$ term) of this potential is responsible for the self-consistent potential of spherical nuclei as well as the pairing force. The terms of higher ℓ contribute the remainder of the interparticle interaction. However, for certain nuclei (in the "deformed" region) the $\ell = 2$ term is incorporated into the self-consistent field. This quadrupole term may be responsible for the quadrupole moment observed in these nuclei. Then the $\ell = 4$ or higher terms give the remaining particle-particle interaction (see Ref. 15 for a discussion of the "pairing plus quadrupole" model).

We are now in a position to discuss the effects of the long-range terms ($\ell \geq 1$) and in particular the quadrupole component ($\ell = 2$). The observation of nuclear excitation levels which have an energy below that expected for single-particle excitations has lead to a classification of these levels in terms of a rotation or vibration of the nucleus as a whole. If this "collective" motion proceeds with periods which are long compared to single-particle rotational periods, then the motion is said to be adiabatic and the Hamiltonian for the system can be separated into a term which contains only the "collective" variables and a term which contains only "intrinsic" or single-particle variables plus, perhaps, an interaction term; thus,

$$H = H_c \text{ (collective)} + H_p \text{ (intrinsic)} + H \text{(coupling)}. \qquad \text{(D2)}$$

The collective modes of motion of a liquid drop were first calculated by Lord Rayleigh.[16] He assumed a surface of general shape described in terms of spherical harmonics as

$$R = R_0 \left[1 + \sum_{\lambda=0}^{\infty} \sum_{\mu=-\lambda}^{\lambda} \alpha_{\lambda\mu} Y_\lambda^{\mu}(\theta,\phi) \right], \tag{D3}$$

where R_0 is the average radius of the surface. The result of letting the $\alpha_{\lambda\mu}$ vary with time is that the Hamiltonian can be expressed as

$$H_{VIB} = \tfrac{1}{2} \sum_{\lambda,\mu} (B_\lambda |\dot{\alpha}_{\lambda\mu}|^2 + C_\lambda |\alpha_{\lambda\mu}|^2). \tag{D4}$$

Assuming a hydrodynamic model, i.e., irrotational flow and constant fluid density with surface tension and Coulomb repulsion, the frequencies of oscillation $\omega_\lambda = (C_\lambda/B_\lambda)^{1/2}$ can be calculated. In order to apply this result to a nucleus the energy must be quantized by assuming that $E_\lambda = \sum_\lambda n_\lambda \hbar\omega_\lambda$, where n_λ is the number of "phonons" of order λ with energy $\hbar\omega_\lambda$. The result is that the first vibrational state has one $\lambda = 2$ phonon (2^+ state). The second state is composed of one $\lambda = 3$ phonon (3^- state) or two $\lambda = 2$ phonons (0^+, 2^+, 4^+ states). These predictions are born out qualitatively by data on even-even nuclei, especially near closed shells.

The nuclei which are not explained by the above arguments are the ones with large quadrupole moments. This is an indication that the energy states may not be vibrational but rotational. In this case the $\alpha_{\lambda\mu}$ are still variable in time but one would not say that the nuclear shape is changing. It is convenient to transform the description of the nuclear system to body centered axes (1, 2, 3) using the Euler angles (θ, ϕ, ψ)[17] as opposed to the space centered axes (x, y, z) previously used. The functions which produce this transformation are the $D_{\mu j}^{\lambda}$ functions found in the study of angular momenta.[18] A transformation from the parameters $\alpha_{\lambda\mu}$ is performed which produces the following parameters: β, a measure of the total nuclear deformation and γ, which indicates the shape of the nucleus (Ref. 7, p. 236). The collective Hamiltonian becomes

$$H_c = H_\beta + H_\gamma + \sum_{a=1}^{3} \frac{L_a^2}{2\mathcal{I}_a} + \tfrac{1}{2} C \beta^2, \tag{D5}$$

where H_β and H_γ jointly express the vibrational kinetic energy and L_a is the component of the angular momentum along the a axis. The result of a calculation using the above Hamiltonian and assuming that the wave function is separable into a rotational and vibrational part yields for an axially symmetric nucleus a rotational energy

$$E_J = \frac{\hbar^2}{2\mathcal{I}} J(J+1), \tag{D6}$$

where J is the angular momentum of the rotational state. This result holds well for several even-even highly deformed nuclei.

Very few nuclei exhibit only vibrational or rotational spectra. In order to explain the levels observed in the vast majority of nuclides the particle and collective motions must be discussed simultaneously.

This description in terms of axially symmetric nuclei was first introduced by Bohr and Mottelson[19,20] in a series of papers during the early 1950's and is summarized in an article by Kerman.[21] The case of the asymmetric rotator has been discussed by Davydov and Filippov.[22] We will treat mainly the symmetric rotator here indicating the results for the asymmetric rotator only briefly.

The Hamiltonian is that of Eq. (D2). The collective part of the Hamiltonian labeled H_c is expressed in terms of β, γ, and the Euler angles and H_p is a shell-model Hamiltonian

$$H_p = \sum_i \left(T_i + V(\beta, \gamma; \bar{r}_i, \bar{\ell}_i, \bar{s}_i) \right). \tag{D7}$$

For weak coupling, i.e., β is small enough to allow a perturbation treatment to be valid, the coupling term in Eq. (D2) represents the perturbation Hamiltonian (see Ref. 7, p. 251). However, one is primarily interested in the case of large deformations where perturbation techniques are inadequate. In this case the single-particle

Hamiltonian must be solved

$$H_p\psi_a = [T + V(\beta, \gamma; \bar{r}_i, \bar{\ell}_i, \bar{s}_i)]\ \psi_a = E_a(\beta, \gamma)\,\psi_a\,, \tag{D8}$$

where a represents all quantum numbers of interest. For a given number of particles one then minimizes the energy using β and γ as parameters. The complete wave function becomes

$$(T_{rot} + \sum_p H_p)\,\psi = E\,\psi, \tag{D9}$$

where

$$T_{rot} = \sum_{a=1}^{3} \frac{R_a^2}{2\mathcal{I}_a} = \sum \frac{(J_a - j_a)^2}{2\mathcal{I}_a}\,, \tag{D10}$$

and $\bar{J}$, $\bar{R}$, and $\bar{j}$ are the total, core and particle angular momenta, respectively.

Let us consider the rotational term in the axially symmetric case

$$T_{rot} = \frac{\hbar^2}{2\mathcal{I}}\,[(\bar{J} - \bar{j})^2 - (J_3 - j_3)^2] + \frac{\hbar^2}{2\mathcal{I}_3}\,(J_3 - j_3)^2\,. \tag{D11}$$

For an axially symmetric potential j_3 is a constant of the motion denoted by Ω. In addition, $\bar{J}^2$ and $J_3 = K$ are constants of the motion with $\mathcal{I}_1 = \mathcal{I}_2 = \mathcal{I}$. Therefore,

$$T_{rot} = \frac{\hbar^2}{2\mathcal{I}}\,[J(J+1) - K^2 - \Omega^2] + \frac{\hbar^2}{2\mathcal{I}_3}\,(K - \Omega)^2 - \frac{\hbar^2}{2\mathcal{I}}\,(J_+ j_- + J_- j_+)$$

$$+ \frac{\hbar^2}{2\mathcal{I}}\,\bar{j}^2\,. \tag{D12}$$

The term involving $J_\pm$ $(J_1 \pm iJ_2)$ and $j_\pm$ $(j_1 \pm ij_2)$ in Eq. (D12) is the rotational and particle coupling term commonly called the RPC term associated with a Coriolis force to be discussed later. The last term contains only particle operators and is added to the intrinsic Hamiltonian to form

$$H_0 = \sum_p H_p + \frac{\hbar^2}{2\mathcal{I}} \left(\sum_p \bar{j}_p \right)^2 . \qquad \text{(D13)}$$

This leaves the Hamiltonian equation

$$\left\{ \frac{\hbar^2}{2\mathcal{I}} [J(J+1) - K^2 - \Omega^2] + \frac{\hbar^2}{2\mathcal{I}_3} [K - \Omega]^2 + H_0 + \text{RPC} \right\} \psi = E \psi , \qquad \text{(D14)}$$

where, since $\mathcal{I}_3$ is observed to be small empirically, we have $K = \Omega$.

After properly symmetrizing the wave function and assuming a solution for the intrinsic motion of the form

$$H_0 \chi_\Omega = \epsilon_\Omega \chi_\Omega , \qquad \text{(D15)}$$

we obtain an energy spectrum

$$E_{J,K} = \epsilon_K + \left(\frac{\hbar^2}{2\mathcal{I}} \right) [J(J+1) - 2K^2 + \delta_{K,\frac{1}{2}} a(-)^{J+\frac{1}{2}} (J + \tfrac{1}{2})] , \qquad \text{(D16)}$$

where the term a is called the decoupling parameter and results from RPC which is only considered for $K = \frac{1}{2}$. We see that a rotational band is built on each intrinsic particle state.

In addition to rotational bands built on single-particle states, certain spheroidal nuclei also exhibit rotational bands built on the collective vibrations expressed in the first two right-hand terms of Eq. (D5). The parameters β and γ are closely related to the symmetry properties of the nucleus. The total deformation of the nucleus is represented by β and for the following discussion may be considered as being proportional to the three-dimensional analog of the eccentricity parameter of an ellipse in plane geometry. The location of a symmetry axis, if one exists, is given by γ (for example, a nucleus having the 3-axis for a symmetry axis would have $\gamma = 0$). The simplest vibration is a β vibration in which axial symmetry is preserved ($\gamma = 0$) and β oscillates about some value β_0. These vibrations have no angular momentum about the symmetry axis and produce

states with K = 0 and total spin and parity 0^+, 2^+, 4^+, · · · . These bands, when observed, appear at about 1 MeV excitation energy. A somewhat lower oscillation energy results from a γ vibration in which β remains fixed while γ oscillates about zero which introduces small departures from axial symmetry but leaves K very nearly a constant of the motion. These vibrations carry two units of angular momentum along the 3 axis and produce states with K = 2 having total spins 2^+, 3^+, 4^+, etc.

Usually at still lower energies a negative-parity rotational band exists, its lowest level being 1^-. It is very likely that these states are based on octupole vibrations of the nuclear shape which can carry from 0 to 3 units of angular momentum along the 3 axis. This motion is coupled to a rotator with 3-component equal to zero producing a band having states with total spin and parity 1^-, 3^-, 5^-, etc. These vibrations are thought to have a pear shape with the large lobe alternating between the two ends of the 3 axis (see Ref. 7, p. 246).

Small departures from the energy spacings of the levels as predicted by the symmetric rotator[20] model are contained in the energy spacings given by the asymmetric[22] rotator model. However, it is difficult to disentangle these effects from the other uncertainties present in the assumptions of the symmetric model. A more significant test for asymmetry is available in that the energies of the first two 2^+ excited states and the first 3^+ state are predicted using the asymmetric model to have the following relationship.

$$E_{21} + E_{22} = 2\hbar^2 (\mathcal{I}_1^{-1} + \mathcal{I}_2^{-1} + \mathcal{I}_3^{-1}) = E_3, \qquad \text{(D17)}$$

where the $\mathcal{I}_a$ are the moments of inertia of the 3-body centered axes. This relationship is born out by approximately a dozen cases to within an error of $\sim$2%.

2. Nilsson Model.

In the previous paragraphs of this section we have been discussing the collective modes of motion for a nucleus. If some nuclei are indeed nonspherical as evidence seems to indicate, then the average potential which is seen by an individual particle will be a function of the "distortion" from a spherical shape. In order to study the motion of a particle outside a distorted core the work done by Nilsson[23] on axially symmetric nuclei will be considered. This work was expanded to include nuclei of a general shape by Newton.[24]

The intrinsic wave function is (D15) using (D13) as the Hamiltonian. In order to keep the calculations simple (and since our discussion is to be in terms of an average potential), we will neglect the particle-particle interaction in (D13) and consider the single-particle equation given by

$$\left[-\left(\frac{\hbar^2}{2\mu^*}\right)\nabla^2 + V_0\left(\frac{r}{f}; \bar{\ell}, \bar{s}\right)\right] \psi_a = E_a \psi_a , \qquad \text{(D18)}$$

where μ^* is defined by $1/\mu^* = 2/M^* - 1/M$ and M^* is the usual reduced mass. The function f describes the nuclear distortion (see Ref. 7, p. 262). Assuming that the isopotential surfaces are ellipsoids with axes in the same ratio as the surfaces of constant density, the anisotropic oscillator potential can be written as

$$V_h = \tfrac{1}{2}\mu^* (\omega_1^2 x_1^2 + \omega_2^2 x_2^2 + \omega_3^2 x_3^2). \qquad \text{(D19)}$$

This result together with the inclusion of an $\bar{\ell}\cdot\bar{s}$ potential, gives the single-particle wave equation

$$\left(-\frac{\hbar^2}{2\mu^*}\nabla^2 + V_h + V_{\bar{\ell},\bar{s}}\right) \psi_a = E_a \psi_a . \qquad \text{(D20)}$$

Since the $V_{\bar{\ell},\bar{s}}$ term is not sufficiently small to allow perturbation methods to apply, the exact solution is found by performing a numerical analysis. This is best done by the introduction of the

coordinates

$$\xi_a = \left(\frac{\mu^* \omega_a}{\hbar}\right)^{1/2} x_a \tag{D21}$$

and

$$\rho^2 = \sum \xi_a, \quad \nabla_\xi^2 = \sum \frac{\partial^2}{\partial \xi_a^2} . \tag{D22}$$

Labeling the first two terms of the Hamiltonian (D20) $H_h = H_0 + H_\epsilon$, this transformation produces

$$\left.\begin{aligned} H_0 &= \tfrac{1}{2} \hbar \omega_0 \ (-\nabla_\xi^2 + \rho^2), \\ H_\epsilon &= \tfrac{1}{2} \hbar \omega_0 \sum_a \delta_a \left(-\frac{\partial^2}{\partial \xi_a^2} + \xi_a^2\right), \end{aligned}\right\} \tag{D23}$$

with

$$\omega_0 = \frac{2k}{\mu^*} \quad \text{and} \quad \omega_a = \omega_0 (1 + \delta_a).$$

The Hamiltonian H_h is that of a three-dimensional isotropic oscillator. In cartesian coordinates the constants of motion are the number of quanta along each of the three axes: n_1, n_2, n_3. In spherical coordinates the appropriate constants are the total number of quanta $N = n_1 + n_2 + n_3$ and a pseudo angular momentum

$$\lambda = -i \hbar \bar{\xi} \times \nabla_\xi , \tag{D24}$$

which differs from the true angular momentum $-i\hbar \bar{r} \times \bar{V}_r$ by terms of first order in δ_a. However, the ξ representation is preferable since it simplifies the numerical procedure. The eigenstates of H_h are expressed as $|N, \ell, \Lambda, \Sigma\rangle$, where $\bar{\lambda}^2 = \ell(\ell + 1)$, $\lambda_3 = \Lambda$, and the spin $s_3 = \Sigma = \pm \frac{1}{2}$ and $\Lambda + \Sigma = \Omega$. Nilsson included a pseudo-spin-orbit coupling term $C\bar{\lambda} \cdot \bar{s}$ and a term $D\bar{\lambda}^2$ which is needed to reduce the higher angular-momentum states from these oscillator values

(observed empirically). These terms are chosen to make the energy levels for spherical nuclei agree with the shell model.

Nilsson and Newton have solved numerically the single-particle wave equation

$$(H_0 + H_\epsilon + C\bar{\lambda}\cdot\bar{s} + D\lambda^2)\,\psi_a = E_a\,\psi_a \tag{D25}$$

and these solutions are exhibited in Refs. 23 and 24. The important parameters include δ, which is a measure of the distortion ($\delta = 0.95\,\beta$), $\eta = 2\delta\hbar\omega_0(\delta)/C$, $\kappa = C/2\hbar\omega_0(0)$, and $\mu = 2D/C$. Reasonable values for the medium-to-heavy nuclei are $\hbar\omega_0(0) = 41\,A^{-1/3}$ MeV and $\kappa = 0.05$ with μ being given in Ref. 23. The states are usually listed by the triad $[N\,n_3\,\Lambda]$ with the value of Ω and parity. The solutions to Eq. (D25) are listed as

$$\psi_a = \sum a_{\ell\Lambda}|N\ell\Lambda\Sigma\rangle. \tag{D26}$$

3. Band Mixing.

Up to this point rotational energy levels of the type (D16) have been considered which are applicable to nuclei whose single-particle energy levels are widely spaced as compared to rotation levels. If this adiabatic condition is not satisfied, the RPC term in Eq. (D14) cannot be neglected. The case of interest is that for which most of the single-particle levels are of high energy but one or two may be of low enough energy so as to allow the RPC, acting through these levels, to partly decouple the particle from the rotor. The effect of this rotation-particle coupling will now be investigated. First, the nonvanishing matrix elements are needed

$$\left.\begin{aligned}(JK|J_\pm|JK\pm1) &= \sqrt{(J\mp K)(J\pm K+1)}\\ (j\Omega|j_\pm|j\Omega\pm1) &= \sqrt{(j\mp\Omega)(j\pm\Omega+1)}\end{aligned}\right\}. \tag{D27}$$

It is seen that only states differing by 1 unit in K are mixed. It should be noted that levels near the ground state have $K = \Omega = 0$ (Ref. 7, p. 240).

Dropping the requirement of axial symmetry and following the discussion by Kerman[25] and later by Brockmeier *et al.*,[26] 4 perturbations on the Hamiltonian remain

$$\begin{aligned} H' &= H_1' + H_2' + H_3' + V'(\bar{r}) \\ &= \left(\frac{\hbar^2}{8\mathcal{J}_1} - \frac{\hbar^2}{8\mathcal{J}_2}\right)[-2(J_+ j_+ + J_- j_-) + (j_+ j_+ + j_- j_-) \\ &\quad + (J_+ J_+ + J_- J_-)] + V'(\bar{r}). \end{aligned} \tag{D28}$$

In the simplest case, namely the situation when one low-lying configuration is coupled to the ground state, this Hamiltonian yields an energy spectrum

$$\begin{aligned} E(J) &= \tfrac{1}{2}[E_{K+1}(J) + E_K(J)] \\ &\quad \pm \tfrac{1}{2}\sqrt{[E_{K+1}(J) - E_K(J)]^2 + 4A_K^2 (J - K)(J + K + 1)}, \end{aligned} \tag{D29}$$

where $E_K(J)$ is the unperturbed solution

$$\begin{aligned} E_K(J) &= E_K^0 + E_K^{(1)}[J(J+1) + \delta_{K,\frac{1}{2}} a(-)^{J+\frac{1}{2}}(J + \tfrac{1}{2})] \\ &\quad + E_K^2 [J(J+1) + \delta_{K,\frac{1}{2}} a(-)^{J+\frac{1}{2}}(J + \tfrac{1}{2})]^2, \end{aligned} \tag{D30}$$

and where

$$A_K = |(K|\frac{\hbar^2}{2\mathcal{J}} \sum J_- |K + 1)| \tag{D31}$$

is the "coupling parameter" and the last term in (D30) is the so-called rotation-vibration correction.[25] The wave function is a linear combination

$$\psi_J^{H,L} = a_J^{H,L}\,\psi_{J,K} + b_J^{H,L}\,\psi_{J,K+1}\,, \tag{D32}$$

with $a_J^2 + b_J^2 = 1$ and the H and L represent the high- and low-energy solution of (D29), respectively. The reduced transition probabilities (see Sec. IIIB) between levels in the same band are given by

$$B(E2) = \frac{5}{16\pi}\,e^2\,(J2J'K|JK20)^2 \left[Q_0{}^K + \left(\frac{A_{K<}}{\Delta E}\right)\sqrt{\frac{2}{3}}\;Q^{K,K'}\,f_{E2}^{KK'}\right]^2 \quad \text{for} \quad K_< \neq \tfrac{1}{2},$$

$$B(M1) = \frac{3}{4\pi}\left(\frac{e\hbar}{2Mc}\right)(J1J'K|JK10)^2 \left[G^{KK'}\left[1 + \delta_{K,\frac{1}{2}}\,\frac{(-)^{J+\frac{1}{2}}}{\sqrt{2}}\,b_{M1}\right] + \frac{A_{K<}}{\Delta E}\,\sqrt{2}\,G^{KK'}f_{M1}^{KK'}\right]^2, \tag{D33}$$

where the parameters are those defined in Sec. IV of Ref. 25. Similarly, for transitions between bands

$$B(E2) = \frac{5}{16\pi}\,e^2\,(J2J'K|JK2,K'-K)^2 \left[\left(\frac{A_{K<}}{\Delta E}\right)\sqrt{6}\;Q_0{}^K + Q^{KK'}\right]^2, \tag{D34}$$

where $Q_0{}^K = Q_0{}^{K'}$, $K' = K + 1$, $K_2 = \frac{1}{2}$. The M1 amplitude is of similar form but usually equal to zero due to the necessity of having $G^{KK} = G^{K'K'}$, where $G^{KK} = K(g_K - g_R)$ and g_K and g_R are the particle and collective g factors, respectively. It should be noted that in the collective model without RPC transitions between bands are not allowed, but RPC enhances these transitions.

These equations have been incorporated into a computer code developed by both Kerman[25] and Brockmeier[26] and used to calculate the energy levels and relative intensities of the transitions for the

states in ^{183}W. A similar code was used in an attempt to describe the spectrum observed in ^{187}W discussed in Sec. VIII.

E. The Core-Excitation Model

As was already discussed, the low-lying excited states of many nuclei, especially those in the deformed region, can be described as a combination of intrinsic particle motion coupled to a rotational and/or vibrational motion. In this section a model will be discussed in which the low-lying excited states of certain nuclei may be described in terms of an excitation of a nuclear core to which one nucleon (or hole) has been coupled.

The core excitation model was first proposed by Lawson and Uretsky[27] and the principles have been expanded somewhat by DeShalit.[28] Consider an even-even nucleus which has a closed-shell (or subshell) configuration for one of the nucleons—say the neutrons. In a closed shell configuration it is expected that the component neutron and proton angular momenta are good quantum numbers for all the low-lying excited states. If one neutron is now added to this nucleus, an odd-A nucleus which is one neutron removed from a closed shell is created. If the coupling of this odd neutron to the even-even core is sufficiently weak so as to allow the component neutron and proton angular momenta to remain constants of the motion, then the states of the odd nucleus may be described using perturbation theory. For each low-lying excited state of the original even-even nucleus, there will be a set of levels in the adjacent odd-A nucleus which corresponds to the several ways that the odd nucleon angular momentum and the angular momentum of the core state can couple to produce a resultant angular momentum.

In the interest of clarity the states in an odd-A nucleus which would correspond to the ground state and the first 2^+ excited state of

an even-even core may be considered. Since the ground state of the core has spin and parity 0^+, the ground state of the odd-A nucleus will result from placing the odd neutron in the lowest allowed shell-model orbital of the potential created by the core and will have the spin and parity of this lowest orbital (denoted by j). A multiplet of states in the odd-A nucleus will result from the coupling of the 2^+ state of the core to the spin j of the odd nucleon which produces a range of levels having spins J_i differing by integral steps such that

$$|2 - j| \leq J_i \leq 2 + j \,, \tag{E1}$$

each state having the same parity as the odd-A ground state.

The following is a summary of the properties of these states and their decay properties provided the core-excitation model is strictly applicable.

(1) The "center of gravity" of the multiplet of states having spins described by Eq. (E1) is defined as

$$E_{CG} = \sum_i E_i (2J_i + 1) \Big/ \sum_i (2J_i + 1) \,. \tag{E2}$$

This energy will be equal to the energy of the first 2^+ excited state in the even-even core.

(2) M1 γ radiation is allowed between members of the multiplet if spin considerations are satisfied.

(3) M1 transitions from the members of the multiplet to the ground state are strictly forbidden.

(4) The reduced transition probabilities (see Sec. IIIB) for the decay of each member of the multiplet to the ground state are equal to each other and further, each is equal to the transition probability for the decay of the 2^+ excited state in the core.

Result (3) is perhaps expected intuitively since the decay of each member of the multiplet is really accomplished through a decay

of the core from $2^+ \rightarrow 0^+$ which is a pure E2 transition. Similarly, since each transition from each member of the multiplet to the ground state is only a core decay, the transition probabilities might be expected to be equal.

DeShalit[28] has given several mass regions in which the model might be expected to be valid. This is not to say that only core-excited states will be observed since some single-particle excitation may also proceed in any reaction which could expose these states. However, the Coulomb excitation reaction (see Sec. III) is perhaps ideally suited for the study of the states corresponding to a 2^+ excitation in the core since E2 transitions are by far the strongest transitions observed in this reaction (see Sec. IIC). Therefore, the states in which we are most interested will yield the most intense transitions. An attempt to apply this model to the ^{105}Pd nucleus has been made, the results of which are reported in Sec. VII.

III. THEORY OF COULOMB EXCITATION

It has long been known that certain nuclear states can be excited by the electromagnetic interaction between a target nucleus and a charged bombarding particle having an appropriate energy. Due to the longevity of the observation of this reaction and various attempts to obtain a theory appropriate to "Coulomb Excitation," this reaction is perhaps the best understood process in nuclear physics. Extensive experimental investigations have been performed to test the theoretical description.

Coulomb excitation proceeds by way of the electromagnetic interaction between the target and projectile nuclei. Since the electromagnetic interaction has a large range compared to the nuclear diameter, Coulomb excitation is an especially efficient means of producing collective excitations. The following sections will describe the classical theory of the reaction.[29] The quantum-mechanical description is contained in the review by Adler et al.[29]; however, most of the features of the reaction are explained well by a classical treatment.

A. The Classical Description

When a bombarding particle with an energy well below the Coulomb barrier approaches a target nucleus, the particle follows a hyperbolic path due to the interaction of the electrostatic fields of the projectile and target nuclei (Fig. 5). The shape of this path and the cross section for scattering into an element of solid angle $d\Omega$ are completely described by the Rutherford scattering formula

$$d\sigma_R = \tfrac{1}{4}\, a^2 \sin^{-4}(\theta/2)\, d\Omega, \qquad (A1)$$

where $a = Z_1 Z_2 e^2/M_o v^2$ is half the distance of closest approach in a head on collision, v is the projectile velocity, and Z_1 and Z_2 are the

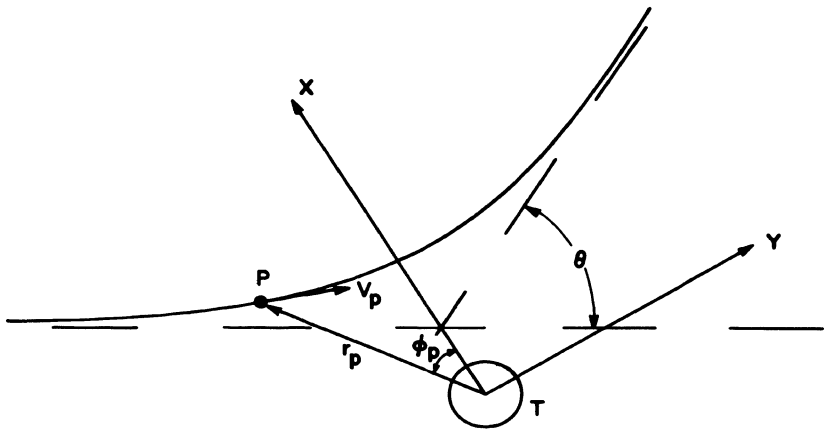

Fig. 5. Classical picture of the projectile orbit in the Coulomb field of the nucleus. The hyperbolic orbit of the projectile p is shown in the center-of-mass reference frame. The position and velocity of the projectile are denoted by ϕ_p, r_p, and V_p, respectively. The total asymptotic deflection angle is denoted by θ.

charge numbers of the projectile and target, respectively. All parameters are expressed in center-of-mass coordinates where M_o is the reduced mass of the target and projectile and θ is the total asymptotic angular deflection of the projectile.

Nuclear excitation is the result of the time-dependent electromagnetic field produced at the target nucleus as the projectile passes. The effective strength of the interaction is expressed by the dimensionless parameter $\eta = Z_1 Z_2 e^2/\hbar v$. When η is small, the velocity of the projectile is high and the Coulomb field does not distort the incoming particle wave appreciably and the particle is able to enter the nucleus. This is an undesirable effect in Coulomb excitation since direct nuclear reactions would then occur which have very large cross sections and would mask any Coulomb excitation which did occur. The requirement placed on η is that $\eta \gg 1$ which is similar to saying that the projectile energy must remain below the Coulomb barrier energy ($E_B = Z_1 Z_2 e^2/R$). In order that a classical description be valid it is further required that the nuclear excitation energy (ΔE) be much less than the energy of the bombarding particle (E_p). The differential excitation cross section can then be expressed as

$$d\sigma = P d\sigma_R , \qquad \text{(A2)}$$

where P is the probability that nuclear excitation of the target will result when the bombarding particle is scattered into solid angle $d\Omega$. This probability can be expressed in terms of the transition amplitudes (b_{if}) from the initial nuclear state i to the final nuclear states f.

In most experimental configurations the probability for excitation in a single encounter is very small so that by first order time dependent perturbation theory we have

$$b_{if} = \frac{1}{i\hbar} \int_{-\infty}^{\infty} \langle f|H|i\rangle \, e^{i\omega t} \, dt, \tag{A3}$$

where H is the interaction Hamiltonian and where

$$\omega = \frac{\Delta E}{\hbar} = \frac{E_f - E_i}{\hbar}, \tag{A4}$$

is the nuclear frequency associated with the excitation energy ΔE.

B. Electric and Magnetic Transition Probabilities

For particle velocities much smaller than that of light the dominant interaction is the Coulomb energy

$$H(t) = \int \rho_n(\bar{r}) \, \phi(\bar{r},t) d\tau, \tag{B1}$$

where

$$\phi(\bar{r},t) = \frac{Z_1 e}{|\bar{r} - \bar{r}_p|} - \frac{Z_1 e}{r_p(t)} \tag{B2}$$

is the electric potential minus the interaction between mass centers (which is responsible for the scattering only and not excitation), and $\rho(\bar{r})$ is the nuclear charge density operator. Expanding (B2) in terms of electric multipole components

$$M(E\lambda,\mu) = \int r^{\lambda} Y_{\lambda\mu}(\theta,\phi) \, \rho_n(\bar{r}) d\tau \tag{B3}$$

yields

$$H(t) = 4\pi Z_1 e \sum_{\lambda=1}^{\infty} \sum_{\mu=-\lambda}^{\lambda} \frac{1}{2\lambda + 1} r_p^{-\lambda-1} Y_{\lambda\mu}(\theta_p, \phi_p) M(E\lambda, \mu), \quad \text{(B4)}$$

assuming the particle remains outside the nucleus.

Equations (B4) and (B3) are inserted into Eq. (A3) and a re-parameterization is performed to yield an expression for the differential cross section

$$d\sigma_{E\lambda} = \left(\frac{Z_1 e}{\hbar v}\right)^2 a^{-2\lambda+2} B(E\lambda) df_{E\lambda}(\theta, \xi), \quad \text{(B5)}$$

where $B(E\lambda)$ is the reduced transition probability (see Ref. 29, Eq. IIA. 18) and $df(\theta, \xi)$ is the differential excitation function.[29]

The total excitation cross section of order $E\lambda$ is obtained by integrating over all scattering directions and is given by

$$\sigma_{E\lambda} = \left(\frac{Z_1 e}{\hbar v}\right)^2 a^{-2\lambda+2} B(E\lambda) f_{E\lambda}(\xi). \quad \text{(B6)}$$

The excitation functions $df(\theta, \xi)$ and $f(\xi)$ have been evaluated numerically in Ref. 29 (Sec. II C). The dimensionless quantity ξ is defined by

$$\xi = \frac{a \Delta E}{\hbar v} = \frac{Z_1 Z_2 e^2 \Delta E}{\hbar v \quad 2E}, \quad \text{(B7)}$$

with

$$E = \tfrac{1}{2} M_o v^2.$$

The ratio of collision time to nuclear period ξ is proportional to and is a measure of the adiabatic nature of the reaction. For large collision time to nuclear period ($\xi > 1$) the f functions decrease exponentially with ξ implying that very little nuclear excitation will occur, i.e., an adiabatic reaction, whereas for $\xi \to 0$ the reaction cross sections are at their highest values. Restrictions are placed on ξ for two reasons. (1) It is desirable to keep the bombarding energy

below the Coulomb barrier

$$E_B = \frac{Z_1 Z_2 e^2}{R}, \tag{B8}$$

where R is the effective radius of interaction which, assuming the projectile to have a small radius when compared to the target, is $r_o A_2^{1/3}$, where $r_o = 1.5 \times 10^{-13}$ cm yielding $E_B = Z_1 Z_2 A_2^{1/3}$ MeV. (2) It is desirable to have an observable spectrum which implies $\xi \lesssim 1$. Both requirements give the range of ξ as

$$\left(\frac{A_1 A_2}{Z_1 Z_2}\right)^{1/2} \frac{\Delta E(\text{MeV})}{13} \lesssim \xi \lesssim 1. \tag{B9}$$

Electric transitions require a parity change of $(-1)^{\lambda}$. Excitations of opposite parity are produced by magnetic transitions resulting from the magnetic field of the passing particle. A similar derivation (see Ref. 29, Sec. IIA. 2) yields a differential cross section for magnetic transitions

$$d\sigma_{M\lambda} = \left(\frac{Z_1 e}{\hbar c}\right)^2 a^{-2\lambda+2} B(M\lambda) df_{M\lambda}(\theta, \xi), \tag{B10}$$

where $B(M\lambda)$ is the reduced magnetic transition probability and df is calculated using Eq. IIA. 51 of Ref. 29. ξ is defined as above. Similarly the total cross section is

$$\sigma_{M\lambda} = \left(\frac{Z_1 e}{\hbar c}\right)^2 a^{-2\lambda+2} B(M\lambda) f_{M\lambda}(\xi). \tag{B11}$$

It can be seen that apart from nuclear matrix elements magnetic transitions are reduced by a factor of $(v/c)^2$ from electric transitions.

C. Important Results

There is a simple relationship between the reduced transition probability to an excited state and the lifetime for radiative decay of

the state by the corresponding multipole transition. The probability per unit time for this part of the transition is

$$T = \frac{8\pi(\lambda+1)}{\lambda\,[(2\lambda+1)!!]^2}\ \frac{1}{\hbar}\left(\frac{\omega}{c}\right)^{2\lambda+1} B(\lambda; I_f \rightarrow I_i), \qquad (C1)$$

where the "downward" reduced transition probability $B(\lambda; I_f \rightarrow I_i)$ is related to the "upward" transition probability by

$$B(\lambda; I_f \rightarrow I_i) = \frac{2I_i+1}{2I_f+1}\ B(\lambda; I_i \rightarrow I_f). \qquad (C2)$$

It should be mentioned that the total lifetime of a state cannot be found without knowing the necessary mixing ratios for the radiative decay of the state. Figure 6 gives the excitation cross sections for different multipole transitions assuming a nuclear excitation energy of 200 keV and using reduced transition probabilities equal to the single particle values

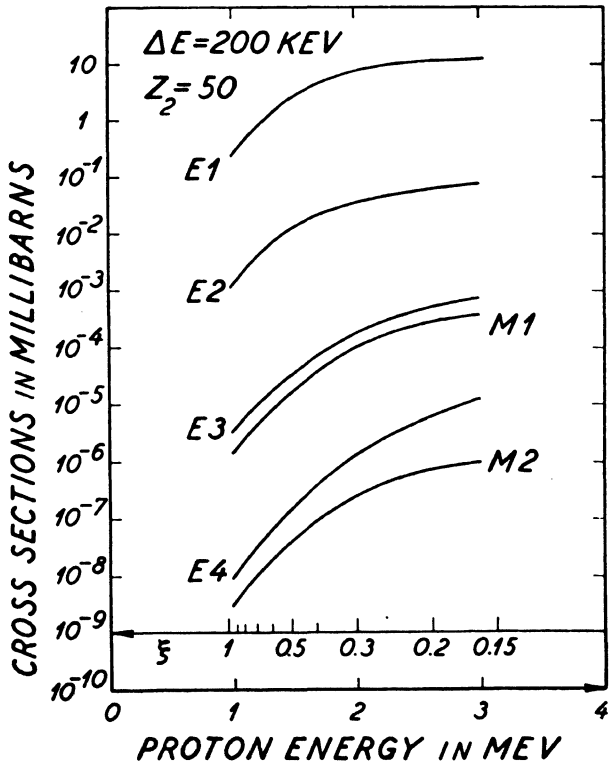

Fig. 6. Excitation cross sections for nuclear transitions of single particle strength. The curves give the total Coulomb excitation cross sections of various multipole orders for proton bombardment of a nucleus with Z = 50. The excitation energy is taken to be 200 keV and the reduced transition probabilities are in single particle units (C3) with $R_0 = 5.9 \times 10^{-13}$ cm. (From Ref. 29.)

$$B_{sp}(\lambda) = (2\lambda + 1)\frac{e^2}{4\pi}\left(\frac{3}{3+\lambda}\right)^2 R_0^{2\lambda}$$

$$\times \begin{cases} 1 & \text{for } E\lambda \\ 10\left(\frac{\hbar}{McR_0}\right)^2 & \text{for } M\lambda\,, \end{cases} \qquad \text{(C3)}$$

where M is the proton mass. (See Eq. IIA.58 of Ref. 29.) An important empirical result is that electric dipole transitions have transition probabilities several orders of magnitude below that given by (C3) and E2 transitions have strengths 10—100 times (C3). The net effect is that E2 transitions are the most strongly excited by Coulomb excitation (by as much as 5 orders of magnitude) in most regions of the periodic table.

The enhancement of the quadrupole transitions is understood to be the result of the long range of the electromagnetic interaction involved in Coulomb excitation. This long range force allows the entire nucleus to undergo collective excitation. We have observed in Sec. IID that many medium-to-heavy weight nuclei have permanent quadrupole deformations and even more undergo quadrupole oscillations in many of the low-lying excited states. It, therefore, is relatively easy to excite these collective states by quadrupole (E2) transitions.[7]

The retardation of the E1 transitions for these nuclei is less well understood but it appears that states differing by one unit of angular momentum and having opposite parity appear to have very different structures. Neither the spherical shell model nor the Nilsson model allow much opportunity for such states to exist with low excitation energies and in the collective model negative parity states are the result of octupole oscillations or permanent pear-shaped deformations. The transition rate to an even parity state will be slow for all these cases due to the dissimilarity of the initial and final states involved in a transition.[7]

It can also be seen from Fig. 6 that given the excitation energy of the state producing a γ ray it is possible to determine the multipole order of the transition by studying the cross section for reaction at several bombarding energies and comparing the experimental curve shape with that which is predicted. This procedure is successful except in the case of differentiating between E1 and E2 transitions (unless the nuclear excitation energy is very low). The multipole order can always be determined by performing Coulomb excitation with different particles. For a given value of ξ the cross section for an excitation of multipole order $E\lambda$ is proportional to $Z_1^2 (A_1/Z_1)^{2\lambda/3}$ (see III.4, IIC.3, IIC.15, IIC.16 of Ref. 29). Therefore, the ratio of the yields obtained with the two particles will depend on the multipole order of the transition. It can also be seen from this result that, in general, heavier particles will produce a larger excitation cross section.

The motivation for performing a Coulomb excitation experiment is an interest in obtaining the transition probabilities to and from certain low-lying excited states. This is accomplished by measuring the excitation cross section and determining the multipole order of the transition as discussed in the previous paragraph. The cross section [Eq. (B6)] can be written as

$$\sigma_{E\lambda} = C_{E\lambda} E^{\lambda-2} (E - \Delta E)^{\lambda-1} B(E\lambda) f_{E\lambda}(\eta, \xi), \qquad \text{(C4)}$$

where $C_{E\lambda}$ is a constant for a given multipole excitation (see Ref. 29, Eq. IIC.16). The energy dependence exhibited explicitly in Eq. (C4) is the result of the closeness of approach of the projectile to the target. The closer the projectile approaches the target the stronger is the electromagnetic force and hence the cross section increases with bombarding energy at a rate dependent on the multipole order of the excitation. The term including the excitation energy ΔE expresses the fact that it is easier for the target nucleus to absorb a small

amount of energy. The dependence of the reaction cross section on the adiabatic nature of the process is expressed in the excitation functions (f). Physically the requirement expressed by these functions is that the electromagnetic field must exist for a short time compared to the nuclear period associated with a transition, otherwise the bombarding particle will produce an electromagnetic field which lasts too long producing only virtual excitations and leaving the nucleus in its ground state. Finally, it is the $B(E\lambda)$ functions which contain all of the properties of the nuclear forces, i.e., state wave function overlaps and the nuclear portion of the dependence of the cross section on ΔE. Since all the other parameters on the right-hand side of Eq. (C4) are known or can be calculated, the transition probabilities $[B(E\lambda)]$ can be found (independent of any nuclear model) by measuring the excitation cross section at a given energy. The number of nuclear models which could be applied to a given nucleus is quickly reduced when one knows the transition probabilities of nuclear states. Most models predict the energy of nuclear states rather poorly; however, certain models may be rejected because the transition probabilities they predict are incorrect by several orders of magnitude. A knowledge of the transition probabilities is a valuable parameter in the selection of applicable nuclear models.

The Coulomb excitation studies discussed in Sec. VII were performed using thick targets; i.e., all the projectiles were stopped inside the target. In this case the amount of total excitation or the yield of the reaction is proportional to an integral of the cross section over the range of energies produced as the projectile slows down in the thick target. It is convenient to express the result of this calculation in terms of the effective target thickness δE_λ[29] which is related to the true thick target yield by

$$Y = \sigma(E_0) \frac{E_0 N}{(dE/ds)_0} \frac{\delta E_\lambda}{E_0}, \qquad \text{(C5)}$$

where Y is the fraction of the incoming particles which produce a particular nuclear reaction and N is the target density. The stopping power $(dE/ds)_0$ is evaluated at the bombarding energy E_0. The fraction $\delta E_\lambda / E_0$ represents the ratio of the observed yield to that which would result if the cross section and stopping power were independent of energy and had values corresponding to E_0. The values of δE_λ as a function of ξ are given in Ref. 29, Sec. IIIB. 2. When thick targets are employed, the consideration of the stopping power reduces the advantage gained in using heavier particles as projectiles (which was mentioned above). The lighter particles normally have a larger range and therefore strike more target nuclei than heavier ones. The net result, however, is that even when using thick targets, larger cross sections are produced when heavier bombarding particles are employed.

However, an additional problem arises in the use of heavy particles as projectiles in that multiple Coulomb excitation may be produced. Consider a nucleus having a 0^+ ground state, a first excited state with spin and parity 2^+ and a second excited state having spin and parity 4^+. If the cross section for excitation of the first excited state is large enough, then some of these states will be in existence when a second projectile strikes the target. Thus the 2^+ state may be excited by an E2 transition to the 4^+ state. Cross sections for multiple excitation may be calculated and the effect has been observed; however, multiple events only produce a complication in the calculation of transition probabilities if the yields of the excited states can be measured without such events.

The angular distribution of the de-excitation γ rays can be described in terms of the correlation function for a hypothetical γ-γ cascade in which the first transition is a pure 2λ-pole radiation,[30] i. e., the Coulomb excitation transition, and the second transition is the de-excitation γ ray (see Ref. 29, Sec. IIA. 4). Since there is

considerable deviation in the predicted angular correlation from the classical limit, even for rather large values of η ($\eta = \infty$ for the classical limit)[29] the quantum mechanical form of the distribution must be used.

$$W_{\theta,\phi}(\Omega_\gamma) = \sum_{K=0}^{\infty} a_{2K}{}^{\lambda}(\theta,\phi,\xi)A_{2K}{}^{\lambda}P_{2K}(\cos\theta_\gamma) \qquad (C6)$$

The $a_{Km}{}^{\lambda}$ coefficients are independent of the nuclear states and the de-excitation process and have been calculated using quantum theory and tabulated in Ref. 29. The $A_K^{(\lambda)}$ coefficients are the usual γ-γ correlation coefficients and are tabulated in Refs. 30 and 31 and the functions P_K are Legendre polynomials. In the conventional case the expansion is carried only to $K = 2$ in Eq. (C6). An additional term must be included in order to correct for the attenuation introduced into the angular distribution by the finite detector solid angle as well as a thick target correction. The detector solid angle corrections are included in the so-called G factors which can be calculated using a computer code written by W. T. Milner.[32] Thick target a coefficients (a^t) are also calculated by Milner[32] and the angular distribution becomes

$$W(\theta) = 1 + a_2{}^{t}A_2G_2P_2(\cos\theta) + a_4{}^{t}A_4G_4P_4(\cos\theta). \qquad (C7)$$

IV. THE (n,γ) REACTION

A. Radiative Capture

In later sections of this paper (Sec. VIII) we will be interested primarily in the low-energy states ($E \leq 2$ MeV) of a nucleus which is formed by the capture of thermal neutrons. However, in order that we may interpret data which is pertinent to the description of the low-lying energy levels it is important to know something about how the capture state is formed and its subsequent decay.[34—39]

The capture cross section for Cd as a function of neutron energy is shown in Fig. 7. The resonance peaks in the cross section result whenever the wave functions of the incoming neutron and the target nucleus have sufficient overlap to allow the neutron to remain within the field of the target nucleus long enough so a reaction may take place. The possible reactions available for low-energy neutrons on medium to heavy weight nuclei are elastic scattering in which the neutron again

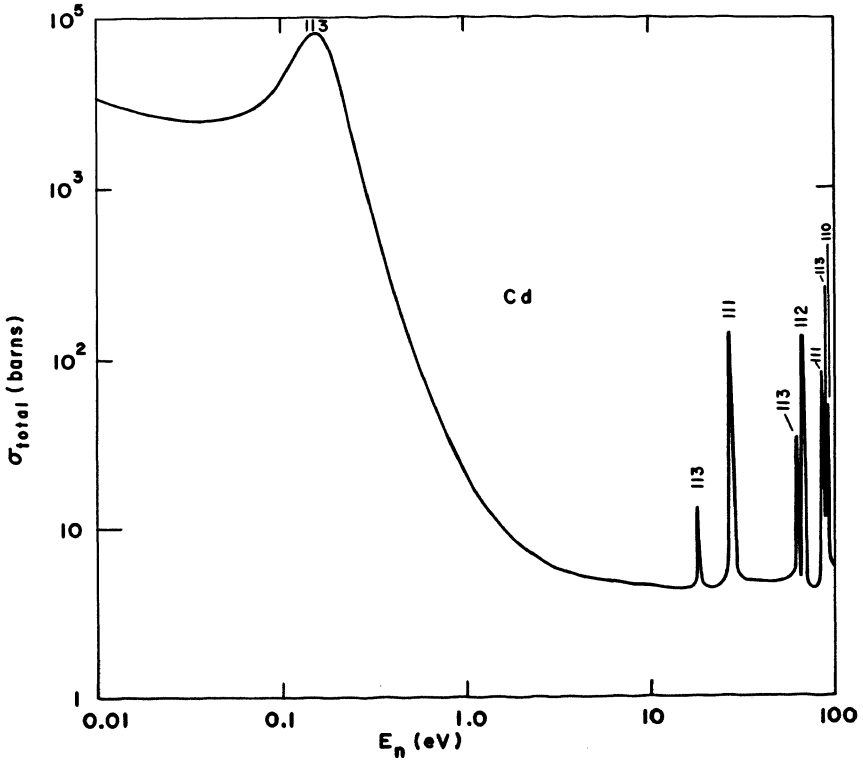

Fig. 7. Total cross section for neutron bombardment of a natural Cd sample. Each resonance has the so-called Breit-Wigner shape.

leaves the target nucleus, radiative capture in which the neutron kinetic and binding energy is given up in γ-ray transitions leading to the ground state of the product nucleus, and in very few cases neutron-induced fission.

The main parameters used to describe a resonance are the spin of the target I_o; the spin s and angular momentum ℓ of the incoming neutron; and the spin I ($\bar{I} = \bar{I}_o + \bar{s} + \bar{\ell}$), energy E_r, and width Γ_s of the resonance. Each resonance gives a contribution to the cross section expressed as

$$\sigma_{cap}(n) = 8\pi\lambda\!\!\!^{-} R g(s) \left(\frac{\gamma_n}{\Gamma_s}\right)\left[1 + \frac{4(E - E_s)^2}{(\Gamma_s)^2}\right]^{-1}, \qquad (A1)$$

where $\lambda\!\!\!^{-}$ is the de Broglie wave length ($\hbar[2ME]^{-\frac{1}{2}}$), R is the channel radius (Ref. 33, p. 463), g(s) is the statistical weight of a resonance of spin s (see Ref. 33, p. 470), γ_n is the reduced neutron width (see Ref. 33, p. 470), Γ_s is the full width at half maximum of the resonance, E_s is the resonance energy and E is the neutron kinetic energy. The important feature of this so-called Breit-Wigner shape for our studies is that for $E \to 0$ the factor $\lambda\!\!\!^{-} \to \infty$ and therefore each resonance will contribute to the cross section at thermal energies. Thermal capture is, however, usually dominated by 1 or 2 of the closest resonances.

One of the most interesting characteristics of the high-energy transitions is the distribution of radiation widths (transition probabilities) for a given multipole transition. Let us consider E1 transitions as these are expected to be the strongest ones involved in a first or "primary" transition following slow neutron capture (Ref. 33, p. 649). We must begin with the analysis by Porter and Thomas[34] of the distribution of reduced neutron widths. They have indicated that the wide fluctuation observed in the reduced widths is the result of the complexity of the wave functions of the highly excited states

formed in neutron capture. After making some reasonable assumptions about the statistical nature of these states they conclude that for a reaction which proceeds by way of a single exit channel, the distribution of widths Γ is

$$P(x) = x^{-\frac{1}{2}} e^{-x/2}, \qquad (A2)$$

where x is the ratio of the reduced neutron width for a given resonance to the average neutron width over all resonances ($\Gamma/\langle\Gamma\rangle$). This distribution belongs to the class of chi-squared distributions

$$P(x,\nu) = \Gamma(\nu/2) \left(\frac{\nu}{2} x\right)^{(\nu/2 - 1)} e^{-\nu x/2}, \qquad (A3)$$

where $\Gamma(\nu/2)$ is the mathematical Γ function and ν is the number of degrees of freedom, i.e., number of exit channels and x is defined as above.

It has been shown by many experiments that the reduced neutron widths do fit a Porter-Thomas distribution with 1 degree of freedom. Since radiative capture from highly excited states seems also to proceed by way of one exit channel and since these states are the same ones involved in neutron emission, the partial radiation widths are also expected to follow the Porter-Thomas distribution. It has also been shown that in most cases the partial radiation widths do follow the Porter-Thomas distribution with 1 degree of freedom as is expected from the statistical model of the resonance states. There still may be individual nuclei where nuclear structure effects may dominate over the statistical nature of a resonance and cause the Porter-Thomas distribution to be violated.[36]

The important result of this discussion is this. Since thermal neutron capture is dominated by one or two resonances, the transition probability, i.e., radiation width, to a given level may or may not be large enough to allow the observation of transitions to the level even if spin and parity selection rules are satisfied.

It should be noted that this dependence of the decay on the Porter-Thomas distribution may be removed by the average resonance technique used by Bollinger and Thomas at Argonne National Laboratory.[38,39]

B. Thermal Capture γ Rays

Figure 8 shows a typical γ-ray spectrum resulting from the capture of slow neutrons in $^{113}Cd(n,\gamma)^{114}Cd$. There are three main regions of interest: (1) a high-energy region (6—10 MeV in the figure) in which individual well-resolved γ rays are observed, (2) an intermediate energy region (2.5—6 MeV in the figure) in which a broad maximum is produced by a myriad of unresolved γ-ray lines, and (3) a low-energy region consisting of individual and usually resolvable γ-ray lines.

First, consider the high-energy transitions. In the single-particle model the widths for the radiation which should be strong enough to be detected are given by

$$\Gamma_{\gamma_{if}}(E1) = 6.8 \times 10^{-2} E_\gamma^{\ 3} A^{2/3} D_i/D_o \qquad \text{(B1)}$$

$$\Gamma_{\gamma_{if}}(E2) = 4.9 \times 10^{-8} E_\gamma^{\ 5} A^{4/3} D_i/D_o \qquad \text{(B2)}$$

$$\Gamma_{\gamma_{if}}(M1) = 2.1 \times 10^{-2} E_\gamma^{\ 3} D_i/D_o, \qquad \text{(B3)}$$

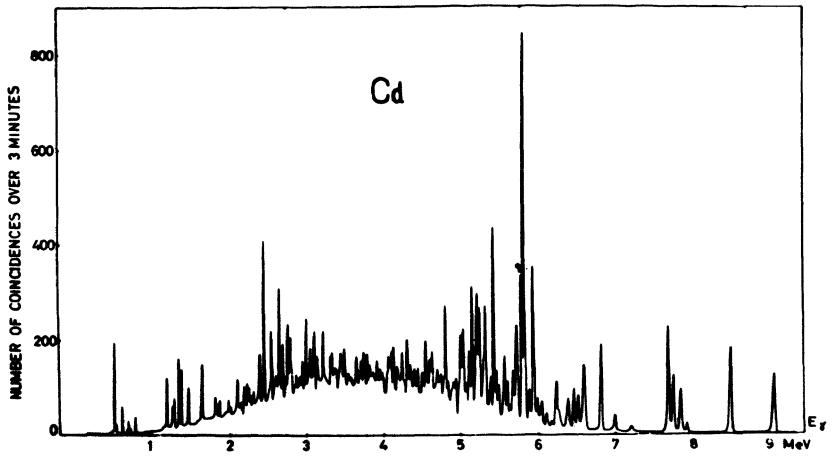

Fig. 8. Gamma-ray spectrum for the reaction $^{113}Cd(n,\gamma)^{114}Cd$. (From Ref. 36.)

where E_γ is the γ-ray energy, A is the mass number, D_i is the spacing of levels having a given spin and parity at the capture state, and D_o is the spacing of the bound single-particle levels of the product nucleus.[36] The energy distribution of the primary γ rays is obtained by multiplying the above widths by the density of final states denoted by $D_f (E_i - E_\gamma)^{-1}$. The result for radiation of multipole order 1 is

$$N_\ell (E_i - E_\gamma) = C_\ell (E_\gamma)^{2\ell+1} D_f (E_i - E_\gamma)^{-1}, \qquad \text{(B4)}$$

where C_ℓ is independent of E_γ.[33] The factor $(E_\gamma)^{2\ell+1}$ favors the emission of radiation with higher energy. However, since the levels become more and more closely spaced as one moves from the ground state to the capture state the factor $D(E_i - E_\gamma)^{-1}$ favors emission of quanta of low energy. With existing state densities and energy differences in medium to heavy weight nuclei, the primary transitions are more likely to be of high energy to states near the ground state.[33]

Let us now consider the effect of a low-energy primary transition to a state near the capture state in the event that it did occur. First, it would be a weak transition because of the dominance of the energy term in Eq. (B4). Secondly, the subsequent "secondary" transition strength would be shared among several transitions of most probably high energy. The net result is to make these secondary high-energy events unobservable. This leads to the general rule that any transition observed with an energy $\gtrsim 75\%$ of the binding energy is a primary transition to a low-energy state of the product nucleus.

It is obvious that by observing primary (high-energy) radiation it is possible to find the energies of many of the low-lying states of the product nucleus, especially if the binding energy of the neutron in the product nucleus is known. Since E1 radiation is the strongest radiation observed in primary transitions, the spin of the final state for the strongest transitions can be found or limited provided the spin of the capture state is known. This does not mean that all of the E1

transitions will necessarily be detected since the Porter-Thomas distribution favors many transitions that are weak compared to the average.

Further, a weak primary transition may be a strong M1 or E2 transition or a weak E1 transition. Therefore, the spin may be limited for the states to which weak primary transitions are observed. In addition, if the parity of the capture state is known, the parity of the low-lying states may be found provided a strong (and therefore E1) primary transition is observed since E1 transitions require a parity change from initial to final states.

The spin and parity of the capture state in thermal neutron capture is often known. This arises from the fact that the energy spectrum of thermal neutrons from a reactor has a Maxwellian distribution about an average energy equal to kT where k is the Maxwell-Boltzmann constant and T is the absolute temperature of the neutron moderator. This average energy is equal to about 1/40 eV and therefore the wavelength associated with a slow neutron is large compared to nuclear dimensions. This implies that the capture process is virtually all s wave capture. Therefore, if the spin and parity of the target nucleus is I^{π}, then the spin of the compound nuclear state is $I \pm \frac{1}{2}$, where the neutron intrinsic spin is $\frac{1}{2}$, and the parity of the product nuclear state is the same as the parity of the target nucleus (Ref. 7, p. 18). For an even-even target nucleus ($I^{\pi} = 0^{+}$) the result is especially simple since the capture state is then known to have spin and parity $\frac{1}{2}^{+}$.

Another consideration which makes thermal neutron capture an especially useful tool for studying the low-lying energy levels of a nucleus is the fact that capture is followed on the average by 3 or 4 cascade γ rays.[33] This means that any levels which are not populated by primary radiation have a high probability of being reached by secondary cascade radiation through the many intermediate energy

levels which are populated by many primary transitions. Therefore, it is seen that even spin states which are greatly different from the capture state may be populated by several secondary transitions of low multipolarity. By studying the low-energy region of the spectrum, states which are not populated by high energy, primary γ rays may be uncovered. Virtually all the levels with an energy ≤ 2 MeV are populated.

V. EXPERIMENTAL PROCEDURE

A. Singles Gamma-Ray Techniques

During the course of the investigations discussed in Secs. VI, VII, and VIII of this dissertation, lithium-drifted germanium [Ge(Li)] detectors were used exclusively for the detection of the γ rays of interest. Three detectors were employed at different times during the course of the studies. An $\sim$30 cc detector was available which was characterized by a line width of 2.9 keV at a deposited energy of 1.33 MeV and having a peak-to-Compton ratio of $\sim$12/1. It is a cylindrical device being drifted with lithium from the circular edge and one of the ends creating a "closed-end coaxial detector." The second detector is a 20 cc Ge(Li) detector having a line width of 2.6 keV at 1.33 MeV deposited energy with an $\sim$17/1 peak-to-Compton ratio. This device has a cylindrical shape being drifted from the circular face only, i.e., a "coaxial detector." The third detector was a "planar detector" (drifted from one face only) of $\sim$3.5 cc volume with a characteristic line width of 1.9 keV at 1.33 MeV deposited energy. (It should perhaps be noted here that the coincidence time distribution for prompt events having an energy below 100 keV produced a time distribution about 40 nsec wide at the base when using the planar or the coaxial detector whereas a distribution about 90 nsec wide resulted with the closed end coaxial detector. The two distributions were virtually the same above 100 keV.)

The charge produced by the detection of a gamma ray in the detector is collected by a charge sensitive FET preamplifier [see Ref. 40 for an explanation of the mechanism of γ-ray detection by a Ge(Li) device and a summary of its uses]. A minimum of pulse shaping is done by the preamplifier so that a pulse from the detector produces a preamplifier output pulse with about 5 nsec rise time and 50 μsec decay time with a voltage height proportional to the energy of the event detected.

The pulses from the preamplifier are applied to the input of a linear amplifier in which the pulses are shaped to an exponential rise time and decay time of 2 μsec while preserving the proportionality of the voltage pulse height to the energy of the event which produced it. These pulses are then applied to a pulse selector and linear gate system which produces an output acceptable to the analog-to-digital converter (ADC) and the multichannel memory.

The pulse-selector-linear-gate system provides the experimenter with the following options.

(1) A single channel analyzer is available to provide that only pulses with heights falling within a certain range are addressed to the analyzer.

(2) A voltage bias may be applied so that any pulse height may be stored in channel 1 of the analyzer.

(3) Artificial dead times of 1, 2, or 3 pulse widths may be inserted after each pulse which is selected. This option is especially useful for high-counting rate experiments with Ge(Li) detectors since the introduction of a dead time after each pulse ensures that the baseline of the system has returned to zero, thus preserving the detector resolution by insuring that one pulse is not riding on the overshoot of a previous pulse.

(4) A pulse-shape discriminator is available which allows the rejection of pulses which do not have rise times or decay times falling within a certain tolerance of a selected "standard pulse shape." This feature allows the rejection of pile-up pulses (one pulse riding on the tail of another) and pulses collected in a bad region of the detector where because of impurities or poor electric field shape the charge is not collected very rapidly which in turn produces a long rise time. This system has been previously described in Ref. 41.

1. The Ramper Method for Energy Determination.

A method for measuring energies to an accuracy of $\lesssim 0.1$ keV has been developed by M. G. Strauss et al. at Argonne National Laboratory.[42] The method is based on the use of a highly linear ramp generator and two standard gamma-ray lines whose energies are well known.

Figure 9 summarizes the use of the system and gives some results obtained from this method. The ramp generator produces a voltage which increases with time in a very linear fashion (linear to 1 part in 10 000). This voltage is then chopped into pulses which are similar to those from a Ge(Li) detector and fed into the preamplifier at the point where detector pulses would enter the system. The detector is removed and replaced with an equivalent capacitance during the

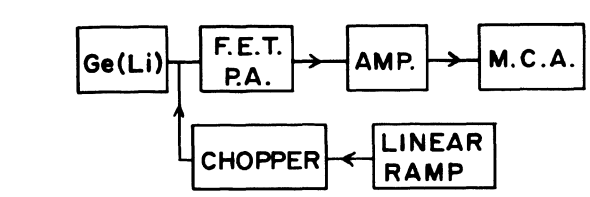

SOURCE	PUBLISHED ENERGY (keV)	THIS WORK ENERGY(keV)
Hg^{203}	279.191 ± 0.008	279.199
MoC^{2}	511.006 ± 0.002	511.000
Cs^{137}	661.635 ± 0.076	661.633
Y^{88}	897.98 ± 0.18	897.983
Na^{22}	1274.54 ± 0.05	1274.551

$$E_s = E_{C1} + \frac{\left(\sum_{C1}^{S} R\right)\left(E_{C2} - E_{C1}\right)}{\sum_{C1}^{C2} R}$$

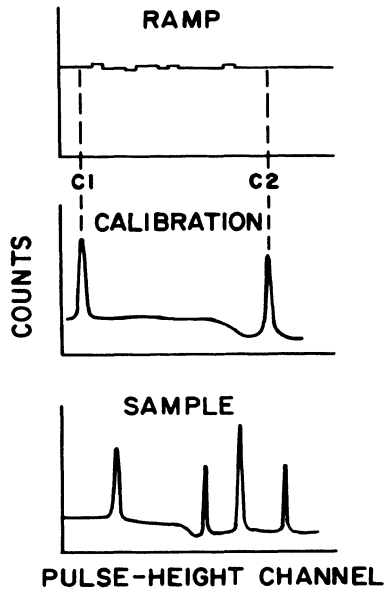

Fig. 9. The ramper method of energy determination in gamma-ray studies. The table represents a comparison of the adopted (published) energies of several well-known γ-ray transitions to those values obtained using the ramper method.

application of ramp pulses to prevent stray pulses from the detector from entering the system during the ramping procedure. If the system were perfectly linear, a horizontal line would be the result of storing the ramper pulses in a multichannel analyzer. Nonlinearities show up as bumps and valleys on the horizontal line. The differential linearity of the entire electronic system from preamplifier to analyzer (excepting the detector itself) is thus measured.

Energies are measured by replacing the detector while leaving all other system settings constant. Two calibration gamma rays whose energies are well known are then addressed to the analyzing system. The energies in the sample run can then be found by using the formula

$$E_S = E_{C1} + \frac{\left(\sum_{C1}^{S} R\right)\left(E_{C2} - E_{C1}\right)}{\sum_{C1}^{C2} R}, \qquad (A1)$$

where E_S in the energy of the sample gamma ray, E_{C1} is the lower calibration energy, E_{C2} is the upper calibration energy, C1 and C2 are the centroids of the lower and upper calibration peaks, respectively, S is the centroid of the sample peak, and R is the spectrum of the ramper, i.e., number of counts in each channel of the ramper spectrum.

Figure 9 also contains a table of adopted values for certain well-known gamma rays and the energies determined by this method. In all cases the determined energy is well within the errors quoted for the adopted values indicating that the maximum possible error is 0.18 keV and the error is probably less than 20 eV. Even under less favorable experimental conditions the errors observed are less than 0.1 keV for single well-isolated peaks.

2. Dead-Time Correction.

The author has been directly involved in the development of a system for the measurement of dead times in the total analyzing system. The necessity of measuring the dead time in the total system (as opposed to only analyzer dead time) was necessitated by the need to know the absolute cross section in the Coulomb excitation experiments described in Sec. VII. However, a knowledge of the dead time is involved in any spectroscopic measurement of an absolute quantity, e.g., detector efficiency. Further, the introduction of an artificial dead time into the analog circuitry to preserve resolution (see Sec. VA) can create an additional dead time which is not negligible compared to the analyzer dead time and thus must be known or measured.

The problem of measuring the system dead time is even more difficult at an ion-beam accelerator where large fluctuations in beam current and thus large fluctuations in the counting rate are encountered. The observed counting rate in a system with an average dead time per pulse (ρ) is

$$n = Ne^{-N\rho}, \qquad (A2)$$

where n is the number of events observed per unit time and N is the counting rate.[43] Thus even to lowest order in ρ (assuming $\rho \ll N$), the losses (N-n), i.e., those counts which are detected but not registered in the analyzer, are proportional to N^2. This creates no particular problem for a constant source rate since the fractional loss remains constant and the measurement of the average dead time is sufficient for spectrum correction; however, at an ion beam accelerator the current may vary over 1 or 2 orders of magnitude creating wild fluctuations in dead time for any given period of spectrum collection time.

This means that a "constant clock" type of dead time measurement such as a dead-time meter on an analyzer is a wholly inadequate indication of the true dead time. In order to make this more clear,

let us consider the following example. Consider a step function counting rate which produces a dead time of 90% in an analyzer lasting for 1 time unit and 0% dead time for 3 time units. It is obvious that virtually all the spectrum was collected in the first time interval (90% dead); however, the dead time given by a clock timer would register the fraction of time dead as 9/40 or 44%. Any measurement employing a correction based on this number would lead to a quantity incorrect by 50%! Similar situations occur during a run on an ion-beam accelerator.

The measurement of the dead time associated with an analyzing system is based on the injection of pulses into the preamplifier at the point where detector pulses also enter. These "sampling" pulses are injected at a rate which is proportional to the activity in which one is interested, the only requirement being that the sampling rate must be large compared to the rate of fluctuation of the activity but not so large as to produce appreciable dead time of itself.

We then have the following relationships. The number of events accepted (N_A) in a given time is proportional to the number of events detected at the input of the preamplifier (N_D).

$$N_A = f(s)\, N_D, \tag{A3}$$

where f(s) is the constant of proportionality indicating that this constant is dependent upon the spectral shape. Since events enter the system in a random nature, each event has an equal probability of being rejected because the analyzer is busy with a previous pulse. This means that Eq. (A3) holds for each pulse height and in particular

$$g = f(s)\, G, \tag{A4}$$

where g is the number of pulser pulses accepted by the analyzer and G is the number generated and introduced to the preamplifier. We also have that

$$G = \frac{1}{K}\, N_D, \tag{A5}$$

where K is a constant of proportionality. By dividing Eq. (A3) by (A4), we have

$$\frac{N_A}{g} = \frac{N_D}{G} = \frac{KG}{G} = K \tag{A6}$$

or

$$N_D = \frac{G}{g} N_A . \tag{A7}$$

Since

$$\begin{aligned} N_D &= D_\gamma + G \\ N_A &= A_\gamma + g , \end{aligned} \tag{A8}$$

where D_γ is the number of γ rays detected and A_γ is the number of γ rays accepted we have

$$\frac{N_A}{g} = \frac{KG}{G} = K$$

$$\frac{A_\gamma + g}{g} = \frac{D_\gamma + G}{G} \tag{A9}$$

$$\frac{A_\gamma}{g} + 1 = \frac{D_\gamma}{G} + 1$$

$$\frac{A_\gamma}{g} = \frac{D_\gamma}{G} = \frac{K(N_D - G)}{N_D} = K - 1 \tag{A10}$$

$$D_\gamma = \frac{G}{g} A_\gamma . \tag{A11}$$

Equation (A10) indicates how the method can be checked. For a given source the ratio of the number of γ rays accepted to the number of pulses accepted should be a constant. Equation (A11) indicates how the number of events recorded is related to the number of events actually detected where G/g is the ratio of the total experimental time to live time.

An assumption which is implicit in Eq. (A5) is that there are no losses associated with the device which is generating the pulser pulses. If there are losses associated with this device, then the rate at which pulses are generated (G') will not be directly proportional to the source rate but will be

$$G' = \frac{1}{K} N_D e^{-\rho N_D}, \tag{A12}$$

where ρ is the dead time per pulse. This reduces to (A5) provided $\rho << N_D$. Therefore, the equations above are valid only to the extent that G' = G.

In order to find an order of magnitude for an acceptable ρ in Eq. (A12), let us expand the fractional difference in G (G - G'/G) in terms of ρN_D

$$\begin{aligned} F &= \frac{G - G'}{G} = (1 - 1 + \rho N_D - \rho^2 N_D^2) \\ F &= (\rho N_D - \rho^2 N_D^2); \end{aligned} \tag{A13}$$

if an average value of N_D exists, then N_D can be written as

$$N_D = N_0 + \epsilon(t),$$

where ϵ is the difference between N_D and the average rate N_0. (A13) becomes

$$F = \rho(N_0 + \epsilon) - \rho^2 (N_0 + \epsilon)^2 . \tag{A14}$$

Assuming that ϵ oscillates about zero on the average, then the term

$$\rho^2 \epsilon^2$$

is the lowest-order term of the expansion which will cause a violation of Eqs. (A10) and (A11). Therefore, to the extent that the second term on the right in Eq. (A13) is small compared to the first, Eqs. (A10) and (A11) will be valid.

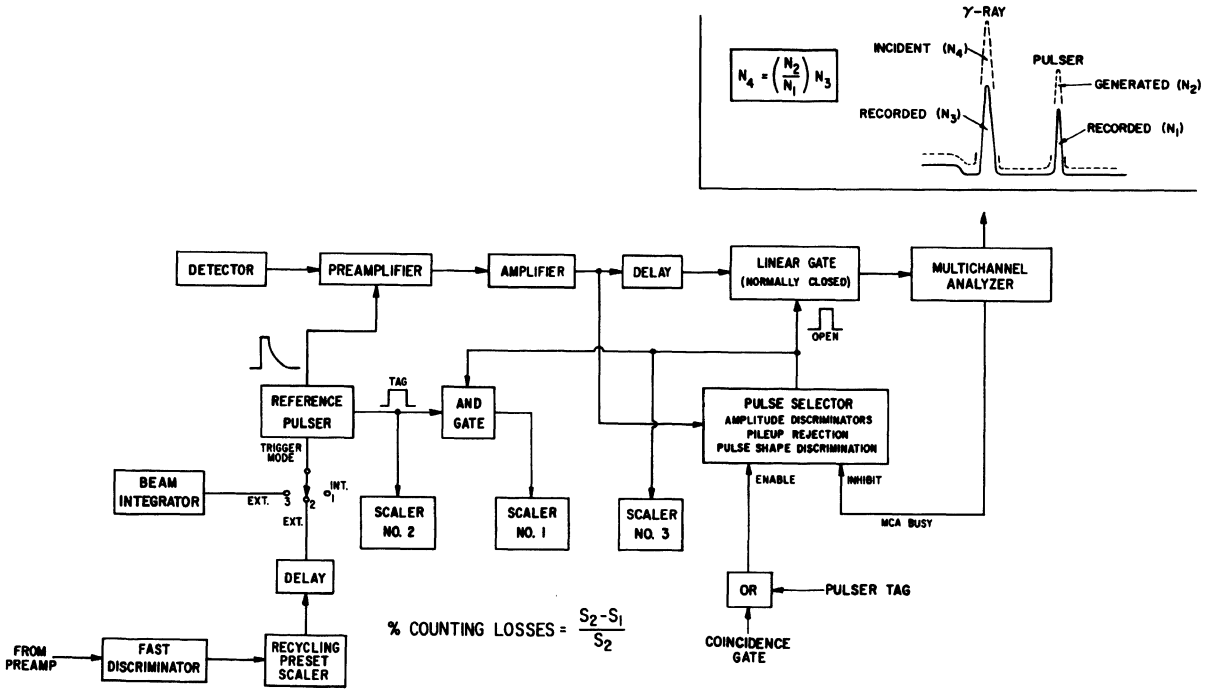

Fig. 10. A block diagram of the system used for the accurate measurement of the dead time associated with the entire analyzing system. The upper left-hand portion of the diagram represents how the actual number of γ-ray detected N_4 may be calculated from the number of γ rays analyzed and the number of pulser pulses analyzed and generated. The equation is exactly equivalent to Eq. (A11). The additional "and/or" circuitry allows the storage of the pulser pulses only during experimental running time and allows stabilization of the spectrum without pulser storage at other times.

Figure 10 shows a block diagram of the system. When performing Van de Graaff studies, the beam current integrator is used to generate injection pulses at a rate which is proportional to the source rate. Since there are no losses associated with the current integrator, Eq. (A11) holds exactly. The number of pulses generated is recorded directly on a scalar and the number accepted while being recorded on another scalar is also stored as a peak in the spectrum. It turns out that because of pile up and other effects, the number of events recorded on the accepted scalar is too high and the number accepted is more accurately obtained by integrating the number of counts in the pulser

peak appearing in the spectrum. We have great confidence in the method used for the Van de Graaff studies because of the agreement found between values for the absolute cross sections calculated by other authors and those we calculated. The values obtained when using this method always agreed with previous values to within the errors quoted by the other experimenters.

Figure 11 shows the results of studies performed using a fast tunnel diode to produce pulser pulses at a rate proportional to the source rate. These studies were performed using radioactive sources solely as a check on the method. The rates were kept low enough to insure that the second term in (A13) was small and therefore Eq. (A10) would be valid. The points marked "UB" represent data taken in an unbiased spectrum, i.e., pulse heights were observed down to the zero of the electronic system. The points marked B are for a spectrum biased so as to accept only the upper portion of the spectrum with the result that most of the dead time occurs in the analog circuitry. The dots represent spectra collected at a constant counting rate. "Low-level sampling" means that pulses just above noise level from the tunnel diode were used to generate the pulser pulses while "high-level sampling" implies that the tunnel diode pulses were biased off so as to insure that only pulses corresponding to large pulse height were used to generate pulser pulses. In the section marked varying source strength the source was run at the constant rates shown and then with the varying rate vs time indicated in the figure. For all cases from 90% losses to 10% losses the ratio of the number of γ-ray counts to pulser counts compared to the average of this ratio remained constant to within 0.5%. The error bars represent errors associated with counting statistics only.

Figure 12 shows a study of the decay of ^{24}Na. It is obvious that the ratio of gamma-ray counts to pulser counts would not remain a constant for a decaying source if the pulses were injected at a

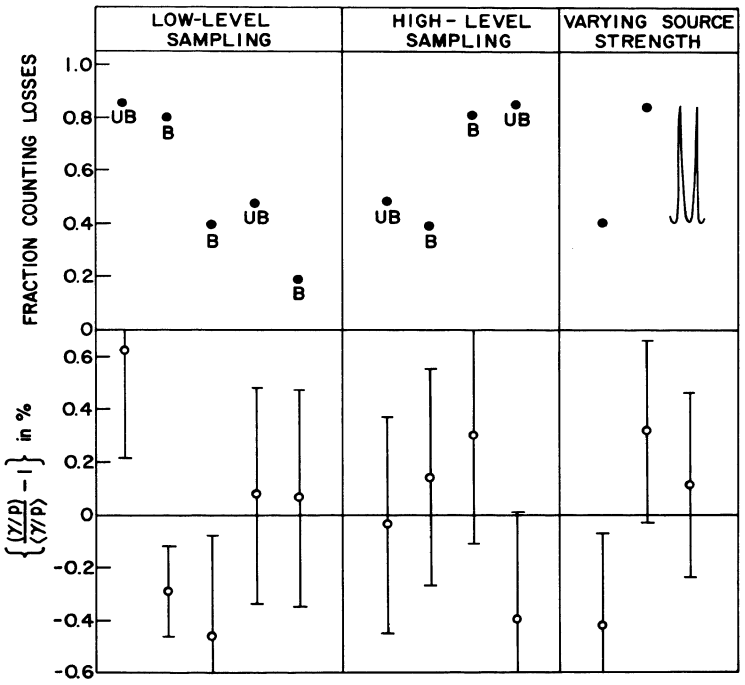

Fig. 11. Results of studies measuring the ratio of the number of γ rays in a ^{60}Co peak to the number of pulser pulses analyzed as compared to the average of this quantity for different source conditions. The points marked UB were unbiased spectra, i.e., the entire ^{60}Co spectrum was observed. The points marked B are for spectra, biased so as to observe only the energy region including the two ^{60}Co γ rays. During the "low-level sampling" runs, the entire ^{60}Co spectrum was used to generate pulser pulses and during the "high-level sampling" runs, only the upper portion of the ^{60}Co spectrum was used to generate pulser pulses. The right-hand portion of the figure shows the result of a run in which the source strength varied approximately as shown with constant source strength runs being taken at the minimum and maximum rate.

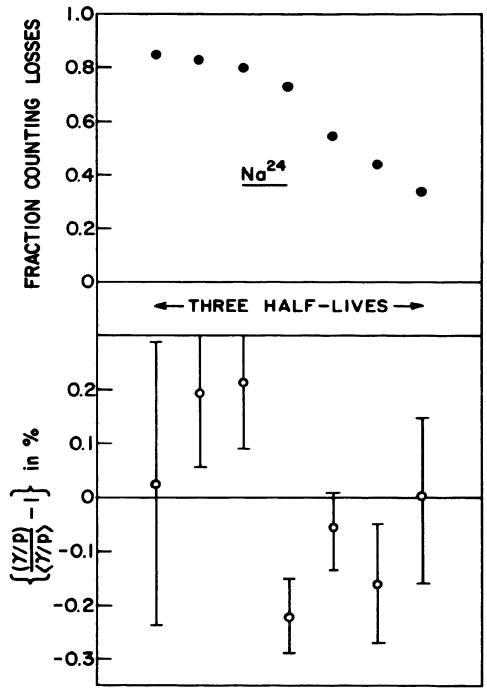

Fig. 12. The ratio of the number of γ-ray counts analyzed from a ^{24}Na source to the number of pulser pulses analyzed as compared to the average of this quantity. This ratio is not expected to be constant for a "constant clock" type dead time measurement; however, the ratio is constant here indicating that the method of dead time measurement is accurate to within one standard deviation for all runs and further, no systematic variation with counting rate is observed.

constant rate (which is equivalent to the dead time meter on an analyzer). However, this ratio does remain constant to within 0.2% for the method described here. These results are to be published in the near future.[44]

3. Spectral Analysis.

As a general rule, gamma-ray spectra are very complicated with multiple peaks appearing rather frequently in spite of the excellent resolution provided by Ge(Li) detectors. Even for single well-resolved lines there is a desire to remove as many of the personal prejudices involved in determining peak centroids and areas as is possible. The desire for some quantitative calculation of peak centroids and areas as well as the necessity of separating multiple peaks which are not fully resolved has led to use of computer programs to "fit" the peaks in a gamma-ray spectrum to a standard peak shape. The program used for the analysis of the data in this dissertation employs a variable metric minimization technique to find the Gaussian curve or curves which best fits the data.

The program takes the data between any two channels specified by the user and subtracts an underlying linear background. The background is assumed to be a straight line with intercept and slope being calculated from the number of counts in two channels supplied by the user. Usually a flat region on either side of a γ-ray peak is assumed to be representative of the underlying Compton (i.e., background) events, and a straight line passing through these points under the γ-ray peak is assumed to represent the part of the peak due to background. After the counts due to background are subtracted from the gross counts in each channel of interest, these net data are given to the variable metric minimization program developed by W. C. Davidon of the Applied Mathematics Division at Argonne.[45]

A Gaussian of the form $g(a, h, X_0, X) = h \exp [-a(X - X_0)^2]$ is used as the standard peak shape where a is proportional to the width of the peak, h is the peak height, X_0 the channel number of the centroid, and X the channel number where g counts are observed. The justification for the use of this peak shape will be indicated later. The three parameters a, h, and X_0 are treated as the coordinates of a 3-dimensional linear space. By simultaneously varying a, h, and X_0 in an iterative procedure designed to find the point, where the function $f(a, h, X_0, X) = Y(X) - g(a, h, X_0, X)$ has a minimum (where $Y(X)$ is the number of net counts at channel X), one is able to find the values of a, h, and X_0 for the Gaussian which supplies the best fit to the data. The minimum in the f function is found by requiring that the partial derivatives of f with respect to a, h, and X_0 are zero and the determinant

$$\begin{vmatrix} \frac{\partial^2 f}{\partial a \partial a} & \frac{\partial^2 f}{\partial a \partial h} & \frac{\partial^2 f}{\partial a \partial X_0} \\ \frac{\partial^2 f}{\partial h \partial a} & \frac{\partial^2 f}{\partial h \partial h} & \frac{\partial^2 f}{\partial h \partial X_0} \\ \frac{\partial^2 f}{\partial X_0 \partial a} & \frac{\partial^2 f}{\partial X_0 \partial h} & \frac{\partial^2 f}{\partial X_0 \partial X_0} \end{vmatrix}$$

be positive definite. When this point is found, within certain tolerances provided to the program, the values of a, h, and X_0 are returned to the user along with the value of χ^2 which is a measure of the "goodness of fit." If more than one Gaussian is to be fitted into one region, the number of parameters is increased to nX(3), where n is the number of Gaussian curves to be fitted with 3 parameters per Gaussian. The same program is used for fitting n Gaussian peaks except that the number of dimensions for the minimization process described above is increased to 3n.

Since there are three parameters for each Gaussian, the minimum number of points which can be used for a meaningful fit is 3n + 1. Any number of points over 3n can be used. The number of degrees of freedom is defined as N-3n, where N is the number of data points used in the fitting region. The value of χ^2 per degree of freedom expected for a fit to a set of data points distributed statistically about a Gaussian curve is 1.0.[45] Typical values for fits obtained for isolated well-resolved peaks in the data shown in the following sections are from 0 to 4. However, these fits are considered "good" even for a χ^2 per degree of freedom equal to 4 for the following reasons:

(1) Various fits were made to isolated peaks using only points on the peaks which were above 50% of the peak height and the parameters obtained were compared to fits made while using points above 10% of the peak height and also to fits made which used the entire peak. It was found that the centroid differed by less than 0.1 channel for all fits; however, the area was strongly dependent on the cutoff height and χ^2 increased as the cutoff was lowered.

(2) The peak area was found to agree well (within 10%) with a straight sum of the number of counts per channel over the peak (with background subtracted) as long as the cutoff was below 20% of the pulse height and agreement usually to within 5% resulted for a cutoff of about 10% of the peak height. However, χ^2 was slightly worse for the 10% cutoff.

(3) The peaks from a Ge(Li) detector are known to produce a tailing effect, especially on the low-energy side of the peak. Therefore, it was decided to accept a slightly worse χ^2 value in order that the area obtained in the fitting program would be equal to the value obtained by straight summing of the counts in a peak.

Experience has shown that the centroids can be found to within 0.1 channel for well-isolated peaks and the error associated with the peak area is about 5%.

B. Coincidence Gamma-Ray Techniques

The interpretation of gamma-ray spectra in terms of transitions between the energy levels of a nucleus is often complicated by the fact that several γ rays have appropriate energies to qualify as transitions between more than two levels. This leads to an ambiguity in selecting the correct level scheme. This is especially true in (n,γ) studies where there are usually more than 200 observed γ rays having an energy less than 2 MeV. Obviously if one had some information about which γ rays are proceeding to a given level and which γ rays result from the decay of the same level, many of the ambiguities could be removed and a unique level scheme could be determined.

Coincidence studies provide just such information. Most low-lying bound energy levels of a nucleus decay by γ-ray emission within nanoseconds (10^{-9} sec) to fentoseconds (10^{-15} sec) after the level is produced. Therefore, by observing the gamma-ray transitions which follow or proceed a given γ-ray transition by several nanoseconds one sees all the observable gamma rays which populate and depopulate an energy level. All γ rays which are separated in time by less than several nanoseconds from a given gamma ray are said to be in coincidence with that gamma ray.

The coincidence studies performed on the nuclei described in Secs. VI and VIII of this dissertation were done using a two-parameter system capable of recording coincidence events resulting between two 1024 channel spectra. Let us call these spectra X and Y. When a coincidence between an event in spectrum X and an event in spectrum Y occurs, the channel numbers of the two events are recorded on magnetic tape. The tape can later be scanned at an associated read-search station so that all the events from spectrum Y which are in coincidence with a given range of channels in spectrum X may be recorded separately. This allows coincidence data for a wide energy

region to be recorded simultaneously while coincidences with specific γ-ray peaks can be studied later.

The basis for the fast timing unit is a time-to-pulse-height converter (TPC).[46] Output pulses from each of the two detector preamplifiers are addressed to individual tunnel diode circuits which produce an output of uniform size for each preamplifier pulse. Leading edge timing is utilized meaning that the output pulse results as soon as the preamplifier signal rises to a given threshold value which, for most applications, is just above the height produced by noise in the circuitry. The output from one tunnel diode is applied to the "ready" input of the TPC and the output from the other tunnel diode is applied to the "start" input of the TPC after being delayed on the order of 50 nanoseconds.

The TPC measures the time (Δt) between the pulses which are obtained from the two detectors by charging a capacitor for a time which is proportional to Δt and producing a voltage pulse which has a height proportional to Δt and duration long enough to allow storage in a multichannel analyzer (these storage times are typically in the μsec range). Figure 13 is a representation of the output voltage (v_1)

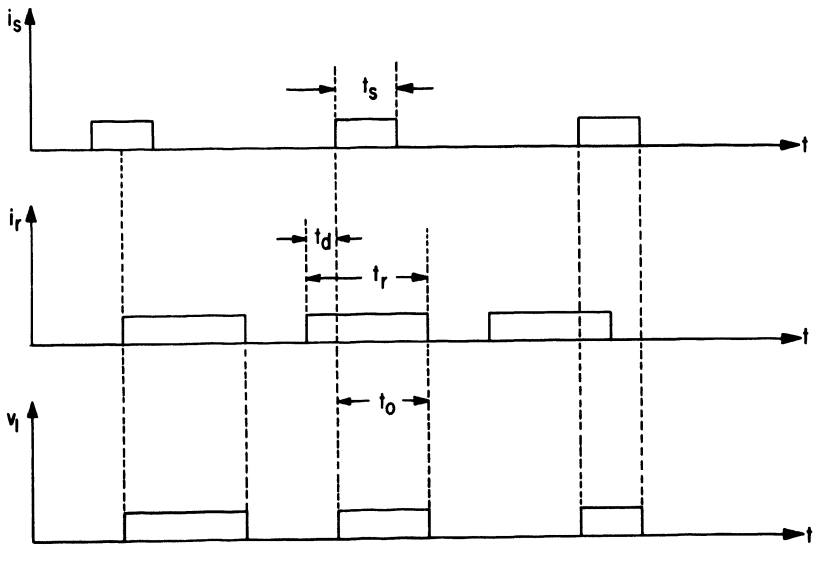

Fig. 13. Wave forms in the ready-start mode of operation of the time-to-pulse height converter. The left- and right-hand portions of the figure indicate how the maximum and minimum output pulse height is produced where i_s is the start pulse, i_r is the ready pulse and the time duration of v_1 is proportional to the output pulse height. The middle portion of the figure represents the sequence of events in which the start pulse for a prompt event is delayed with respect to the ready pulse.

produced when the pulses from the two detectors are in coincidence. As stated above, the output of a tunnel diode corresponding to one of the detectors is connected to the "ready" input of the TPC. This input produces a square wave voltage pulse lasting for a constant time (t_r) which is determined by an external shorted clipping line. In our application the ready pulse lasted for 200 nsec. This pulse is represented by i_r in Fig. 13. The output of the other tunnel diode is connected to the "start" input which produces a square wave pulse (i_s) lasting for a very short time (t_s) ($t_s \leq 1$ nsec). The capacitor begins to charge when these two pulses overlap in time and the charging process is terminated by the end of the ready pulse. The output voltage from the capacitor is then proportional to the time difference between the arrival of the start pulse and the end of the ready pulse. From the left-hand portion of the figure it can be seen that two pulses which are in coincidence will always give the maximum output proportional to t_r as shown on the left in the figure. In order to get a distribution of output pulses, the start pulse is delayed of the order of 50 nsec so that the ready pulse of a coincidence event always arrives before the start pulse and the output pulse is proportional to t_0 as shown in the central portion of the figure.

If there were no uncertainties involved in the time measurement, the spectrum resulting from this device would be a delta function peak in the channel representing t_o say channel C. In fact the time resolution is determined by the charge collection time of the detector and FET so that the resulting time distribution has a centroid equal to C and a full width at half maximum equal to τ as shown in Fig. 14, where τ is the time resolution of the detector FET system. The flat distribution under the peak is due to events which are not in "prompt" coincidence but represent events occurring randomly in time, i.e., an event was detected in each detector within the ready time just by accident, arising from the decay of two different nuclei.

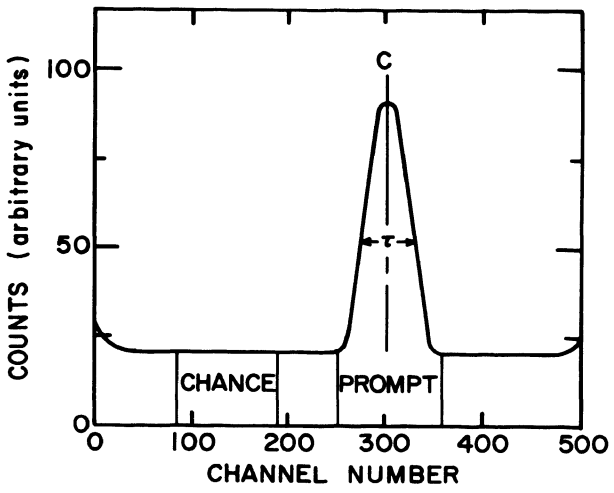

Fig. 14. A representative pulse-height spectrum produced by the TPC. The prompt and chance distributions may be observed independently with the use of separate discriminator windows.

The nonlinearities observed at the beginning and end of the time spectrum are due to events which are represented on the right- and left-hand portions of Fig. 13.

Let us now consider the coincidence rates which are expected in an experiment involving a nucleus with a constant decay rate equal to R. Consider a coincidence event between two gamma rays a and b, where a and b represent the gamma ray as well as its intensity

$$a = \frac{\text{number of times a is observed/unit time}}{R} \qquad \text{(B1)}$$

and a similar equation holds for b. If the detection efficiency (including any geometrical factor) of the two detectors are represented by ϵ (a) and ϵ(b), then the rate at which gamma ray a is observed in detector 1 is

$$R_a = \epsilon\,(a)\; a\, R \qquad \text{(B2)}$$

and similarly for b observed in detector 2.

$$R_b = \epsilon\,(b)\; b\, R\,; \qquad \text{(B3)}$$

the number of true coincidences observed per unit time is given by

$$R_{ab} = \epsilon_a \epsilon_b\; a\; b\; R\,.$$

(Note that a and b must result from the same nucleus in order to be in prompt coincidence; hence the factor is R, not R^2.) The number of chance events will be

$$N_c = \frac{(\text{time TPC can accept pulses}) \times (\text{no. of ready events})}{\text{total experimental time}}$$

$$N_c = \frac{2\tau \times (R_a\ T)}{T} \times (R_b\ T)\ , \tag{B4}$$

where R_a and R_b may be interchanged. We then have a chance rate equal to

$$R_c = 2\tau\ R_a\ R_b$$

$$R_c = 2\tau\ \epsilon\,(a)\ \epsilon\,(b)\ a\ b\ R^2\ . \tag{B5}$$

The ratio of true to chance events is then

$$F = \frac{R_{ab}}{R_c} = \frac{1}{2\tau R} \tag{B6}$$

which is independent of ϵ and the fractional occurrence of γ rays a and b.[47]

It can be seen that in order to have a high true to chance ratio one must reduce τ as much as possible. Once this is done, the maximum rate for a desired true to chance ratio is fixed by Eq. (B6). The true to chance ratio in the studies of Secs. VI and VIII was typically ≈ 10 with a resolving time of ≈ 60 nsec.

Figure 15 shows a block diagram of the two-parameter coincidence system. An additional feature of the system not mentioned before is the ability to distinguish between events occurring in the prompt time distribution and events recorded in a chance distribution of equal width (see Fig. 14) by the use of an appropriate tag bit which is recorded on the magnetic tape. In this way the number of chance events may be considered in the final analysis of the data.

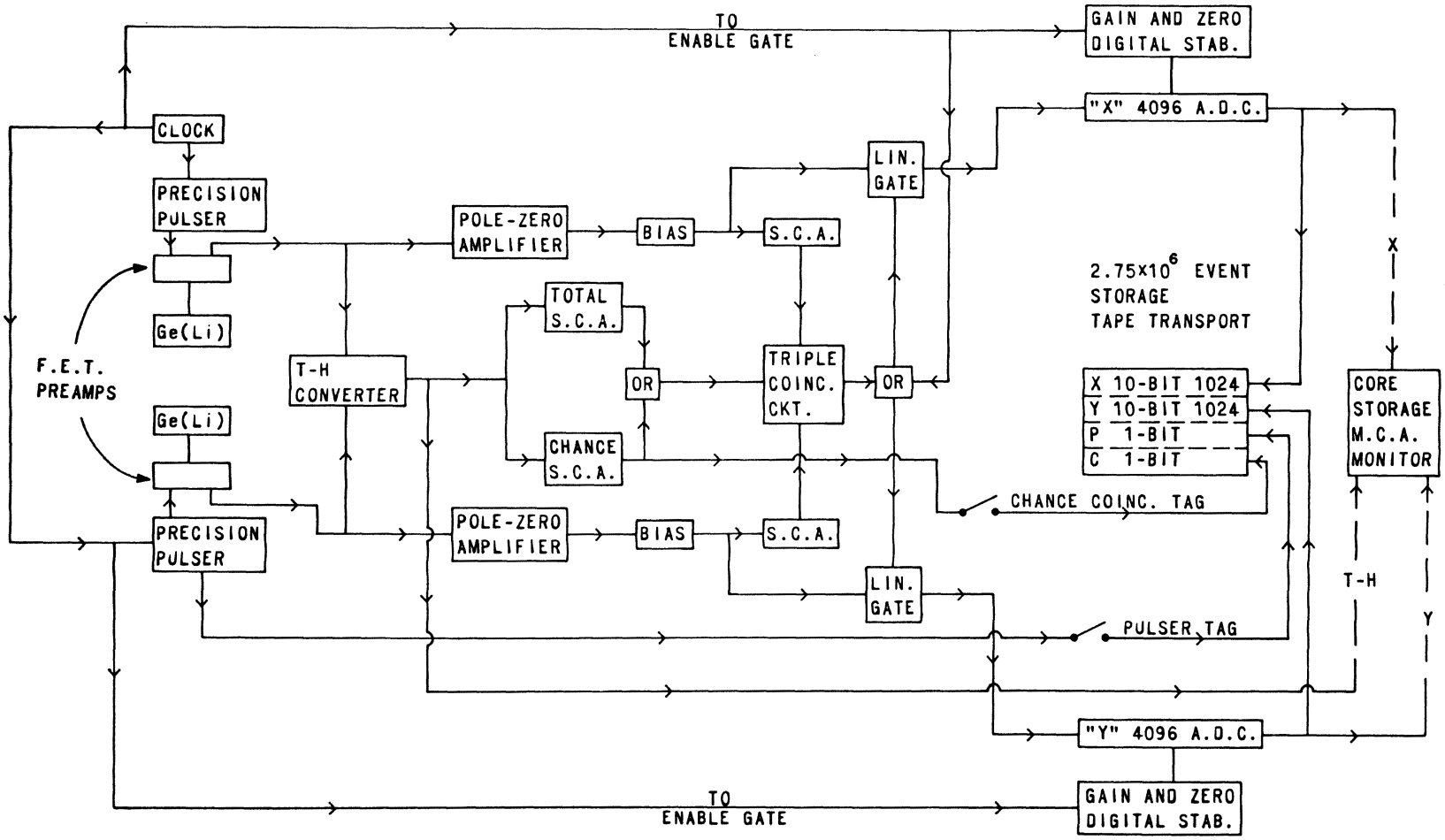

Fig. 15. A block diagram of the two-parameter coincidence system.

It should be noted that the experimenter also has the ability to stabilize the two 1024 channel spectra. This feature is desirable due to the fact that coincidence studies may be of several days duration and line broadening due to gain and zero shifts in the electronic system must be avoided during this time in order to preserve the high resolution of the Ge(Li) detector. Stabilization is based on the use of two highly stable dual pulsers which introduce pulses into each arm of the coincidence system. A tag is provided by the pulsers each time a pulser pulse is injected into the system and this tag is used either to prevent storage of these pulses or to produce an identifying bit which is recorded on tape along with the pulser events.

VI. LEVEL STRUCTURE OF LOW-LYING EXCITED STATES OF ^{66}Ga POPULATED BY THE DECAY OF 2.2-h ^{66}Ge

A. Introduction

The low-lying states of odd-odd $^{66}_{31}Ga_{35}$ have been the subject of only a few previously reported experimental investigations. Although the levels of this nuclide are accessible by means of some particular charged-particle reactions, no reports of studies of this type have appeared in the literature. All prior investigations[48—50] of these states have been based upon their population by the β decay of 2.2-h ^{66}Ge. Since the ground state of ^{66}Ga is itself unstable to β decay[51] ($t_{1/2}$ = 9.5 h) to ^{66}Zn, the γ-ray complexities of the combined parent and daughter activities make the investigation of the ^{66}Ge decay difficult. Therefore, it is not surprising that these complications have deterred many earlier investigations.

The ^{66}Ga nuclide contains three protons outside the closed $f_{7/2}$ shell and presumably the configurations of the ground state and low-lying excited states would be dominated by the odd proton in the $2p_{3/2}$ orbital, although the $2p_{1/2}$ and $2f_{5/2}$ proton orbital might also be expected to play non-negligible roles. The valence neutrons are also expected to occupy similar orbitals. Thus, the low-lying excited states of ^{66}Ga may be expected to be characterized by positive parity. Since the ground-state spin and parity of ^{66}Ga is known[52] to be 0^+, all transitions from higher levels to ground are of pure multipolarity. The spin of the parent ^{66}Ge is also 0^+, and allowed β decay to excited states of ^{66}Ga is expected to populate levels whose spin and parity are at most 1^+. These facets of the decay characteristics and of the expected shell-model configurations of the low-lying states combine to lead to the expectation of low-spin excited states and relatively simply defined multipole character for many of the γ-ray transitions.

In addition, β transitions to 0^+ states in ^{66}Ga are forbidden by isobaric-spin selection rules, and such Fermi-type transitions would proceed by way of isobaric spin impurities present in the wave function of the 0^+ parent level of ^{66}Ge. Thus, identification of 0^+ levels in ^{66}Ga together with experimental stipulation of the β branching (if any) to these states can provide illuminating estimates of the amount of isobaric spin impurities present.

Previous studies[48,49] have shown the γ-ray spectrum to be very complex, with many closely spaced transitions. The earlier work[48,49] utilized NaI(Tl) detectors and, despite the numerous detailed γ-γ coincidence studies, the resulting level scheme for ^{66}Ga appeared to contain several important inconsistencies and ambiguities which demanded clarification.

The present work describes an investigation of the levels in ^{66}Ga populated in the β decay of ^{66}Ge. High-resolution Ge(Li) detectors were used exclusively, both for γ-ray singles spectra and for coincidence spectra. The purpose of this investigation was to determine a clear, self-consistent, and unambiguous level scheme. In addition, since the expected shell-model configurations of the levels in this nuclide may lead to the occurrence of forbidden M1 transitions, this investigation included efforts to determine the lifetime of states that could signify the presence of such retarded transitions.

B. Sample Preparation and Half-Life of the Parent Activity

The 2.2-h ^{66}Ge activity was produced by means of the ^{64}Zn(α,2n)^{66}Ge reaction at the Argonne 60-in. cyclotron. A natural Zn target was employed. In order to maximize the ratio of the (α,2n) reaction cross section to that of competing reactions, the target thickness was selected such that the α-particle energy decreased only

from 36 to 28 MeV in traversing it. As a result of the use of the natural target and the necessarily incomplete discrimination against these other reactions, some vestiges of short-lived ^{65}Ge (1.5 min) and ^{67}Ge (19 min) were present. To permit these contaminating activities to decay to negligible proportions, three hours were allowed to elapse from the termination of the α-particle bombardment to the initiation of the chemical separation. Traces of long-lived ^{69}Ge (40 h) were also unavoidably produced, but the γ rays from this activity were readily identified.

The desired ^{66}Ge activity was chemically separated from both the target material and the sizable Ga daughter activities of the short-lived Ge parents produced in the bombardment. In this separation by benzene solvent extraction, the target was first dissolved in concentrated HCl and thoroughly mixed with the benzene solvent. The Zn and Ga fractions were selectively retained in the acid and were removed by repeated scrubbings with concentrated HCl. The aqueous layer was finally removed by titration, centrifuging, and vigorously bubbling with air. The Ge activity was finally back-extracted with a few drops of 0.1 N HF. The desired fraction of the ^{66}Ge yield was placed in small plastic vials for counting.

Because of the build-up of the 9.5-h ^{66}Ga daughter activity, all samples of ^{66}Ge activity were only used for ~1.5 half-lives of the parent. Repeated bombardments and chemical separations were therefore required for those investigations lasting longer than ~3.5 h except as noted in the next paragraph.

The half-life of the ^{66}Ge activity was determined with a single sample in a study of ~12 h duration. The γ-ray spectrum was periodically recorded with a Ge(Li) detector, and the decay characteristics of several of the stronger transitions known to be associated with ^{66}Ge were analyzed together to obtain the half-life. (The dead-time of the system varied considerably over the duration of this study

because of the decay of the activity and the presence of the 9-h ^{66}Ga daughter. This deadtime was carefully determined and corrections for it were applied.) The resulting half-life $T_{1/2} = 2.23 \pm 0.10$ h disagrees with the value 2.4 ± 0.2 h reported previously.[2] Each individual γ ray assigned to ^{66}Ge also displayed a half-life consistent with this value. A few of the observed transitions were due to the much longer lived Ge activities and the ^{66}Ga daughter but were easily identified.

C. Gamma-Ray Energies and Relative Intensities

The singles γ-ray spectrum (Fig. 16) was obtained with the aid of the 30-cm^3 Ge(Li) detector (see Sec. VA). The energies and relative intensities of the γ rays observed in the ^{66}Ge → ^{66}Ga decay are listed in Table I. All transitions appear to be fully resolved. Of special interest is the clear separation of the 182- and 190-keV gamma rays previously accepted as a single 185-keV transition in earlier NaI(Tl) studies of this spectrum. In addition, several previously unreported transitions were observed.

The γ-ray energies were determined by comparison with the positions of the γ-ray transitions at 121.970 ± 0.030 keV in ^{57}Co and at 1332.483 ± 0.046 keV in ^{60}Co, both of which are known[53,54] to high accuracy. The comparison was made with the aid of the extremely linear ramp generator and a chopper which was discussed in Sec. VA1. This method yielded the energies of the transitions in the ^{66}Ge → ^{66}Ga spectrum to the accuracies quoted in Table I. The self-consistencies of the γ-ray energies determined are given in Table II. This table lists the various sums or differences of cascade and crossover transitions whose placements are defined in the final proposed level scheme presented in Sec. E. Many of these sums and differences involve rather weak transitions. Nevertheless, as is

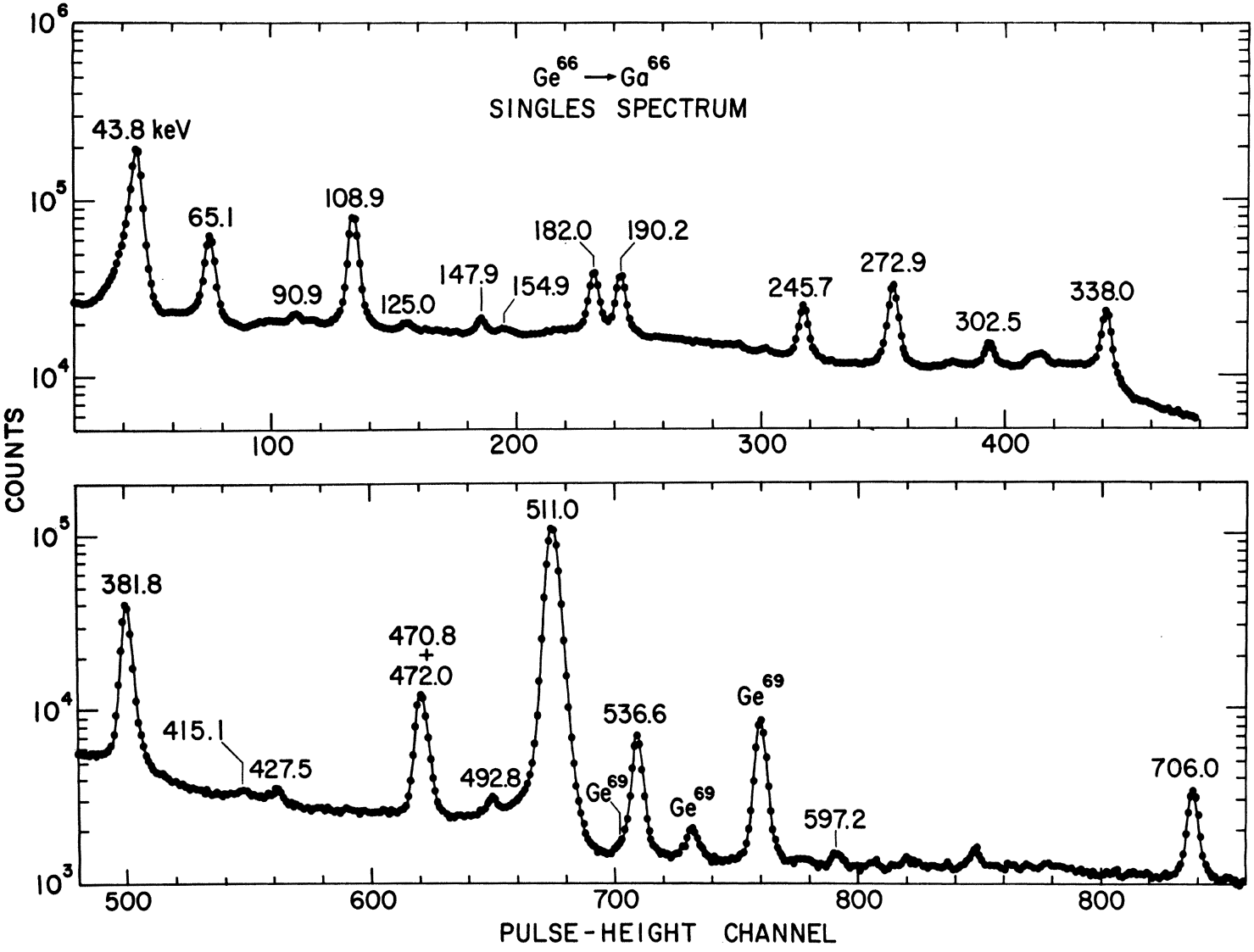

Fig. 16. Singles spectrum of γ rays following the decay of ^{66}Ge. All energies are in keV. The γ rays from the ^{69}Ge impurity are labeled.

TABLE I. Transitions in ^{66}Ga.

Gamma-ray energy (keV)	Relative gamma-ray intensity[a]	Initial state (keV)		Final state (keV)
43.83 ± 0.05	76.4	43.8	→	0
65.10 ± 0.05	21.8	108.9	→	43.8
90.90 ± 0.10	1.5	381.8	→	290.9
108.93 ± 0.05	45.1	108.9	→	0
125.05 ± 0.10	1.4	234.0	→	108.9
147.87 ± 0.08	3.3	381.8	→	234.0
154.85 ± 0.10	1.9	536.6	→	381.8
181.96 ± 0.05	25.7	290.9	→	108.9
190.17 ± 0.05	26.2	234.0	→	43.8
245.75 ± 0.05	21.0	536.6	→	290.9
272.90 ± 0.05	41.1	381.8	→	108.9
290.99 ± 0.10	1.1	290.9	→	0
302.51 ± 0.07	8.4	536.6	→	234.0
338.01 ± 0.05	34.0	381.8	→	43.8
381.85 ± 0.05	100	381.8	→	0
415.13 ± 0.10	1.8	706.0	→	290.9
427.51 ± 0.10	1.0	536.6	→	108.9
470.76 ± 0.07	31[b]	514.6	→	43.8
472.0 ± 0.25[c]	5[b]	706.0	→	234.0
492.76 ± 0.10	1.5	536.6	→	43.8
536.58 ± 0.05	20.8	536.6	→	0
597.16 ± 0.15	1.2	706.0	→	108.9
706.04 ± 0.07	13.4	706.0	→	0

[a] The intensities of the gamma rays are relative to that of the 381.85-keV γ ray taken as 100. The errors in the relative γ-ray intensities are 5—8% of the listed value for intensities >10, 10—20% for weaker transitions.

[b] After chance and underlying Compton coincidences were subtracted, a knowledge of the placement of all pertinent transitions in the level scheme allowed the relative intensities of the 147.9- and 302.5-keV gamma rays in the singles spectrum to be compared with that obtained for these γ rays and that of the resolved 472.0-keV gamma ray in coincidence with the 190.2-keV transition. From this one obtains the relative intensity of the 472.0-keV transition. This intensity was determined to be 5 ± 1 relative to that of the 381.8-keV gamma ray. Further, the combined γ-ray intensity of the two unresolved 470.8- and 472.0-keV transitions in the singles spectrum is 36 relative to the 381.85-keV transition (taken as 100). From a very careful peak fit of the "470-keV" γ-ray peak in the singles spectrum, ~15% of the unresolved doublet strength can be attributed to the 472.0-keV transition, in good agreement with the relative intensity presented in this table as obtained from the coincidence study.

[c] The listed γ-ray energy and its estimated error have been obtained from the observed shift in peak position relative to the much stronger 470.76-keV transition in the coincidence spectra. However, the mandatory placement of this transition dictated by the coincidence results imposes a smaller uncertainty on the listed energy of this γ ray when coupled with the listed errors in the energies of the 706.04-, 190.17-, and 43.83-keV transitions.

evident in Table II, those cascade and crossover energies that involve only the stronger transitions defining the energies of the various excited states in ^{66}Ga show a maximum energy spread of $\leq$0.06 keV, while the maximum energy spread is $\leq$0.13 keV for those sums involving weak transitions, and is $\leq$0.2 keV for those involving even the very weakest γ-ray transitions.

The relative γ-ray intensities listed in Table II were obtained with the aid of well-calibrated γ-ray intensity standards run at the same source-to-detector distance. They served to define the peak detection efficiency of the detector as a function of γ-ray energy. The deadtime losses in the counting system were carefully determined in

TABLE II. Comparison indicating the degree of consistency between the values obtained by independent computations of the excitation energy.

Excitation energy (keV)	Cascade energy sum (keV)	Crossover energy (keV)	Maximum energy spread (keV) of cascade sum	Average deviation (keV) of cascade sum[a]
43.8	43.83	43.83	0.02	0.01
	43.84			
	43.82			
108.9	108.93	108.93	0.02	0.04
	108.95		0.10*	
	108.97*			
	109.03*			
	108.95*			
234.0	234.06	234.00	0.06	
	233.98*		0.08*	0.03
	233.98*			
290.9	290.83	290.89	0.06	0.07
	290.95*		0.12*	
	290.99**		0.16**	
381.8	381.83	381.85	0.02	0.05
	381.83		0.12**	
	381.73**			
536.6	536.64	536.58	0.06	0.08
	536.64		0.13*	
	536.51*		0.20**	
	536.70**			
	536.44**			
	536.59**			

[a]The values listed in this column are obtained by taking the energy of the crossover transition as the standard.

*Includes weak transitions.

**Includes weakest transitions.

each intensity calibration and suitable corrections were made; otherwise the determinations of the detection efficiencies at the peaks would have been spuriously low.

D. γ-γ Coincidence Studies and Measurement of Excited-State Lifetimes

1. γ-γ Coincidence Studies.

Gamma-gamma coincidence spectra were obtained with the 1024×1024-channel two-parameter γ-ray spectrometer which was

discussed in Sec. VB. Ge(Li) detectors were employed in each arm of the coincidence system. An $\sim$4-cm^3 planar drifted Ge(Li) detector and the $\sim$30-cm^3 closed end coaxial Ge(Li) detector were used in the coincidence studies. Availability, not experimental criteria, dictated the choice of these detectors. [The coincidence counting time would have been materially reduced had both Ge(Li) detectors been of the larger volume.] Both 1024 channel spectra were stabilized using the two highly-stable dual pulsers discussed in Sec. VB. The two pulsers were master-slave driven and the tag produced by the pulsers at the time of the output pulses was used to simulate a coincidence in the 2-parameter system. Pulses were injected at a rate of 10 pulses/sec. Thus, even in the coincidence mode of operation, each ADC received a sufficient number of stabilization pulses to assure proper zero and gain correction and yet the pulser repetition rate was small enough that it contributed only negligible deadtime to the system so that the ADC's were virtually always free to process and record actual γ-ray coincidence events. The stabilization was necessitated by the lengthy coincidence running time required and by the replacement of new source material approximately every 3 h. These replacements produced large and abrupt counting-rate changes, which are conducive to shifts in gain and/or zero.

The tag pulse from the pulser was also utilized to gate the stabilizers so that the stabilization concerned itself only with the peaks produced by the precision pulser and was thus unaffected by the presence of γ-ray pulses. Consequently, excellent stabilization is achieved even when the pulser peaks are inadvertently superimposed on γ-ray peaks. In addition, the pulser tag was employed to reject storage of the pulser peaks. The success of the stabilization was attested by the absence of any observable line shifts during coincidence runs lasting 14 h.

The fast-slow coincidence circuitry used leading-edge triggering and employed a fast resolving time (90 nsec) with 100% coincidence efficiency over the entire pulse-height range accepted by both detectors. The rather long fast-coincidence resolving time was dictated by the requirement to attain 100% coincidence efficiency even for the lowest energy transitions (44 and 65 keV) present. The fast coincidence circuit consisted of the time-to-pulse-height converter[46] discussed in Sec. VB. Coincidences were recorded for all events satisfying the fast-slow requirements. Even for the 90-nsec fast-coincidence resolving time employed, the contributions from chance coincidences were negligible.

Figure 17 displays some coincidence spectra typical of those obtained. These particular ones were selected to show some particularly interesting coincidence relationships which were new and/or crucial to the establishment of an unambiguous level scheme. These three coincidence spectra were obtained by gating on specific γ-ray transitions in the direct singles spectrum displayed in the upper portion of this figure. The spectra in coincidence with the 44-, 65-, and 190-keV γ rays not only show unambiguously that the "185-keV" line (previously thought to be a single transition) is a 181—190-keV doublet (Fig. 17a) but also demonstrate that the members of this doublet are not in coincidence with one another (Fig. 17d) and that each terminates at a different excited state (Figs. 17b and 17c). The other point of special interest is that the "470-keV" gamma ray, which appears to be a single transition even in the high-resolution Ge(Li) singles spectrum (Fig. 17a), is in coincidence with the 44- and 190-keV transitions but not with the 65-keV line (Fig. 17c). However, inspection of Fig. 18 (an enlarged plot of the 470-keV region of Figs. 17b and 17d) shows a shift in the pulse height of this "470-keV" gamma ray and therefore proves it to be a doublet. From the observed shift (1.2 keV) the energies of these transitions are

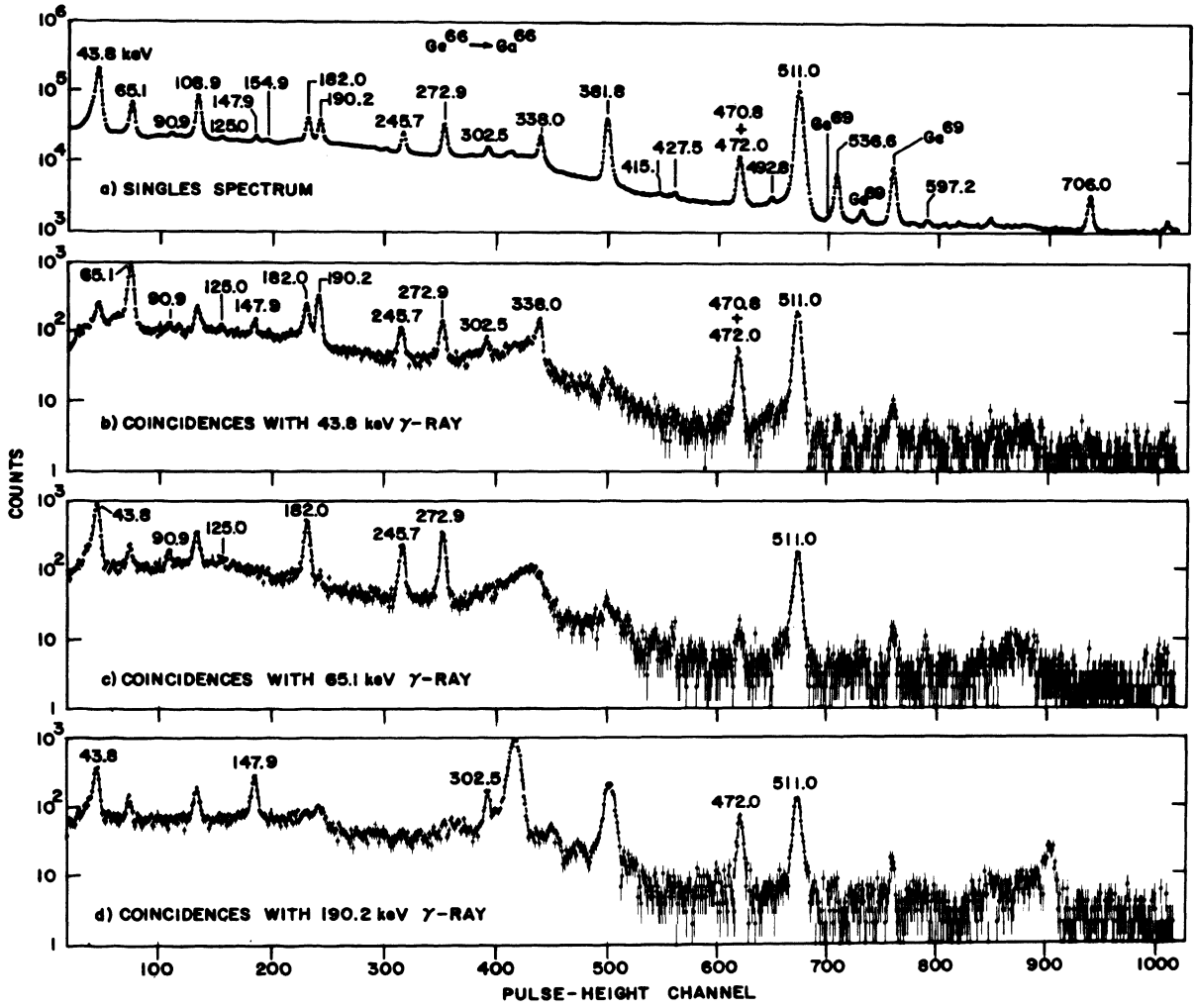

Fig. 17. Typical γ-ray spectra in coincidence with the 43.8-, 65.1-, and 190.9-keV gamma rays are shown in secs. (b), (c), and (d), respectively. For comparison, a singles spectrum taken under identical conditions, is shown in sec. (a) of this figure. All energies stated are in keV. Coincidences with Compton distributions underlying γ-ray peaks used as gates have not been subtracted in this figure. Small chance-coincidence contributions have not been subtracted. True coincidence γ-ray peaks are labeled by energy in spectra (b), (c), and (d). Broad unlabeled "peaks," most evident in spectrum (d), are due to detector-to-detector scattering.

found to be 470.8 and 472.0 keV, the former being in coincidence only with the 44-keV gamma ray and the latter in coincidence with both the 44- and 190-keV transitions. From a careful unfolding of the singles "peak" into two transitions, the intensity of the 472-keV gamma ray was

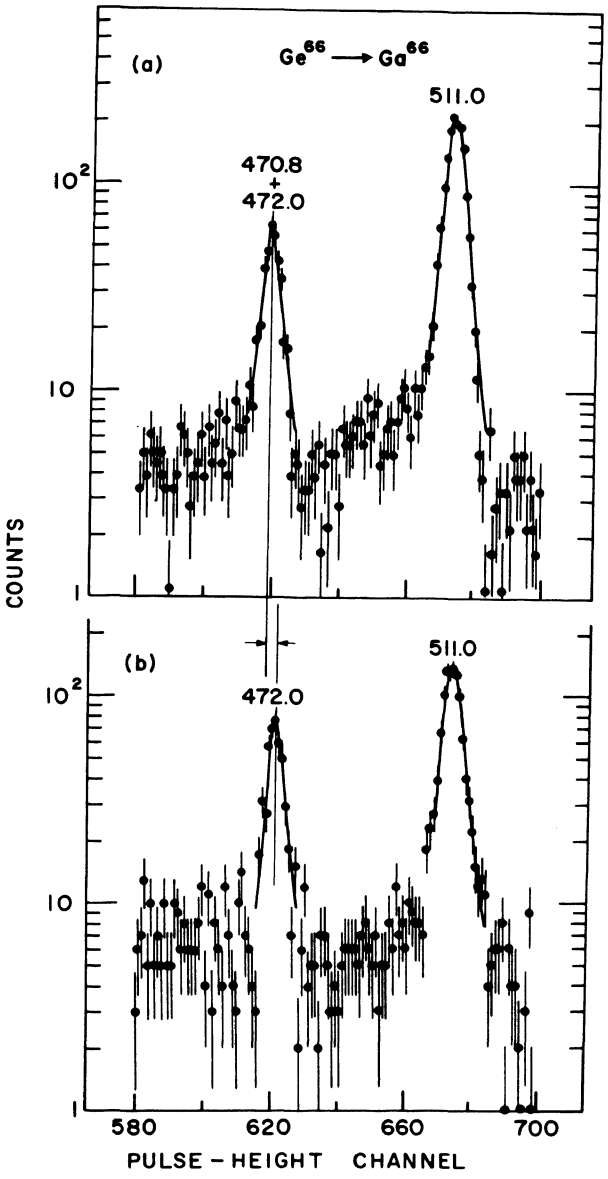

Fig. 18. Enlarged section of γ-ray spectrum in coincidence with (a) the 43.8-keV gamma ray, and (b) the 190.2-keV gamma ray. Note the displacement of the 472.0-keV peak in (b) from that of the conglomerate 470.8 + 472.0-keV peak in (a). The positions of the 511-keV annihilation radiation peaks are the same. All energies are in keV. Small chance or underlying Compton coincidences have not been subtracted in this figure.

determined to be $\leq 15\%$ of the intensity of the unresolved doublet seen in the singles spectrum. Slight tailing, present for all lines seen, restricts the determination of the relative intensities of these two components to a specification of this upper limit and does not permit a more accurate decomposition of these two lines.

Several relatively broad peaks seen in Fig. 17b, c, and d result from coincidences with Compton distributions underlying the γ-ray peaks used as gates. Although these "peaks" are evidently too

wide to be γ rays; their identity was clearly established by setting equal (but slightly displaced) pulse-height gates on the underlying Compton distributions. However, one of the pulse-height gates is set on the γ-ray peak and the other on the adjacent Compton distribution, and the slight energy shift between these two gates displaces these "peaks." Consequently, the "peaks" do not completely disappear when the spectra in coincidence with the underlying Compton distributions are subtracted from those obtained by gating on the associated adjacent γ-ray lines. The Compton "peaks" arise principally from scattering from each of the two unshielded Ge(Li) detectors to the other placed $\sim 135^{\circ}$ from it. Although somewhat broader than real γ-ray peaks, these Compton "peaks" are still narrow enough that they are readily identified and do not mask true γ-ray peaks. If these "peaks" had caused trouble, they obviously could have been obviated by placing appropriate shielding between the detectors.

Table III summarizes the coincidence relationships thus established among the γ rays. All transitions listed in this table were seen in the coincidence spectra. As will be noted from a comparison with Table I, even some rather weak transitions were unambiguously observed to be present in some coincidence spectra.

2. Lifetime of the 43.8-keV Excited State.

As reported earlier,[50] the lifetime of the 43.8-keV first excited state was determined with the aid of two 2×1-in. NaI(Tl) scintillators. Figure 19 displays the time-to-pulse-height conversion spectrum obtained by gating one arm of the coincidence system on the 44-keV gamma ray while the second arm viewed only the full-energy peak of the annihilation radiation. The two scintillators were placed at 90° to each other and were shielded from crystal-to-crystal scattering by an appropriately placed graded Pb wedge. The time calibration pertaining to this spectrum is 1.15 nsec/channel. The

TABLE III. Observed γ-γ coincidences.

γ-ray energy (keV)	Coincidence γ-ray energies[a]
43.8	65.1, 90.9, 125.0, 147.9, 182.0, 190.2, 245.7, 272.9, 302.5, 338.0, 470.8, 472.0
65.1	43.8, 90.9, 125.0, 182.0, 245.7, 272.9
108.9	90.9, 125.0, 182.0, 245.7, 272.9
182.0	43.8, 65.1, 90.9, 108.9, 245.7
190.2	43.8, 147.9, 302.5, 472.0
245.7	43.8, 65.1, 108.9, 182.0
272.9	43.8, 65.1, 108.9, 154.9 (?)
302.5	43.8, 125.0, 190.2
338.0	43.8, 154.9 (?)
381.8	154.9 (?)
470.8 + 472.0	43.8, 190.2

[a]Those γ-ray energies followed by (?) appear only faintly in the coincidence spectra and unambiguous establishment of their presence in these spectra is not claimed. The coincidence relationships of these transitions are consistent with the proposed level scheme but their placements in the scheme were established on the basis of energy and intensity fits.

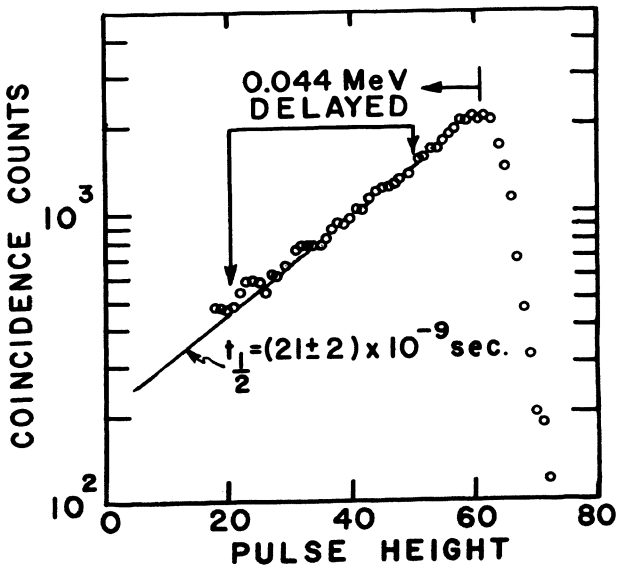

Fig. 19. Observed time-to-pulse height delayed-coincidence spectrum between the 43.8-keV gamma ray and the annihilation radiation. The slope on the left arises from delayed emission of the 43.8-keV gamma ray and corresponds to a half-life of 21 ± 2 nsec. The time calibration for this spectrum is 1.15 nsec/channel. The detectors used were NaI(Tl) scintillators.

left-hand slope corresponds to the delayed emission of the 44-keV gamma ray and yields a half-life of 21 ± 2 nsec.

Since β^+ decay populates most of the high excited states, there could be doubt whether the delayed state was the one from which the 44-keV gamma ray originates or a higher one that feeds this state. In order to resolve this ambiguity about the state with the 21-nsec half-life, a delayed coincidence experiment was performed in which the first scintillator viewed the entire spectrum while the second arm of the system remained gated solely on the full-energy peak of the annihilation radiation. In this spectrum only those events occurring within the delay-time interval specified by the bracketing arrows in Fig. 19 were accepted. This delayed-coincidence spectrum is shown in Fig. 20. Shown for comparison in this figure is a portion of the singles spectrum viewed by the same scintillator. The presence of the 44-keV gamma ray and the absence of all other transitions in this delayed spectrum at once certifies

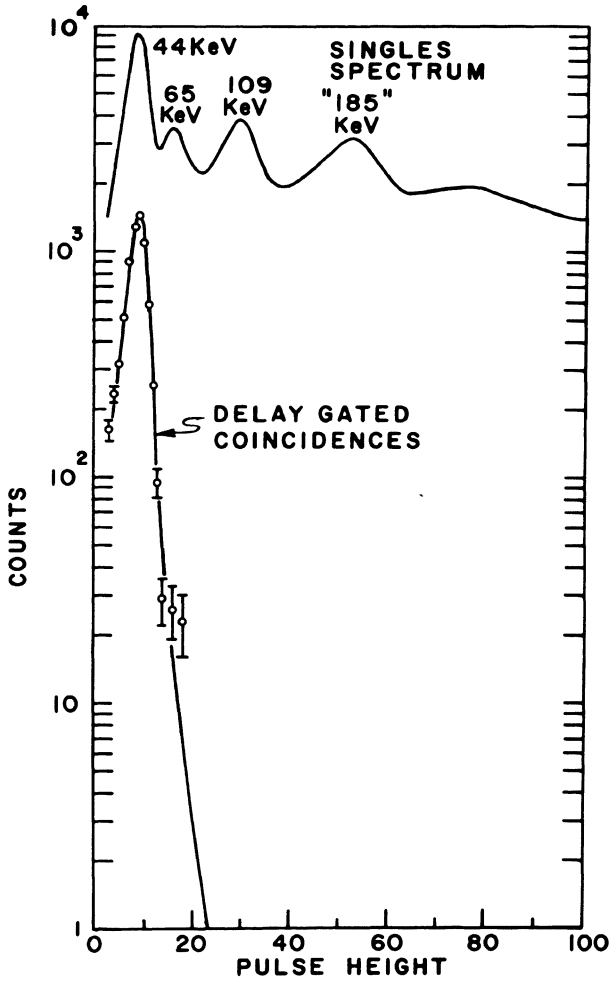

Fig. 20. Delayed-coincidence γ-ray spectrum (lower curve) obtained by viewing the entire γ-ray spectrum with one NaI(Tl) scintillator while gated by a second NaI(Tl) detector set on annihilation radiation. The delay time and the requisite time-duration "window" for pulses from the gating detector are specified by the bracketing arrows in Fig. 19. A small chance-coincidence contribution has been subtracted. Shown for comparison is a singles γ-ray spectrum (upper curve) viewed by the same detector.

(a) that the delayed state is the one from which the 44-keV gamma ray originates, (b) that the 44-keV transition is the sole transition issuing from this state, and (c) that 44-keV gamma ray populated no lower-lying excited state that decays within the 35-nsec time interval specified by the pulse-height gate set on the time distribution. Since all γ rays found to be in "prompt" coincidence with the 44-keV transition (Table III) are absent in the spectrum of Fig. 20, this study not only establishes that the measured half-life of 21 nsec is associated with the state from which the 44-keV gamma ray issues, but ensures that the 44-keV gamma ray originates from the first excited state of ^{66}Ga.

E. Discussion

The combined information gleaned from the spectrum in coincidence with the 44-keV gamma ray (Fig. 17b) and from the delayed-coincidence study places the 44-keV transition between the first excited state and the ground state. The results of the γ-γ coincidence spectra that involve all but the weakest transitions (Table III) unambiguously define the ordering of these γ rays and establish the energies of the excited states between which each transition proceeds. The self-consistency and precision of the energies determined for the γ rays observed in this decay allow precise definition of the excitation energies of these states and permit those few very weak transitions observed in the singles spectrum to be positioned among these states with great confidence. Some very weak peaks in the coincidence spectra are consistent with these placements. Therefore, the proposed ^{66}Ge $\rightarrow$ ^{66}Ga decay scheme presented in Fig. 21 is felt to be unambiguously defined and is in strong disagreement with the one most recently proposed by Ricci et al.[49] (This disagreement obviously arises from the complexities of the γ-ray spectrum,

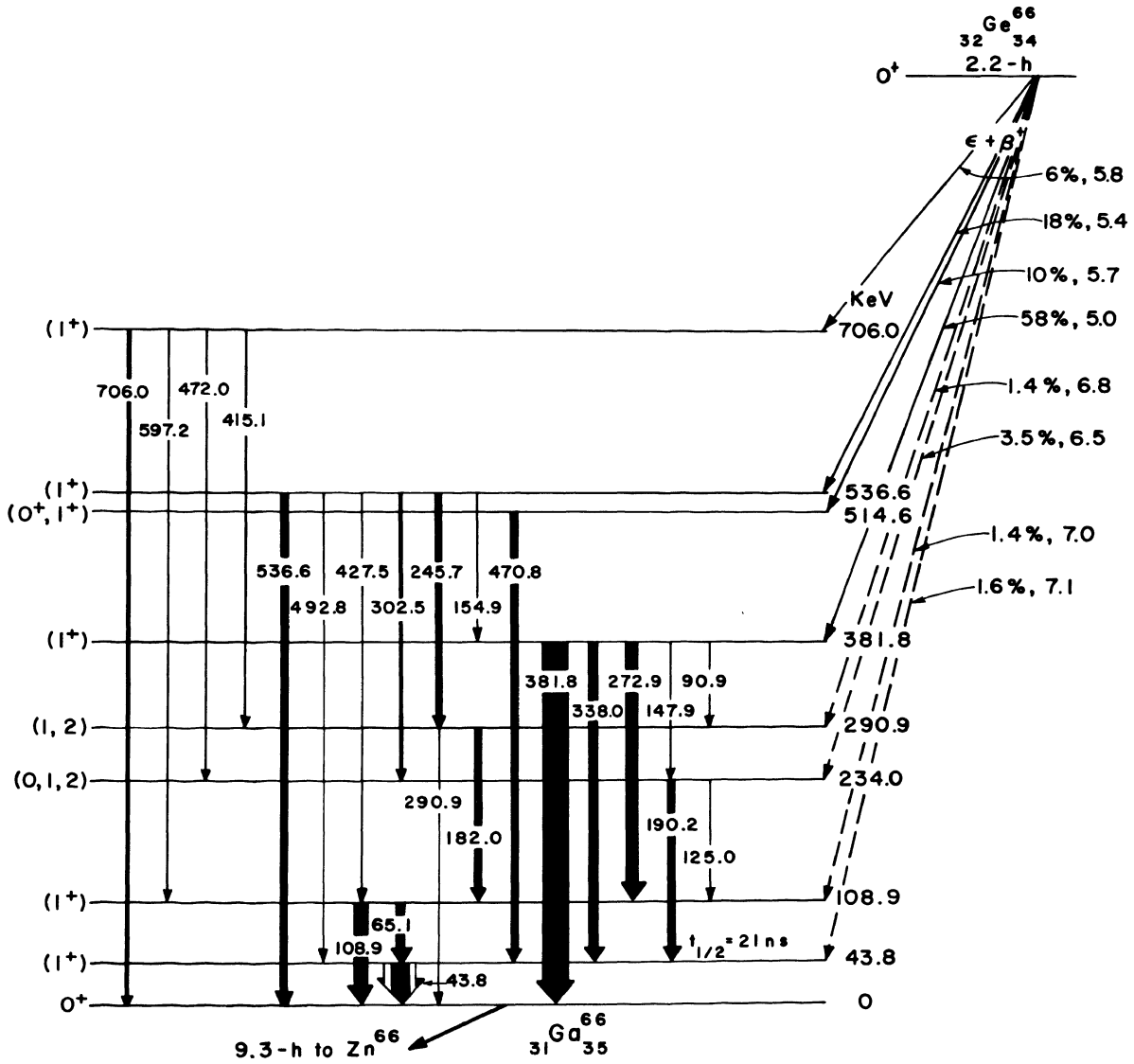

Fig. 21. Proposed β decay and level scheme of 2.2-h ^{66}Ge. All level excitation energies in ^{66}Ga are in keV, as are the energies of the γ-ray transitions. The β branches indicated by dotted lines correspond to upper limits on the relative intensities of these groups (in %) and consequently to lower limits on stated values of log ft. The spins and parities shown in parentheses are inferred from the results of the present experimental study. However, in no case should these be considered as experimentally measured parameters. The relative intensities of the γ-ray transitions are indicated by the breadths of the arrows. The open areas shown in the arrow representing the 43.8-keV transition indicate that fraction of the transition intensity proceeding by internal conversion.

which remained unresolved in the earlier NaI(Tl) investigation despite their extensive coincidence studies.)

The half-life of the 44-keV state (21×10^{-9} sec) can be compared with single-particle estimates[56] of the lifetime. When corrected for internal conversion by use of the theoretical total-internal-conversion coefficients[57] for pure M1 and E2 transitions (a mixture of both multipolarities is ruled out by the 0^+ ground-state assignment) and compared with single-particle estimates, the 44-keV transition displays a retardation factor of 129 if M1, and an enhancement factor of 769 if E2. The E2 enhancement, unrealistically large even for the most highly collective nuclei, is certainly ample reason to reject this multipolarity assignment in ^{66}Ga. However, the M1 retardation factor associated with the 44-keV transition is consistent with those of retarded M1 transitions (presumably ℓ-forbidden) observed in this mass region.[58,59] Thus, an M1 assignment appears the most appropriate for this transition.

Further evidence for an M1 assignment for the 44-keV transition comes from the combination of the intensity of the 44-keV gamma ray relative to the intensities of those feeding the first excited states (Fig. 21 and Table I) and the β^+ spectrum end-point energies reported by Ricci et al.[49] These authors observed two major β^+ groupings associated with the decay of ^{66}Ge; one is an ~100% branch with a β^+ end-point energy of 1.3 ± 0.1 MeV and the other a <10% branch with a β^+ end-point energy of 2.0 ± 0.2 MeV. They attributed the lower energy branch to the highest energy inner β^+ group. The weak higher energy branch, if it is correctly assigned to this decay, establishes that the β^+ feeding to levels near the ground state (including the level at 44 keV) is less than 9% of the total β^+ decay. If the 44-keV transition were E2, the large theoretical total conversion coefficient ($\alpha_T = 12$) would demand that ~75% of all the ^{66}Ge decay populate the 44-keV state, in clear disagreement with the relative

intensities of the β^+ groups reported earlier. On the other hand, an M1 assignment for this transition ($\alpha_T = 0.62$) requires an upper limit of only ~2% for the total ^{66}Ge decay branch to this state and is in keeping with the β^+ findings of Ricci et al.[49] Thus, the above arguments strengthen the M1 assignment of the 44-keV transition.

On the basis of this multipolarity assignment and the relative intensities of the transitions present in the decay, the branching of the ^{66}Ge decay to each level in ^{66}Ga is as presented in Fig. 6. The four decay branches to the 381.8-, 514.6-, 536.6-, and 706.0-keV states in ^{66}Ga account for more than 93% of all β decay. This branching, the 2.2-h half-life of the parent, and the reasonable assumption that the 1.3-MeV β^+ end-point energy is associated with the most energetic and intense branch to the 381.8-keV state in ^{66}Ga, lead (after correction for orbital capture[14]) to log ft values of the β-decay branches to the four highest excited states shown in Fig. 6. These values are consistent with allowed decay.

Similarly, the data presented here lead to log ft >6.5 for the decay to each of the four lowest excited states. (The log ft values of the decay branches to these lower states must be considered lower limits since they are based on the maximum β feeding of these states, the intensity of feeding being derived from the intensity balance of the γ-ray transitions to and from each of these states.) These log ft values are consistent with categorizing the β branches to the four lowest excited states as either ℓ-forbidden ($\Delta\ell = 2$) or first-forbidden transitions.

Even if a possible higher energy β^+ branch to these low-lying states were treated as a single branch to the ground state, the 9% upper limit assigned to it by Ricci et al.[49] would demand log ft = 6.3. This log ft value must be considered a lower limit, since the β feeding to the first four excited states can, by itself, account for the full intensity of the higher energy β group reported by Ricci et al.[49]

In addition, within the errors associated with the relative intensities of the γ rays, the present data are equally well consistent with the absence of all direct β feeding to any of the four lower excited states. In short, no β feeding has been established to any state below 381.8 keV in ^{66}Ga, including the ground state. Further, the value log ft = 6.3 for the possible $0^+ \rightarrow 0^+$ ground-state-to-ground-state β transition would be forbidden by isobaric-spin considerations. If this log ft is used to estimate the amount of isobaric-spin impurity required to permit this possible transition, a value of 5.5×10^{-2} is obtained. This amount of isobaric-spin admixture exceeds that established[15] for the $0^+ \rightarrow 0^+$ beta decay of ^{66}Ga $\rightarrow$ ^{66}Zn by a factor of $\sim$15. In order to bring the amount of isobaric-spin impurity into accord with the upper limit of that found for other $0^+ \rightarrow 0^+$ beta transitions in this mass region would require the intensity of the β branch to the 0^+ ground state to be $< 1\%$. This upper limit on the intensity of this possible β branch is totally in accord with the above experimental findings which are consistent with no established, observed, or inferred direct β branch populating the ground state of ^{66}Ga. On the basis of the association between the 1.3 $\pm$ 0.1 MeV end-point energy of the strongest β^+ group seen by Ricci *et al.*[49] and the 381.8-keV excited state in ^{66}Ga, a total decay energy of 2.7 $\pm$ 0.1 MeV is inferred.

The 381.8-, 514.6-, 536.6-, and 706.0-keV levels are fed by allowed β decay from the 0^+ ground state of ^{66}Ge and must therefore be assigned spins of 0^+ or 1^+. However, the 381.8-, 536.6-, and 706.0-MeV states decay to the 0^+ ground state of ^{66}Ga by means of γ-ray transitions. This, as well as isobaric-spin forbiddenness for Fermi transitions, rules out the possible 0^+ assignments and restricts their spin and parity assignments to 1^+. Because of the natural breadth of the annihilation-radiation peak in the γ-ray spectrum, it was not possible to ascertain with certainty whether or not

a 514-keV ground-state γ-ray transition was present in the decay of the state at this excitation energy. In addition, the coincidence studies were not performed under sufficiently favorable conditions to unequivocally establish or reject this possibility. Thus, with no direct experimental evidence for the decay of the 514.6-keV state to the 0^+ ground state, there are no adequate experimental grounds to reject the possible 0^+ assignment for this state. However, since a $0^+ \rightarrow 0^+$ beta transition would be possible only if there were isobaric-spin impurities, the value log ft = 5.7 for the β branch to the 514.6-keV level would imply an isobaric-spin impurity of $\sim$10%, a value much larger than those ascribed[60] to other such admixtures in this region (e.g., $\sim$27 times that established in the $^{66}Ga \rightarrow {}^{66}Zn$ decay). Thus, the spin 1^+ for the 514.6-keV level is strongly favored on these grounds.

The pure M1 assignment of the 44-keV transition establishes the first excited state as 1^+.

The 108.9-keV state decays both to the 0^+ ground state and to the 1^+ first excited state. If the spin of the 108.9-keV level were as great as 3, a 108.9-keV octupole transition to the ground state could not be expected to successfully compete with the 65.1-keV transition to the 1^+ first excited state. The comparable transition probabilities of the 272.9- and 338.0-keV transitions from the 381.8-keV 1^+ state to the 108.9- and 43.8-keV levels rule out a spin >3 for the 108.9-keV state. Thus, the spin of the 108.9-keV level can be restricted to 1 or 2 (a spin-0 alternative is inadmissible because of the direct γ-ray transition from this state to the 0^+ ground state), and the 108.9-keV transition must be either pure dipole or pure quadrupole. The ratio of the theoretical K conversion coefficient[57] of the 108.9-keV transition to that of the pure-M1 43.8-keV transition is 0.04 if the former transition is M1, and is 0.4 if it is E2. A six-gap "orange" spectrometer was used to study the

internal-conversion spectrum. Although not of high statistical quality and therefore not presented here, the results are sufficiently reliable to reject the E2 possibility and is consistent with an M1 assignment. Therefore, the 108.9-keV state can be assigned spin 1. Although none of the above data can distinguish between an E1 or M1 assignment for this transition (the theoretical conversion coefficients are almost identical), shell-model considerations strongly suggest positive parity; indeed, it is difficult to concoct a reasonable shell-model configuration that would lead to a negative parity. Thus, all of the foregoing imply a spin and parity of 1^+ for the 108.9-keV state.

The theoretical K-conversion coefficient of the 65.1-keV transition is 0.19 or 2.8 for M1 or E2, respectively. On the basis of the relative intensities of the γ-ray and K-conversion lines associated with the 65.1- and 43.8-keV transitions, the 65.1-keV transition can be assigned as M1 with admixture of $< 15\%$ E2—again consistent with a 1^+ assignment for the 108.9-keV state.

A definitive spin assignment cannot be made for the 234.0-keV level. The absence of a ground-state γ ray from this state does not make it possible to reject a 0^+ assignment for this level, although such an argument was possible for some of the higher excited states. The internal-conversion data were carefully scrutinized for the possible presence of a totally converted E0 234.0-keV transition, but none was observed within spectral statistical limitations. However, theoretical considerations[61] strongly disfavor such a transition in competition with the 190.0-keV transition (if M1 or E2) to the first excited state. Thus, the lack of observation of the possible E0 transition does not rule out a 0^+ spin assignment. Three of the higher 1^+ states decay to the 234.0-keV level, each decay being in competition with higher energy M1 transitions to lower levels. On the basis of single-particle transition probabilities[56] and what is known of the largest M1 retardations and E2 enhancements in this mass

region, it is possible to restrict the spin of the 234.0-keV level to ≤ 2. These arguments restrict the spin of the 234.0-keV state to 0, 1, or 2. Again, shell-model considerations strongly suggest positive parity. Since only a lower limit can be set on the log ft value of the β decay to this level, it cannot be used to place further spin restrictions on this level.[62]

The presence of the ground-state transition from the 290.9-keV state rules out a possible spin-0 assignment for this level. From arguments similar to those used for the spin of the 234.0-keV state, the γ ray branching from higher excited states of spin 1^+ allows the spin of the 290.9-keV level to be restricted to ≤ 2. Thus, this state has spin 1 or 2, with strong shell-model arguments for positive parity.

The above spin, parity, and log ft values are summarized in the level scheme (Fig. 21).

On the basis of probable shell-model configurations for the levels in odd-odd $^{66}_{31}Ga_{35}$, it becomes fairly evident that a sizable degree of configuration mixing would be expected in any meaningful description of these states. Alternatively, if one adopts a more collective approach by assuming some moderate degree of oblate deformation, then the applicable Nilsson orbitals[63] available for the protons are $K_\pi = \frac{5}{2}^-$, $\frac{3}{2}^-$, and $\frac{1}{2}^-$ while those of the neutrons are $K_\nu = \frac{3}{2}^-$ and $\frac{5}{2}^-$. These can couple in a variety of ways to lead to K = 0, 1, 2, 3, 4, and 5. Of most significance, these couplings lead to two K=0 bands and five K=1 bands as well as several bands with $K \geq 2$. From these considerations, a large number of $J^\pi = 1^+$ low-lying excited states and two $J^\pi = 0^+$ states can be anticipated, in agreement with the spin assignments and possible spin limitations for the low-lying states of this nuclide. Similarly, a moderate degree of prolate deformation results in like conclusions. The retarded M1 44-keV transition can be understood on the basis of

K-forbiddenness by assigning the ground state and first excited state to $(K^{\pi}, J^{\pi}) = (0^{+}, 0^{+})$ and $(1^{+}, 1^{+})$, respectively.

Further inferences would require rather extensive theoretical calculations, and it is doubtful that the results would justify the effort without additional experimental determinations of, say, the lifetimes of higher excited states and unequivocal spin assignments for the few levels for which only spin limitations could be prescribed. However, the experimentally determined characteristics of the low-lying levels of ^{66}Ga appear to be consistent with general theoretical considerations and expectations.

These results have been published in Ref. 64.

VII. COULOMB EXCITATION OF ^{105}Pd

A. Introduction

The level scheme of $^{105}_{46}Pd_{59}$ has been obtained previously from radioactive decay studies[65,66] and the B(E2) values for one or two excited states of the stable even-even Pd isotopes have been known for some time.[32,67—69] The measurement of enhanced B(E2) transitions in several nearby nuclei[70] suggests that ^{105}Pd may be somewhat deformed and, therefore, may exhibit a spectrum characteristic of a transition region between spherical and deformed nuclei.

In the simple single-particle description, ^{105}Pd is expected to have all levels filled up to the $1g_{7/2}$ level. However, the fact that the ground-state spin and parity are observed[71] to be $\frac{5}{2}^+$ indicates that the $1g_{7/2}$ level lies below the $2d_{5/2}$ level in this mass region. This fact implies that ^{105}Pd has one neutron in the $2d_{5/2}$ level, i.e., it is one nucleon removed from a closed subshell. The single-particle energies for excitation to the $d_{5/2}$, $d_{3/2}$, $s_{1/2}$, and $h_{11/2}$ orbitals which lie within the same major shell are expected to require an excitation energy $\lesssim 1.5$ MeV. At least 10 levels are observed below this energy. The observation of very strong E2 transitions to several of these levels[32,67—69] indicates that there must be appreciable collective excitation associated with them.

A determination of the E2 transition strengths to the other low-lying levels of this nucleus is clearly of value in trying to understand the collective nature of these states. Because of its high resolution, the Ge(Li) detector is especially valuable in the determination of E2 strengths to many of the low-lying states by Coulomb excitation which cannot be resolved or observed over background when a NaI(Tl) crystal is used. In particular, we have been able to observe E2 excitation probabilities for 10 levels in ^{105}Pd whereas previous

investigations[67—69] have yielded E2 probabilities for only 2 levels with the use of NaI detectors.

B. Experimental Techniques

Coulomb excitation of ^{105}Pd was accomplished using α particles from the Argonne Tandem Van de Graaff to bombard a thick target of self-supporting Pd metal foil which had been enriched to 77% in ^{105}Pd. The de-excitation γ rays were observed in a Ge(Li) detector (nominally 30 cc, see Sec. V) placed at ~1.5 in. from the target at an angle of 55° with respect to the beam direction in order to remove the effect of any angular distribution. Singles γ-ray spectra were collected at 7 α bombarding energies from 4.4 MeV to 8.0 MeV. Gamma rays having an energy from ~40 keV to ~2.4 MeV were recorded using the pulse-height analysis system described in Sec. V except that the spectra were recorded in a Nuclear Data 4096 channel analyzer.

As was discussed in Sec. III, the measurement of the relative excitation probabilities of the different states as a function of bombarding energy allows one to determine the branching of the γ rays and to confirm that the dominant mode of excitation of the levels is indeed E2 Coulomb excitation.

The absolute yield of γ rays was determined using an efficiency curve for the Ge(Li) detector obtained by using several calibrated intensity sources covering the energy range from ~88 keV to 1.3 MeV. These intensity calibration sources were placed at the exact position of the target so that exactly the same amount of absorber (target chamber, detector housing, etc.) was traversed by the calibration γ rays as for the Coulomb excitation γ rays. Corrections for dead time in the total analyzing system were made in a manner very similar to that described in Sec. VA.

The construction of the decay scheme depends heavily on the data from the radioactive decay studies.[65,66] In all cases the energies determined in the present study using the ramper method (Sec. VA1) agree with those from the radioactive decay studies.[65,66] Similarly, the branching ratios of all the γ rays observed in the Coulomb excitation spectra agree with those of the radioactive decay studies.[65,66] Since the 344-keV level was found to be weakly excited in the Coulomb excitation study and was known to be fed strongly in the $^{105}Ag \rightarrow {}^{105}Pd$ β decay, a companion study of the latter decay was performed to more accurately determine the branching ratio of the 64- and 344-keV γ rays depopulating this state.

C. Results

1. Ge(Li) Spectra and Decay Scheme.

Ge(Li) spectra were taken of the de-excitation γ rays following Coulomb excitation in ^{105}Pd for bombarding energies of 4.4, 5.2, 5.6, 6.0, 6.4, 7.2, and 8.0 MeV. Typical running times were $\sim$5 h. Figure 22 shows the spectrum obtained at 7.2 MeV. A list of the γ rays observed is given in Table IV. The energies for all of the lines were determined by the ramper method discussed in Sec. V. The energy scale was determined by the use of standard γ-ray sources whose energies are well known.[53] Errors assigned to the energies are based mainly on the internal consistency of the energy of γ rays which represent cascade and crossover radiation from the same level. The absolute intensity (number of γ rays/bombarding α particle) was determined by correcting the observed intensities for detector efficiency and analyzing system dead time as mentioned above. The number of bombarding particles was calculated from the total charge which was collected by the target. The intensities

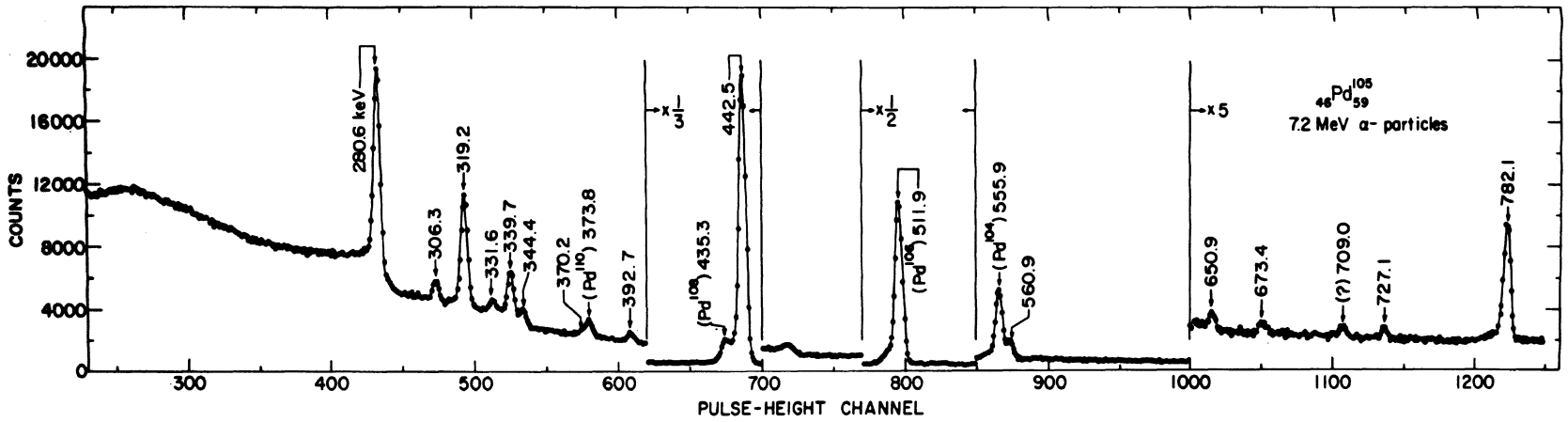

Fig. 22. The gamma-ray spectrum resulting from Coulomb excitation of ^{105}Pd with 7.2-MeV alpha particles. The contaminant radiation resulting from the even-even isotopes of Pd did not mask any radiation in which we were interested while serving as a check on our method for determining the B(E2)'s. (See text.)

TABLE IV. Gamma-ray energies and intensities for the 7.2-MeV alpha bombardment.

γ-ray energy	Excitation/α particle
280.6 ± 0.4	$12.7 \pm 0.4 \times 10^{-9}$
306.3 ± 0.5	1.20 ± 0.9
319.2 ± 0.4	7.8 ± 0.6
331.6 ± 0.5	0.67 ± 0.08
339.7 ± 0.4	3.18 ± 0.09
344.4 ± 0.6	0.87 ± 0.09
370.2 ± 0.8	0.27 ± 0.07
392.7 ± 0.7	0.68 ± 0.09
442.5 ± 0.5	89.0 ± 5.0
560.9 ± 0.7	2.3 ± 0.3
650.9 ± 0.8	0.37 ± 0.06
673.4 ± 0.9	0.37 ± 0.06
727.7 ± 0.8	0.31 ± 0.04
782.1 ± 0.8	4.8 ± 0.03

given in Table IV for the 7.2-MeV bombardment are accurate to ~5% for the stronger lines and ~15% for the weaker ones. The spectra taken at other bombarding energies have similar errors and, of course, different relative intensities due to the dependence of the cross section for the population of a given level on the bombarding energy.

Figure 23 is the spectrum obtained in a study of ^{105}Pd following β decay of ^{105}Ag. Since the 64-keV transition was not observed in the Coulomb excitation spectra, the branching ratio of the 64-keV transition was obtained from this spectrum (the 64-keV γ ray represents 31% of the decay of the 344-keV level). This transition must be

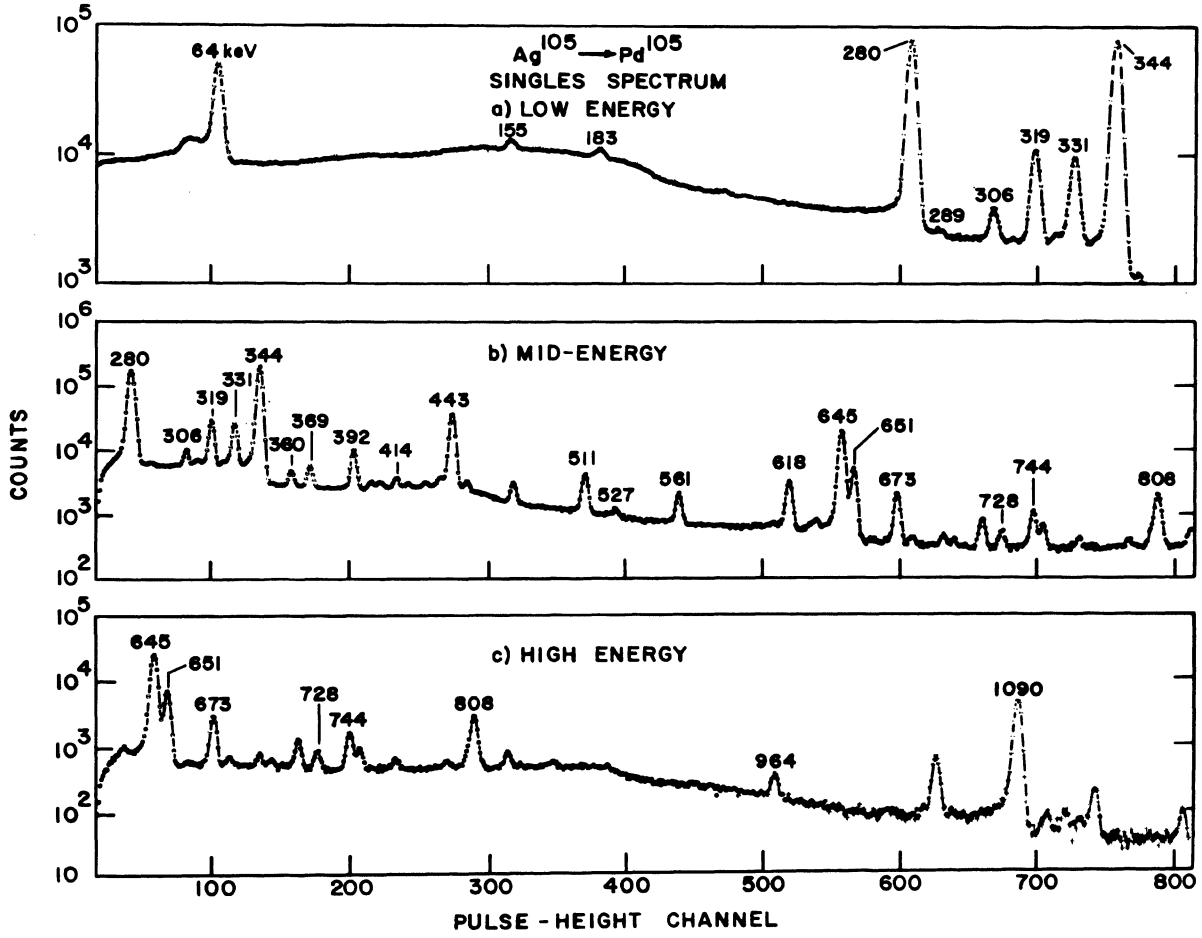

Fig. 23. The gamma-ray spectrum of ^{105}Pd following β decay from ^{105}Ag. The branching ratio of the 64 to 344 keV transitions important for the accurate determination of the B(E2)'s was obtained from this study.

considered in the calculation of the yield of the 344-keV state and of the 280-keV state since some of the observed population of this state occurs via the 64-keV cascade radiation from the 344-keV state.

Figure 24 shows the decay scheme deduced from the Coulomb excitation data with the exception of the 489-keV level observed in the radioactive decay studies[65,66] but unobserved in this study (due to its high spin and negative parity). The 782-keV level is not observed in the radioactive decay studies.[65,66] The spins and parities indicated in the figure are those of Refs. 65 and 66. The transition probabilities

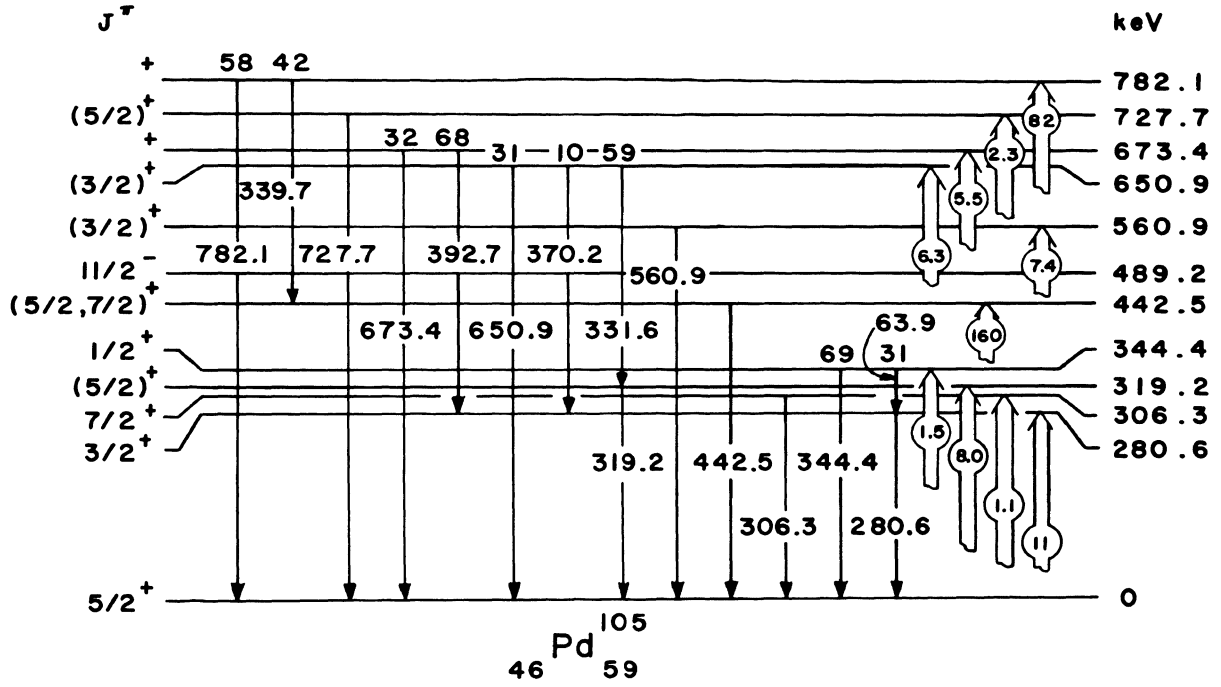

Fig. 24. The level scheme of ^{105}Pd. Only those transitions which were observed in this study are included. However, the $\frac{11}{2}^-$ state at 489.2 keV observed in the β decay studies but not seen in Coulomb excitation is included so that all of the excited states observed in this nucleus below 782 keV are shown on this figure. The spins indicated on the left are those of Refs. 65 and 66. Those spins which are assigned with less certainty are enclosed in parentheses. The positive parities of states so marked are confirmed by their observation in the E2 Coulomb excitation process. The branching ratios of the levels are indicated above the appropriate gamma ray and the energies of the gamma rays appear within the arrows representing the transition. The pot-bellied arrows represent transitions observed by E2 Coulomb excitation with the B(E2)↑ (in units of 10^{-51} e^{2}cm^4) appearing in the rounded portion of the arrow.

[B(E2)↑] are indicated within the pot-bellied arrows in units of 10^{-51} e^{2}cm^4.

2. Determination of B(E2)↑ Values.

The theoretical excitation functions were all calculated from the graphs, tables, and formulas given in the review article of Alder et al.[29] For all the bombarding energies used, the value of the

parameter η_i (see Sec. III) was greater than 10, so the function f_{E2} could be read directly from the graph of Ref. 29. For the calculation of the thick target yields (see Sec. III) it is necessary to know dE/dx for protons given in Ref. 72. The usual formula for the relationship between the stopping power for an ion of mass M, charge Z, and energy E to the stopping power of protons in the same material is assumed

$$(dE/dx)_{Z,M,E} = Z^2 (dE/dx)_{p,E/M} . \qquad (C1)$$

Thus the stopping power for α particles of energy E is four times that for protons of energy E/4. In addition it is assumed that dE/dx is inversely proportional to the square root of the target atomic number. Thick target yields were calculated from the formulas of Sec. III and the graphs of Ref. 29, Sec. IIIB. The error associated with the uncertainties in the stopping power and the use of the graphs is expected to be ~4%.

Figure 25 shows the relative γ-ray yield for the 13 transitions observed in this study. The points represent the data and the line results from using the weighted average of the B(E2)'s calculated for the appropriate level in Eq. (C5) of Sec. III. The yield of each γ ray is consistent with E2 Coulomb excitation. It is interesting to note that the γ rays of energy 339.7, 392.7, and 331.6 keV obviously do not originate from levels of the same energy. Otherwise their yield curves would have a shape more like that of the 344.4-keV transition. Thus the shape of the curve is an indication that these γ rays originate from a level of higher energy. In fact, the experimental points for these three γ rays follow exactly the shape of the yield curve for the level energy which is indicated in the figure.

In order to determine the absolute B(E2)↑ for the levels in ^{105}Pd it is necessary to determine the absolute intensities for the population of each level. The intensities of all the γ rays depopulating a level are summed and the intensity due to any transitions which feed

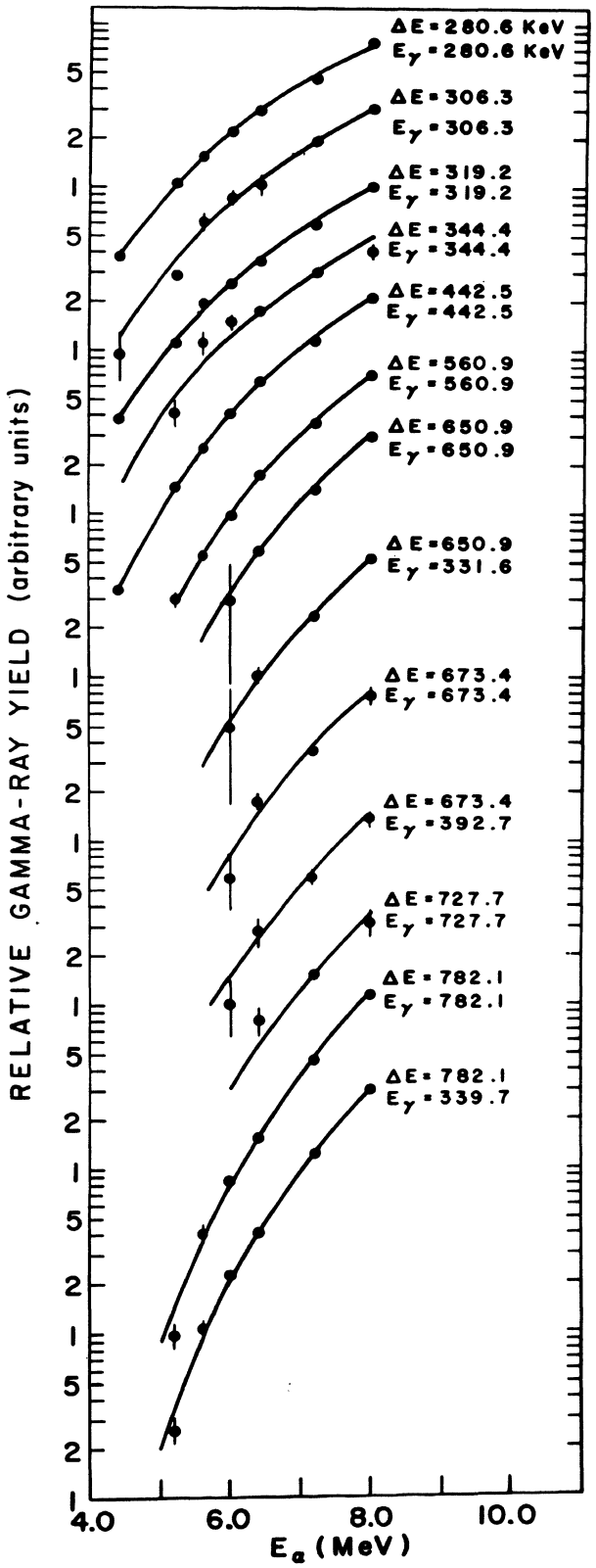

Fig. 25. Relative γ-ray thick target yields obtained in this study. The points represent the data and the line represents the theoretically predicted yield using a weighted average of the B(E2)↑ for each state. The yields of all of the observed de-excitation γ rays are consistent with E2 Coulomb excitation.

TABLE V. Transition probabilities from the ground state of ^{105}Pd.

Energy	J^*	B(E2) (10^{-51} e^2 cm^4)	$B_M(E2)^a$ (10^{-51} e^2 cm^4)
280.6	$\frac{3}{2}$	11.0 ± 0.2	0.84
306.3	$\frac{7}{2}$	1.1 ± 0.02	0.56
319.2	$(\frac{5}{2})$	8.0 ± 0.2	3.3
344.4	$\frac{1}{2}$	1.5 ± 0.2	2.9
442.5	$(\frac{5}{2}, \frac{7}{2})$	160 ± 10	(3.5, 0.59)
560.9	$\frac{3}{2}$	7.4 ± 0.4	0.84
650.9	$\frac{3}{2}$	6.3 ± 0.6	0.84
673.4	?	5.5 ± 0.6	2.9
727.7	$\frac{5}{2}$	2.3 ± 0.4	3.3
782.1	?	82 ± 6	2.9

[a] $(2J^* + 1) \times C^2$ was set equal to 1.0 in the calculations for which the spin is unknown. Two calculations are given for those levels for which the spin is uncertain.

this level from above is subtracted. In calculating the various transition intensities, the conversion coefficients of the various transitions were taken into account. The conversion coefficients used were those of T. Sutter et al.[65] [The only large correction was for α_T (63.9) = 1.13.[65]]

After correction for feeding and branching, the absolute direct excitation yields are obtained for the 10 levels. Values of B(E2)↑ were calculated at each bombarding energy. Weighted averages of the B(E2)↑'s were calculated and are listed in Table V. In all of these calculations the statistical errors were negligible. The systematic errors arising from uncertainties in efficiency calculations, beam-current integration, stopping power calculations, and peak area

calculations are included in the errors quoted in Table V. The even Pd contaminant γ-ray lines observed in the Coulomb excitation spectrum allowed the calculation of the B(E2)↑ for several levels in the even-even Pd isotopes, known amounts of which were present in the target. These values had been measured previously[32,67—69] and the values determined in this study always agreed with the values quoted by previous investigators to within the errors quoted by them.[32,67—69] This agreement confirms that the corrections for detector efficiency, dead time, etc., have been accurately assessed and is evidence that the B(E2) values determined for the levels in ^{105}Pd are equally reliable.

The right-hand column in Table V shows the B(E2)↑ calculated from the Moszkowski single-particle estimate.[73] The Moszkowski limit can be written as

$$B_M(E2) = 2.8\,(A/100)^{4/3}(2J^* + 1) \times [C(J^*, J_0, 2; \tfrac{1}{2}, -\tfrac{1}{2}, 0)]^2\, e^2 \times 10^{-51}\ \mathrm{cm}^4, \qquad \text{(C2)}$$

where A is the nuclear mass, J^* is the excited-state spin, and $J_0 = \frac{5}{2}$. The values for the factor $(2J^* + 1)C^2$ are 1.0, 0.3, 1.14, 0.19, 2.38 for $J^* = \frac{1}{2}, \frac{3}{2}, \frac{5}{2}, \frac{7}{2}$, and $\frac{9}{2}$, respectively.

D. Discussion

The level structure of ^{105}Pd is not easily understood. Although the γ-decay studies[65,66] are quite complete and have been in existence for some time, very little nuclear reaction work has been published and only two levels have been observed previously in Coulomb excitation.[67—69] Similarly, very little theoretical discussion appears in the literature on this nucleus.

The observation of several enhanced E2 transitions in ^{105}Pd implies that there must be appreciable collective effects associated

with several of the low-lying excited states of this nuclide and that the simple shell model cannot be expected to adequately describe the observed properties of these states.

It is probably not possible at present to explain all the B(E2) values which we have determined. There are, however, two levels (the 442- and 782-keV levels) that display markedly enhanced B(E2)↑ values. These levels may be associated with the collective 2^+ excitations of the even-even core (^{104}Pd).

The core-excitation model (see Sec. IIE) should be applicable to nuclei which are one particle removed from a closed subshell. Since the ground-state spin of ^{105}Pd is known to be $\frac{5}{2}^+$, this is an indication that the $g_{7/2}$ subshell may be filled with one neutron outside of this shell in the $d_{5/2}$ orbital. According to this model, a set of states should exist which correspond to the various ways in which the odd-neutron can couple to the collective 2^+ excitation of the core. Publications by Lawson and Uretsky[27] and deShalit[28] describe the properties that such a nucleus is expected to exhibit (see Sec. IIE). As applied in its simplest form to ^{105}Pd, this model predicts the existence of a multiplet of excited states having spins of $\frac{1}{2}$, $\frac{3}{2}$, $\frac{5}{2}$, $\frac{7}{2}$, and $\frac{9}{2}$, each of which has a ground-state transition probability B(E2) equal to that of the $2^+ \rightarrow 0^+$ transition in the next lower even-A isotope. In addition, the M1 transition to the ground state from one of these excited states should be forbidden, whereas, an M1 transition between members of the multiplet should be allowed provided ΔJ selection rules are met. The center of gravity [see Sec. II, Eq. (E2)] of this multiplet should equal the energy of the 2^+ state in ^{104}Pd.

We have two prime candidates for the core-excited states, whereas, five members of the multiplet of levels associated with the 2^+ excitation of the ^{104}Pd core are expected. Furthermore, even when using only the two levels that have been observed and assigning the lowest possible values for the unknown spins, the center-of-gravity

is considerably greater than 556 keV, the energy of the 2^+ state in ^{104}Pd. Since the members of this multiplet are expected to have large B(E2)↑, all of the levels below 782 keV should certainly have been observed. It is significant that no levels above 782 keV were observed although the experimental spectrum extended to ~2.5 MeV. Any of the higher members of this multiplet would be expected to have enhanced B(E2)↑ values (see Table VI) and, again, should have been easily observed. Even in the event that one or more members of this multiplet above 782 keV have been missed, the only effect is to increase an already-too-high value for the center-of-gravity.

Model predictions for the values of the individual B(E2)↑'s may be obtained by combining the result from the core-excitation model; $B_{105}(E2; J_i^* \rightarrow J_0) = B_{104}(E2; 2^+ \rightarrow 0^+)$ and the fact that $B(E2; J_0 \rightarrow J_i^*) = (2J_i^* + 1)/(2J_0 + 1)B(E2; J_i^* \rightarrow J_0)$.[29] Since the spins of the final states are not known definitely, a tabulation of the possible values of B(E2)↑ for the various members of the multiplet is given in Table VI. The observed values of B(E2)↑ for the 442- and

TABLE VI. Transition probabilities predicted by the core-excitation model.
$B_{105}(E2; \frac{5}{2} \rightarrow J_i^*) = (2J_i^* + 1)/30 \times B_{104}(E2; 0^+ \rightarrow 2^+)$
$B_{104}(E2; 0^+ \rightarrow 2^+) = 550 \times 10^{-51}\, e^2\, cm^4$.

J_i^*	$(2J_i^* + 1)/30$	$B(E2; \frac{5}{2} \rightarrow J_i^*)$
1/2	1/15	$36.7 \times 10^{-51} e^2 cm^4$
3/2	2/15	73.3
5/2	1/5	110
7/2	4/15	147
9/2	1/3	183
	TOTAL	$550 \times 10^{-51} e^2 cm^4$

B(E2)↑ (442) = 160 B(E2)↑ (782) = 83

the 782-keV levels are 83 and 160 (in units of $10^{-51} e^2 cm^4$), respectively. These values are consistent with the magnitude expected. However, the experimentally determined values fall about half way between two of the expected values. If there had been a one-to-one correspondence between the levels observed and those predicted, it would have been tempting to tentatively assign the spins of these two states based on the core-excitation model. However, an exact correspondence was not found and, therefore, such assignments cannot be made because of the inadequate experimental verification of the model.

The failure to find such verification could be interpreted as an indication that some single-particle excitation is also present in the make-up of these levels. Unfortunately, the magnitude and sign of the correction factor depends on the exact ratio of single-particle to core excitation and, therefore, no theoretical help is currently available for the exact interpretation of this data.

In addition to the results discussed above, the core-excitation model predicts that the sum of the $B(E2)\uparrow$ for the multiplet should equal the value for $B(E2; 0^+ \rightarrow 2^+)$ in ^{104}Pd which is $550 \times 10^{-51} e^2 cm^4$. In order to obtain an upper limit on the amount of core excitation observed in this study, the sum of all the $B(E2)\uparrow$'s for all levels was taken. The $\Sigma B(E2)\uparrow$ is equal to $290 \times 10^{-51} e^2 cm^4$. This sum is equal to approximately 53% of the expected value of $B(E2; 0^+ \rightarrow 2^+)$ in ^{104}Pd.

In Ref. 29 it is noted that it may be necessary to add a term to the $\Sigma B(E2)\uparrow$ to account for the quadrupole moment of the ground state of the nucleus. In an analogy to the discussion presented in Ref. 74, the ground state of ^{105}Pd may undergo a polarization caused by the field of the last neutron so that part of the expected transition strength may go into unobserved transitions between the magnetic substates of the nuclear ground state. In order to account for the

missing transition probability the ground-state quadrupole moment would have to be large enough to account for ~47% of the B(E2)↑ of the $0^+ \rightarrow 2^+$ in ^{104}Pd. From this fact the ground-state quadrupole moment is calculated as being ~0.9 b. This value is not unreasonable since the values observed for the odd Cd isotopes, which also have spin $\frac{5}{2}$, is ~0.8 b. These results are very similar to those reported previously by Kistner and Schwarzschild[74] for ^{99}Ru and ^{101}Ru.

In summary, although two states in ^{105}Pd were observed that could correspond to the excitation of the ^{104}Pd core, the overriding conclusion is that the simple core-excitation model does not provide an adequate description of the states of ^{105}Pd, at least not to the extent that had been expected.[28] The low-lying excited states of this nuclide seem to display characteristics of both a collective and a single-particle nature.

VIII. LEVEL STRUCTURE OF LOW-LYING EXCITED STATES OF ^{187}W POPULATED IN THE THERMAL NEUTRON CAPTURE REACTION $^{186}W(n,\gamma)^{187}W$

A. Introduction

The low-lying states of odd-odd $^{187}_{74}W_{113}$ have been the subject of several previously reported experimental investigations.[75,79,80] The (d,p) work of Erskine[75] has resulted in the excitation energies of a number of levels up to ~1800 keV and in assignments for the orbital angular momentum of several excited states up to an energy of ~1 MeV. Erskine has proposed Nilsson orbital specifications of five levels up to an excitation energy of 434 keV. The spectrum of primary radiation has been studied by Martin et al.[79] who has defined states in ^{187}W up to an energy of ~1150 keV, some of which were not seen in the stripping study of Erskine. Finally, Prokofev et al.[80] employed the thermal-neutron-capture reaction in a magnetic spectrograph study of the internal-conversion electron spectrum of the secondary transitions in ^{187}W and reported the energies of several low-energy γ rays. Despite these efforts, many details of the level structure are still unknown or poorly established.

The odd-A deformed tungsten isotopes are near the edge of the deformed region where rotational characteristics are not expected to be as prevalent as in nuclei which are closer to the center of the deformed region. However, the low-lying excited states of ^{183}W have been successfully interpreted in terms of a model in which a core rotator is coupled to an odd nucleon.[76,77] When proper account is made for Coriolis band mixing, a striking agreement between the predictions of this model and the experimentally observed parameters occurs. The low-lying levels of ^{185}W and ^{187}W also appear to display rotational structure; however, fewer low-lying states are observed experimentally in these nuclei. The degree of correspondence

between the levels in these nuclei and the predictions of the model is, therefore, less clear. While ^{183}W and ^{185}W are populated by β decay, ^{187}W is not; consequently, less experimental information is available about the low-lying excited states and the radiative decay of the levels of this nuclide.

Due to the multiplicity of the cascade γ-ray transitions from the compound nuclear state formed in thermal-neutron-capture to low-lying levels of the product nucleus (see Sec. IV), virtually all of the low-lying excited states are readily populated. The combination of primary and secondary gamma radiation following thermal-neutron-capture leads equally well to states characterized by excited neutron or proton configurations, by particle or hole makeup, or by an intrinsic, rotational, or vibrational nature. At the same time, this wide population of the low-lying excited states leads to spectra of a very complicated nature. If sufficiently sophisticated experimental techniques are employed in the investigation of this reaction, these studies may provide a valuable extension of the information obtained from charged particle studies.

To this end the present experimental investigation of the levels in ^{187}W was performed in an attempt to provide additional information about the level structure of ^{187}W which might permit a more critical test of the applicability of the simple rotational model to the low-lying excited states in ^{187}W and/or point up any systematic behavior indicative of the approach of this nuclide to the edge of the deformed region.

The thermal-neutron-capture reaction $^{186}W(n,\gamma)^{187}W$ was employed to populate the low-lying levels of ^{187}W. This investigation included studies of the primary and secondary transitions by means of singles and coincidence γ-ray techniques using Ge(Li) detectors exclusively. Coincidence data were recorded between the high-energy ($\sim$4—5.5 MeV) and the subsequently emitted low-energy

transitions (~50—1300 keV), as well as among the low-energy cascade γ rays.

B. Experimental Facilities and Techniques

An external neutron beam facility was employed in the measurement of low-energy singles γ-ray spectra and two-parameter γ-ray spectra for both high-energy transitions coincident with low-energy transitions (hereafter referred to as high-low coincidences) and low-energy γ rays coincident with low-energy γ rays (hereafter called low-low events). A highly collimated beam of thermal neutrons was extracted from a modified thermal-column at the Argonne CP-5 reactor. A schematic diagram of this facility is shown in Fig. 26. Great care has been taken to insure that the neutron beam is free of fast neutrons (Cd ratio ≈550) and pile γ rays. An extremely well defined beam (thermal flux $\approx 5 \times 10^7$ neutrons/cm^2-sec, height ≈2 cm, width ≈0.5 cm) was obtained by the use of conventional collimators fitted with defining apertures of Li^6F discs* enriched to 95.5% in Li^6. The targets consisted of pressed cylindrical pellets of WO_3 enriched to

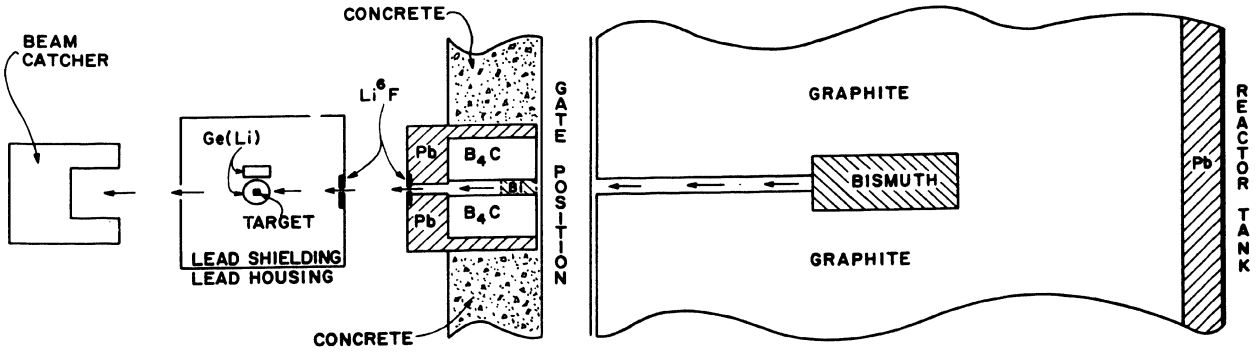

Fig. 26. Representation of the external thermal neutron beam facility. (Not to scale.)

*Fabricated by Oak Ridge Stable Isotope Sales, Oak Ridge National Laboratory, Oak Ridge, Tennessee.

97.2% in ^{186}W contained in thin-walled (4.5 mg/cm^3) aluminum holders.

Two coaxially drifted detectors (see Sec. V) were mounted at 180° to each other and positioned 2.9 cm from the beam axis. Both detectors were shielded by thin (0.25 cm thick) Li^6F discs to prevent scattered neutrons from entering the detectors or the detector housings. The coincidence data were recorded on a two-parameter magnetic tape storage unit described in Sec. VB. A 4096 channel ADC was employed in each arm of the coincidence system in order to obtain the pulse-height resolution capabilities of large ADC's while any 1024 channel segment could be selected for storage in the 1024 × 1024 channel array. The storage capacity of the magnetic tape was $\sim 2.75 \times 10^6$ event-address pairs.

The basis for the fast coincidence timing unit was a time-to-pulse-height converter (TPC) which is described in Sec. VB. Prompt and chance events were simultaneously but separately recorded on the magnetic tape by the use of a tag bit associated with the chance distribution in order to allow a proper consideration of chance events in the final data reduction. The fast-slow* resolving time was ~90 nsec. Digital gain and zero stabilization was employed in the ADC of each arm of the coincidence system.

Two separate sets of coincidence data were collected. One detector was always set to record the low-energy portion of the spectrum while the second detector registered either (a) the high-energy spectrum or (b) the low-energy spectrum. The energy resolution of the Ge(Li) detector is sufficient to resolve single lines in the primary spectrum which represent transitions to and population of individual low-lying states (each primary transition yields three peaks

---

*"Fast-slow" refers to the fact that a triple coincidence is required in order that an event be recorded: (a) a "fast" output from the TPC and (b) a "slow" output from each of the two ADC's.

in the high-energy spectrum due to the production of electron-position pairs in the detector by the primary γ ray and the subsequent escape of zero, one or both of the quanta resulting from the annihilation of the positron). Coincidence spectra recorded between these γ rays and the low-energy γ rays representing transitions from the low-lying level being populated to the ground state may define both the decay characteristics of these states and the subsequent population of lower levels. The low-low coincidence relationships serve to complement and expand the information obtained from the high-low coincidence studies.

C. Results

1. High-Energy Transitions.

Figure 27 displays the primary high-energy capture γ rays observed in the high-energy arm of the high-low coincidence study of the $^{186}W(n,\gamma)^{187}W$ reaction. The energies indicated on the figure

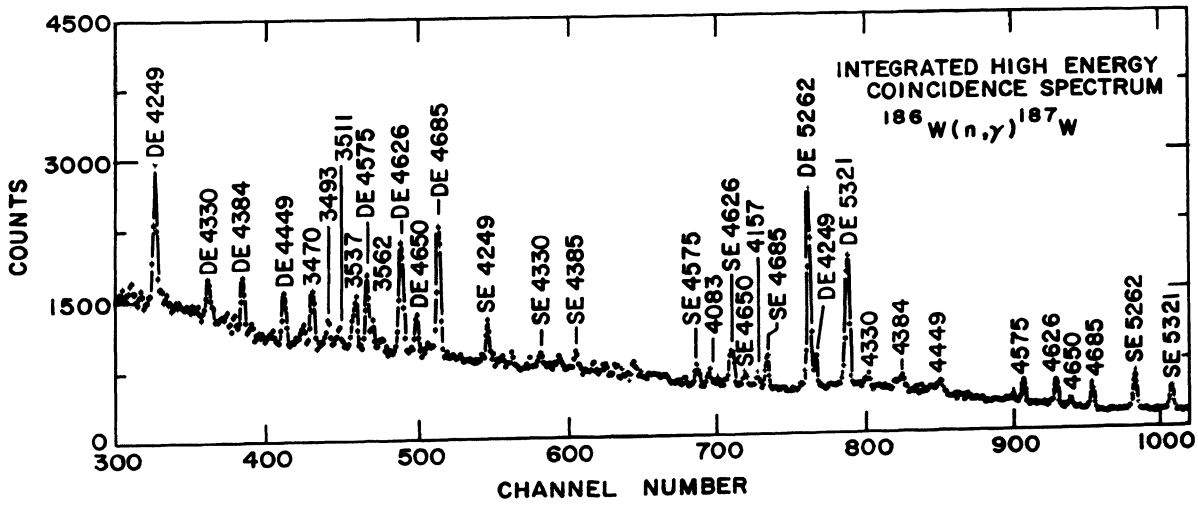

Fig. 27. Integrated high-energy coincidence spectrum for the $^{186}W(n,\gamma)^{187}W$ reaction. No coincidences are observed for the 5467-keV transition indicating that this is the ground-state transition from the capture state.

are those of Martin.[79] The analysis of this spectrum yielded assignments of double-escape, single-escape, and full-energy peaks that are felt to be unambiguous. The excitation energies of terminal states populated by these γ rays have been obtained under the usual and well-established assumption that, in this mass region, γ rays having energies $\geq 70\%$ of the neutron binding energy are primary transitions proceeding directly from the capture state to the low-lying excited states. Martin et al.[79] have determined the neutron binding energy to be 5467 ± 2 keV from an observation of the primary γ-ray transition to the ground state (this assignment is confirmed in Sec. C2). This value of the neutron separation energy agrees with the mass adjusted value 5460 ± 5[81] calculated from the (d,p) Q value reported by Erskine.[75]

2. Low-Energy Transitions and γ-γ Coincidence Studies.

a. Low-energy γ-ray singles measurements. The spectrum of low-energy γ rays from the $^{186}W(n,\gamma)^{187}W$ reaction recorded at the external beam facility is shown in Fig. 28. The energy calibration was accomplished using well-known energy standards and a highly linear ramp generator as discussed in Sec. VA. 1. The detection efficiency of the Ge(Li) detector was determined for each peak by use of several single γ-ray lines from intensity calibrated sources. Over 100 γ rays were observed with an energy ≤ 1200 keV and the energies and intensities of the observed lines are listed in Table VII. The errors quoted for the energies are substantiated by the excellent agreement of crossover to cascade sums which appear in the proposed level scheme.

b. High-low coincidences. Two-parameter γ-γ coincidence spectra were recorded with a nominal 20 cc detector set to accept the high-energy primary transitions (energy range ~ 2.4—5.8 MeV) while a nominal 30 cc Ge(Li) detector (see Sec. V) was set to observe

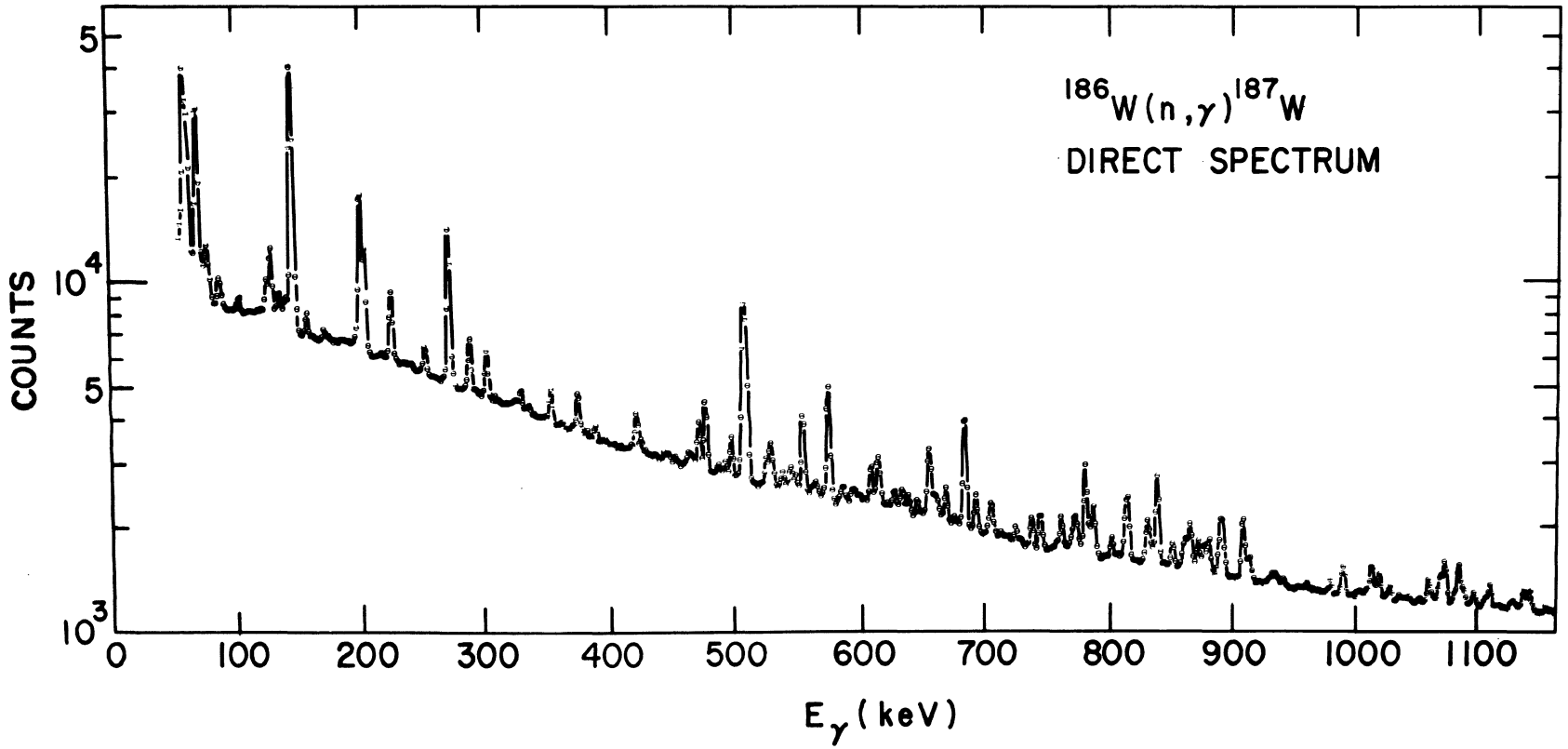

Fig. 28. Typical low-energy Ge(Li) singles pulse-height spectrum obtained for the reaction $^{186}W(n,\gamma)^{187}W$. Gamma-ray energies are listed above the appropriate peaks with lines indicating the position of the γ ray in the case of unresolved multiple peaks. The energies and relative intensities are also listed in Table I.

TABLE VII. Energies and relative intensities of low-energy γ rays observed in W^{187}.

Gamma-ray energy (keV)	Relative gamma-ray intensity[a]	Gamma-ray energy (keV)	Relative gamma-ray intensity[a]	Gamma-ray energy (keV)	Relative gamma-ray intensity[a]
101.8 ± 0.2	1.4	548.0 ± 0.8	3.8	840.1 ± 0.2	23.5
124.3 ± 0.4	5.4	557.2 ± 0.1	23.4	852.3 ± 0.2	4.6
127.7 ± 0.2	12.3	566.7 ± 0.6	2.2	860.6 ± 0.5	3.4
139.8 ± 0.6	4.2	574.2 ± 0.9	2.3	863.0 ± 0.5	5.6
145.7 ± 0.1	100	577.3 ± 0.1	36.8	866.0 ± 0.3	10.5
149.0 ± 0.4	4.1	580.9 ± 0.8	1.9	872.7 ± 0.2	6.5
157.4 ± 0.2	3.6	588.8 ± 0.4	3.3	877.4 ± 0.2	6.3
171.6 ± 0.2	1.7	611.2 ± 0.2	8.6	881.5 ± 0.2	7.8
175.1 ± 0.8	0.8	616.1 ± 0.3	9.0	889.1 ± 0.3	3.8
198.2 ± 0.4	3.0	628.9 ± 0.2	3.0	891.8 ± 0.2	13.8
201.4 ± 0.1	51.6	634.5 ± 0.4	2.0	894.6 ± 0.4	2.4
204.9 ± 0.3	23.0	635.9 ± 0.4	2.7	909.0 ± 0.2	15.2
219.0 ± 0.5	1.0	640.5 ± 0.3	3.2	912.3 ± 0.5	3.1
225.9 ± 0.2	13.6	647.4 ± 0.3	2.7	914.7 ± 0.5	4.2
227.4 ± 0.6	2.6	656.1 ± 0.3	8.4	931.5 ± 0.7	1.9
250.7 ± 0.8	0.7	657.8 ± 0.5	12.2	934.4 ± 0.7	1.9
253.4 ± 0.2	6.0	661.5 ± 0.5	4.3	936.7 ± 0.7	1.4
273.0 ± 0.1	51.8	664.0 ± 0.5	3.0	941.3 ± 0.5	1.7
276.3 ± 0.6	2.5	670.3 ± 0.2	6.9	979.2 ± 0.3	2.1
287.0 ± 0.3	1.6	676.9 ± 0.4	1.0	988.8 ± 0.5	3.7
289.9 ± 0.1	11.6	694.3 ± 0.3	7.3	990.4 ± 0.6	2.9
294.3 ± 0.3	1.0	703.9 ± 0.8	1.4	1008.6 ± 0.9	1.2
303.3 ± 0.1	10.4	706.5 ± 0.3	6.2	1012.3 ± 0.3	6.9
330.7 ± 0.3	3.1	708.4 ± 0.9	1.3	1015.7 ± 1.0	1.3
337.7 ± 0.6	1.1	726.1 ± 0.3	2.5	1018.3 ± 0.4	4.5
354.8 ± 0.2	6.2	738.9 ± 0.2	5.7	1027.2 ± 0.4	2.3
376.7 ± 0.1	8.8	746.1 ± 0.3	6.9	1034.1 ± 0.8	1.8
390.6 ± 0.4	2.7	759.1 ± 0.7	1.5	1042.3 ± 0.8	1.7
423.9 ± 0.2	9.0	762.9 ± 0.3	7.1	1050.5 ± 0.7	1.3
428.1 ± 0.2	2.9	770.1 ± 0.9	2.1	1058.0 ± 0.3	5.5
466.0 ± 0.5	2.6	775.1 ± 0.7	6.2	1061.7 ± 0.8	1.8
469.0 ± 0.6	2.3	778.2 ± 0.9	1.7	1067.3 ± 0.3	6.9
474.0 ± 0.1	12.0	782.3 ± 0.2	23.2	1071.2 ± 0.2	10.6
489.4 ± 0.3	1.9	786.0 ± 0.5	5.2	1078.6 ± 0.5	2.3
495.0 ± 0.4	2.8	789.0 ± 0.3	11.1	1082.3 ± 0.2	9.6
500.0 ± 0.2	8.6	803.3 ± 0.2	4.4	1086.1 ± 0.4	3.4
528.0 ± 0.3	5.7	808.8 ± 0.8	1.2	1094.3 ± 0.4	2.7
531.3 ± 0.3	9.2	813.8 ± 0.4	6.6	1103.8 ± 0.8	1.6
533.3 ± 0.6	3.5	816.1 ± 0.4	15.1	1107.4 ± 0.3	4.4
541.1 ± 0.4	3.5	832.0 ± 0.4	10.0	1126.4 ± 2.0	0.9
546.3 ± 0.7	2.8	835.4 ± 0.8	3.8	1134.8 ± 0.2	4.8
				1139.6 ± 0.2	4.8

[a]The listed intensities of the gamma rays are relative to that of the 145.7-keV γ ray taken as 100. The errors in the relative γ-ray intensities are 5—10% of the listed values for intensities >10, 10—20% for the weaker transitions.

the low-energy events up to a γ-ray energy of ~1.3 MeV. These spectra required a collection time of ~50 hours. Representative high-low coincidence spectra are given in Fig. 29. The upper portion is the singles spectrum obtained at the same gain as the coincidence spectra. The coincidence spectra shown were obtained by adding the

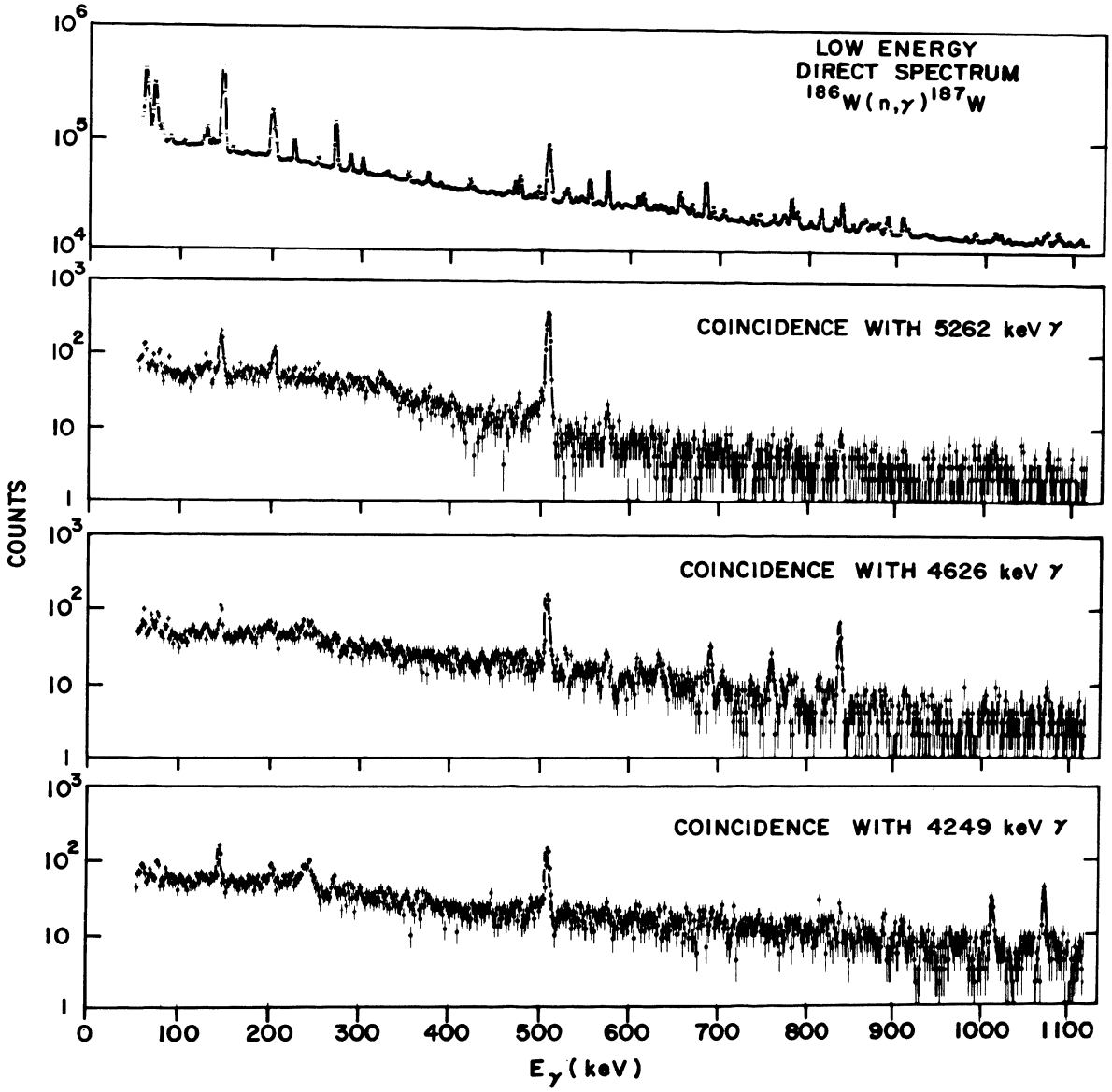

Fig. 29. Representative portions of the low-energy spectra in coincidence with the indicated high-energy gamma rays. The upper curve is the low-energy singles spectrum recorded under the same experimental conditions as the three lower coincidence spectra. In this figure no corrections have been made for chance coincidence events or events resulting from coincidences with higher-energy transitions whose continua underlie a particular high-energy coincidence gate. The contribution of chance events can be assessed by noting the relative heights of the 146, 201, and 273 transitions as compared to the direct spectrum in the upper curve whose shape is followed by the chance coincidence spectrum. In all cases the number of chance and underlying coincidence events were small compared to the number of real coincidence events.

two spectra obtained by gating on the double escape peak and the full-energy peak.

The high-low coincidence data, besides producing other invaluable information, strongly suggest that the 5467-keV transition seen by Martin et al. does indeed represent a transition to the ground state since no coincidence events were observed between this transition and low-energy transitions. Therefore, this energy was adopted as the neutron binding energy. Table VIII summarizes the results of the γ-ray coincidences obtained from these spectra.

The γ-ray decays of those low-lying states which are directly populated by given primary transitions are seen to be readily identified and relatively uncomplicated. It is evident that the use of a NaI(Tl) detector as the high-energy detector would have prevented such clear

TABLE VIII. Low-energy transitions observed to be in coincidence with high-energy primary γ rays in ^{187}W.

Gamma-ray energy (keV)	Coincidence gamma-ray energies[a] (keV)
5321	146
5262	146, 205
4685	146, 205(?), 577, 782
4650	146, 205(?), 611, 670, 739, 816
4626	146, 694, 763, 840
4575	146, 746, 814, 892
4449	1018
4384	1082
4250	146, 205(?), 1012, 1071

[a]Those γ-ray energies followed by (?) appear only faintly in the coincidence spectra and unambiguous establishment of their presence in these spectra is not claimed.

cut identification and analysis due to the poor energy resolution of that device. Even in the event that a Ge(Li) detector had been used for the observation of these events and a NaI(Tl) detector for the low-energy γ rays, it would have been impossible to provide the important separation of closely spaced doublets (such as the 201- and 205-keV transitions). Thus the use of Ge(Li) detectors in both arms of the coincidence system was necessitated in the interest of obtaining definitive spectra for the removal of ambiguities from the decay scheme. The detection efficiency of the solid state system is considerably lower than a Ge(Li)-NaI(Tl) system; however, the increased spectral clarity more than compensates for any loss of efficiency. In fact the solid state system is required in order to establish unambiguous coincidence relationships between individual γ rays.

c. Low-low coincidences. The two Ge(Li) detectors were set to record the low-energy spectrum ($\leq$1300 keV) and low-low coincidence data were collected for $\sim$20 hours resulting in the observation of $\sim 7 \times 10^6$ events. Typical spectra resulting from this data are shown in Fig. 30. The upper curve is the singles spectrum and the lower curves A, B, and C represent coincident spectra for the 145-, 290-, and 424-keV transitions, respectively. The chance and Compton coincidence events have been subtracted from the three lower spectra. The number of Compton events is estimated by taking a coincidence spectrum which is gated on a region of width equal to the γ-ray peak of interest lying either to the right or left of that peak. Again, if either arm of the coincidence system had been a NaI(Tl) detector, the individual lines of close lying multiplets could not have been selected individually as gates nor could these close peaks have been unambiguously separated in the gated coincidence spectra. Thus, in the observation of low-low coincidences the use of Ge(Li) detector in both arms of the system is demanded by the experimental

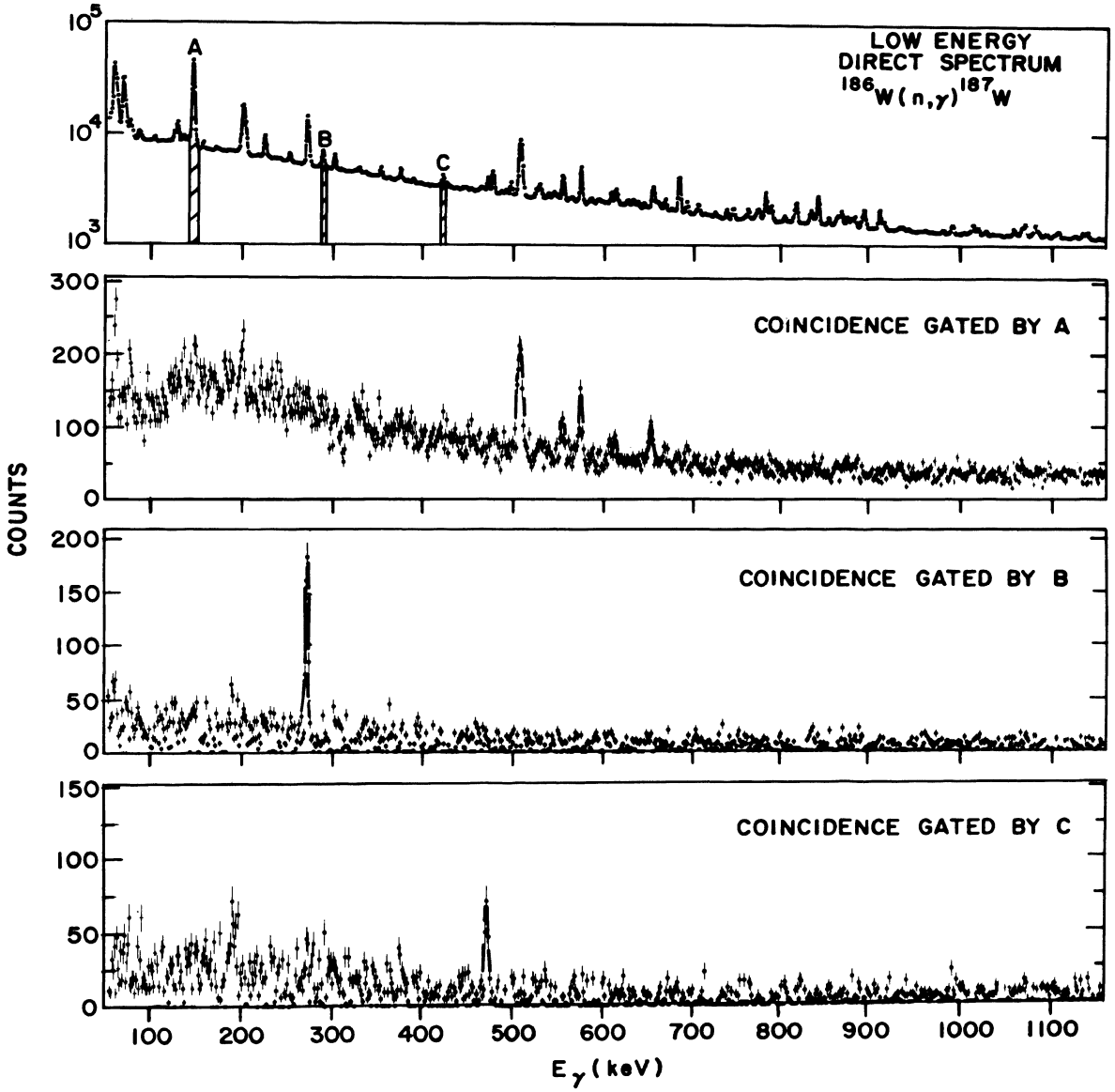

Fig. 30. Typical portions of the low-energy spectra in coincidence with the particular low-energy coincidence gates specified by the cross-hatched peaks of the singles spectrum shown in the upper portion of this figure. The three lower coincidence spectra shown have been corrected for chance coincidence events and for events due to those portions of the Compton distributions of higher energy transitions which underlie the respective coincidence gates employed. It should be noted that the direct spectrum (upper curve) is plotted on a semi-log scale while the coincidence spectra (three lower curves) are plotted on a linear scale.

TABLE IX. Coincidence relationships observed among the low-energy transitions in ^{187}W.

Gamma-ray energy (keV)	Coincidence gamma-ray energy[a] (keV)
57—60	146, 201, 273, 557(?), 577, 611
128	577
146	557, 577, 611(?), 616(?), 658
273	290
290	273
424	474
474	424
500	225
557	146
577	146, 205(?)
616	146
658	146

[a]Those γ-ray energies followed by (?) appear only faintly in the coincidence spectra and unambiguous establishment of their presence in these spectra is not claimed. The coincidence relationships of these transitions are consistent with the proposed level scheme but their placements in the scheme were established on the basis of energy and intensity fits.

situation. A summary of the low-energy coincidence studies appears in Table IX.

D. Level Scheme

The proposed level diagram is shown in Fig. 31. The properties of 24 excited states up to an energy of 1217 keV are summarized in this figure. The levels which are populated by primary γ rays are

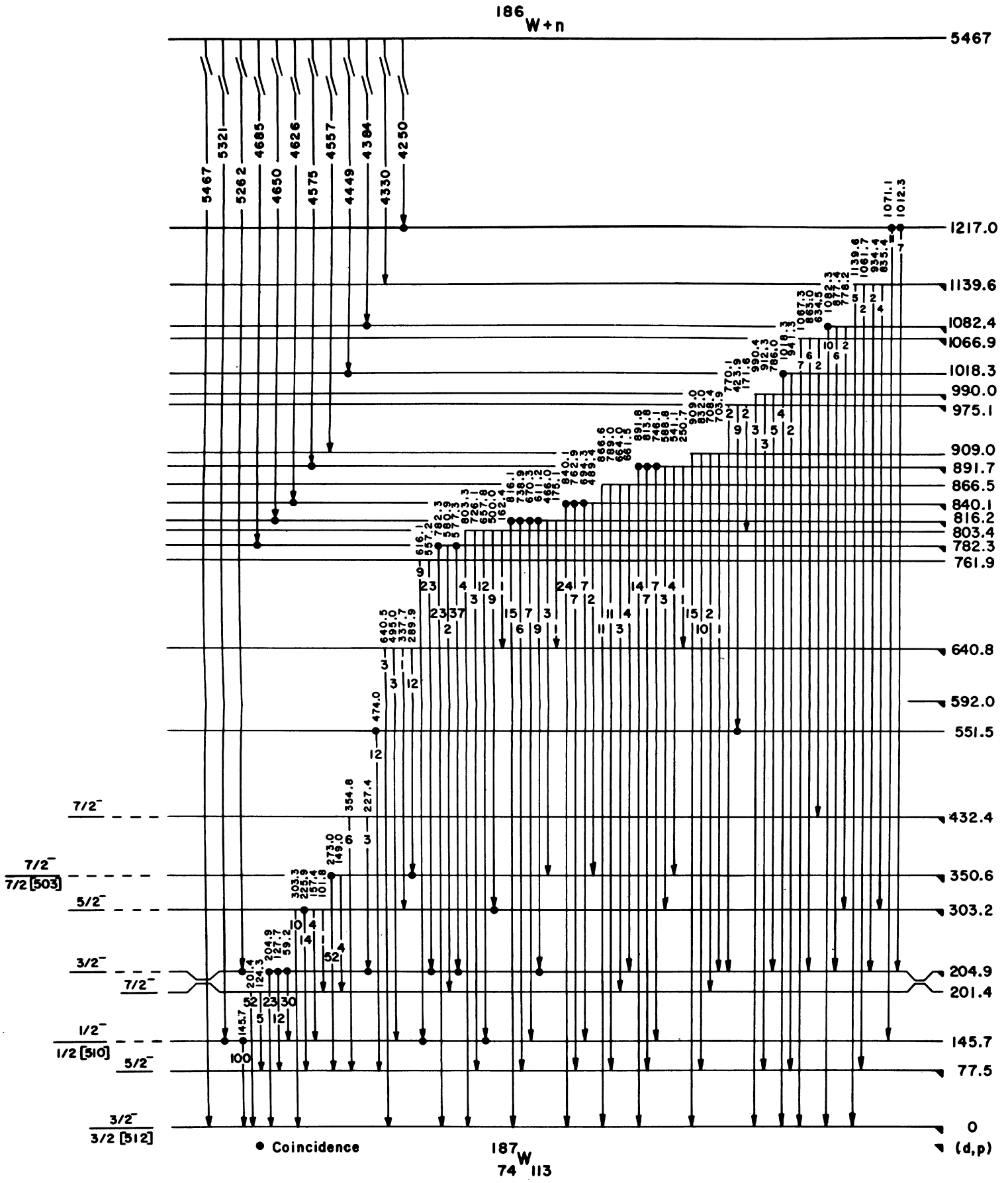

Fig. 31. Proposed level scheme of ^{187}W deduced from the various coincidence and singles γ-ray investigations of the present work. The excitation energies are expressed in keV. Those levels marked on the right by downward-pointing flags are levels associated with reported (d,p) population. The dots at the beginning or ending of the arrow representing a γ-ray transition indicate an observed coincidence between the γ ray so marked and another γ ray(s) proceeding to or from the same level. The levels observed to be populated in the present work are designated by full horizontal lines across the level scheme. The (d,p) state which has not been observed in this study is marked by a short horizontal line at the right of the diagram. All levels which have been observed in the primary high-energy γ-ray spectrum are indicated by a high-energy γ-ray transition. States which are based solely upon the energy and intensity balance of low-energy transitions (indicated by the lack of coincidence indication and primary γ-ray transition to the level) are not proposed as confidently as are the states assigned on the basis of coincidence results. The spins, parities, and rotational band configurations resulting from this study are indicated to the left of the level diagram.

indicated by an arrow originating from the capture state and terminating at a low-lying level and labeled with the energy of the primary γ ray. The γ rays observed to be in coincidence with primary γ-ray transitions are indicated by a dot at the lower end of the arrow representing the primary γ ray with a corresponding dot at the beginning of the arrow representing the secondary γ ray(s). The results of the low-energy coincidence studies are indicated by a similar notation. The levels observed in this work that correspond to levels observed in the (d,p) studies of Erskine[75] are indicated by downward pointing flags at the right of the figure. Only one level (592-keV level) observed in the (d,p) studies[75] was not observed in this work and it is indicated schematically by an incomplete horizontal line and downward pointing flag at the right of the diagram.

As expected (see Sec. IV), primary γ-ray transitions (predominantly of dipole character) are not seen to populate all the levels observed in the (d,p) investigation. However, when both primary and secondary γ radiation is considered, all of the levels below 1217 keV seen in the (d,p) work are observed in this study with the exception of the 592-keV level.[75] In addition, the present studies have also defined states in this region which were not observed in the (d,p) work. This confirms the introductory expectation (see Sec. IV) that the combination of primary and secondary γ-ray transitions following thermal neutron capture—which are unencumbered by the same type of selection and intensity rules which govern (d,p) studies—could populate low-lying states independent of their constitution.

The first considerations in the construction of the proposed level scheme were the results of the γ-γ coincidence studies. Seventeen of the 24 proposed levels were observed to be populated and/or depopulated in the coincidence studies as is indicated in Fig. 31. This scheme differs in many respects from that proposed previously by Prokefev *et al.*[80] Several new levels have been observed in the

present study and one level proposed in the previous studies is conspicuously absent. The electron-conversion studies of Prokefev et al.[80] indicate the possible existence of a 185-keV excited state which decays by a 185-keV transition to the ground state. This transition was totally unobserved in our studies. However, a 201-keV transition which was observed in our studies may have also been observed in the electron-conversion spectrum of Prokefev et al.[80] In addition, no transitions were observed in our γ-γ coincidence studies to indicate the presence of a 185-keV level nor were energy sums found for γ rays which could populate and/or depopulate such a level. These facts have prompted us to discard the 185-keV energy level in favor of the 201-keV level and its associated 201-keV transition to the ground state.

Many of the transitions observed in the singles γ-ray spectrum were too weak to be seen in the coincidence studies. Several of these γ rays have been included in the decay scheme of Fig. 31 on the basis of their satisfaction of stringent energy balances and intensity considerations. All but the very weakest transitions observed were found to be accommodated in this level scheme.

E. Discussion

Because ^{187}W lies near the edge of the deformed region, it is expected that this nuclide may not be adequately described in terms of the simple particle plus rotator model. The necessity to include the Coriolis band mixing term (see Sec. IID) in a comparison of the rotational model with experimental findings in ^{183}W has been previously demonstrated.[76,77] Such a comparison was made by Erskine[75] who sought the best agreement with this model for the excitation energies and (d,p) strengths to those levels observed in his studies. The radiative decay characteristics determined in the

present work allow a more critical comparison to be made between the model and experiment since the degree of band mixing imposed is expected to be more sensitive to electromagnetic transition rates and branching ratios than to (d,p) stripping strengths.

The ground-state spin of ^{187}W has been measured by atomic beam methods[82] as being $\frac{3}{2}$, and the (d,p) stripping studies of Erskine[75] yield a negative parity for the same state. The ground state thus becomes a candidate for the $[512]\frac{3}{2}^-$ Nilsson state. The apparent success with which the Nilsson model, including Coriolis mixing, has met in explaining the levels[76,77] in ^{183}W and ^{185}W has prompted us to apply this model to ^{187}W employing very similar Nilsson parameters and intrinsic states.

The γ-ray spectrum for the ^{186}W(n,γ)^{187}W was calculated in the following way. The transition probabilities predicted by the model are found to be only slightly dependent on the Nilsson parameters δ, κ, and μ. Therefore, the parameters found empirically by Kerman[76] and Brockmeier et al.[77] for ^{183}W were used for the ^{187}W calculations. The Nilsson wave functions for a deformation $\delta = 0.2$ were adopted and only the $[510]\frac{1}{2}^-$, $[512]\frac{3}{2}^-$, and $[503]\frac{7}{2}^-$ intrinsic states were used (see Sec. IID and Ref. 23).

On the basis of one-particle theory, the $[510]\frac{1}{2}^-$ and $[512]\frac{3}{2}^-$ intrinsic states are filled in ^{187}W. The residual pairing interaction, however, allows these and other close lying intrinsic states to be filled or unfilled in varying degrees. The pairing theory treats intrinsic states as one-quasiparticle states (see Sec. IIC) which behave as before except that the transition probability now depends on the probability of occupation U^2 of the quasiparticle states. Pairing effects have been considered in these calculations.

The spectrum for ^{187}W was calculated using a computer code written by M. E. Bunker.[83] The choice of the positions of the intrinsic states was guided by the work of Erskine[75] and the energies

TABLE X. Parameters and excitation energies of Nilsson states in $^{184}_{74}$W.

$E_K = E_0 + A[J(J+1) + a(-)^{(J+\frac{1}{2})}(J+\frac{1}{2})\delta_{K,\frac{1}{2}}] + B[J+1) + a(-)^{J+\frac{1}{2}}(J+\frac{1}{2})\delta_{K,\frac{1}{2}}]^2$ coupling constant = 1.0928.

J	K	E_0 (keV)	A (keV)	B (keV)	a	E (theo) (keV) mixed	E (exp) (keV)
				[510]			
$\frac{1}{2}$	$\frac{1}{2}$	140.8	18.6	-57.0	-0.01566	145.7	145.7
$\frac{3}{2}$	$\frac{1}{2}$					204.8	204.9
$\frac{5}{2}$	$\frac{1}{2}$					303.0	303.2
$\frac{7}{2}$	$\frac{1}{2}$					432.6	432.4
				[512]			
$\frac{3}{2}$	$\frac{3}{2}$	0.0	14.7	182.0	0.0	0.0	0
$\frac{5}{2}$	$\frac{3}{2}$					77.6	77.5
$\frac{7}{2}$	$\frac{3}{2}$					200.5	201.4
				[503]			
$\frac{7}{2}$	$\frac{7}{2}$	345.6	17.0	0.0	0.0	350.6	350.6
$\frac{9}{2}$	$\frac{7}{2}$					503.5	not obs.

of the states within a band were calculated using Eqs. (D29) and (D30) of Sec. II. The parameters of these equations were varied in order to obtain agreement with the experimental excitation energies. The calculated branching ratios were then compared with experiment.

Table X lists the parameters used, the excitation energies calculated, and the experimentally observed excitation energies. Certain irregularities develop in the values of the parameters which must be used to fit the observed data.

The $[510]\frac{1}{2}^-$ band requires a large negative B coefficient (see Table X). A term very similar to the term associated with the B coefficient results from the band mixing interaction. Since the two levels involved in band mixing are usually repelled,[83] i.e., the energy of the higher level is usually increased while the energy of the lower level is decreased, the levels in the [510] band would be expected to move upward in proportion to a term like $[+B'(J)(J+1)]$ even if the B coefficient appearing in Table X were zero. The fact that a negative

B coefficient must be used to fit the data is an expression of the fact that some of the effects of band mixing must be overcome in order to obtain level energies which correspond to the observed energy levels. However, this value for the B coefficient is not an unreasonable result if the transition probabilities are predicted accurately.[83]

A more serious objection is the fact that an enormous positive B coefficient must be used in order to predict a $\frac{7}{2}^-$ member of the $[512]\frac{3}{2}^-$ band at an excitation energy of 201 keV.[83] A negative B coefficient of much smaller magnitude would be expected from arguments similar to those in the previous paragraph. In addition, the values of B coefficients quoted for nearby nuclei are typically negative with a magnitude ≤ 0.1 keV.[78]

If B is set equal to zero for the [512] band, then a $\frac{7}{2}^-$ member of this band would appear at 185 keV. It is expected that this level should be observably populated; however, such a level is completely unobserved in the present study although a perhaps fortuitous indication for the existence of this level appears in the electron conversion studies of Prokefev et al.[80] One other possibility exists as explanation for the 201-keV state, namely, that it might be the head of a $[651]\frac{1}{2}^+$ band which has been observed in neighboring nuclei.[78] However, the population of this level from the $[503]\frac{7}{2}^-$ level and its decay to a $\frac{5}{2}^-$ level make this explanation a rather remote possibility. Therefore, the 201-keV state has been assigned as the $\frac{7}{2}^-$ member of the ground-state rotational band.

The proximity of ^{187}W to the edge of the deformed region produces the possibility that strong deviations from the rotational model may occur. In ^{189}Os (isotonic with ^{187}W) the $\frac{7}{2}^-$ member of the $[512]\frac{3}{2}^-$ band lies at a much higher energy than expected, and it is therefore not unreasonable that the 201-keV state is the $\frac{7}{2}$ member of the $[512]\frac{3}{2}^-$ band.[78]

The branching ratios which are calculated using the parameters in Table X including the assumption that the 201-keV state

TABLE XI. Branching ratios of the low-lying excited states in ^{187}W.

Initial state (keV)	Final state (keV)	Branching Ratio[a] (theory)	(exp.)
145	0	1.0	1.0
145	78	0.002	Not observed
201	0	1.0	1.0
201	78	0.12	0.10
205	0	1.0	1.0
205	78	0.0056	0.52
205	146	0.61	1.30[b]
303	0	1.0	1.0
303	78	1.46	1.4
303	146	0.65	0.4
303	201	0.86	0.1
303	205	0.02	Not observed
351	0	22	Not observed
351	78	1.0	1.0
351	201	0.019	0.077
433	78	1.0	1.0
433	201	0.31	Not observed
433	205	0.34	0.50
433	303	0.61	Not observed

[a]The parameters used to generate the theoretical values are given in Table IV. The transition with branching ratio equal to 1.0 was used as the comparison state for each level.

[b]The 59 keV transition was not well resolved in the singles spectrum. The error associated with this value is therefore $\approx$ 50%.

belongs to the $[512]\frac{3}{2}^-$ band are given in Table XI along with the experimentally determined ratios. The agreement between the experimental and theoretical values is good for at least two of the states: the 201-keV and the 303-keV levels. Transitions which should have been observable according to the calculated transition probabilities for the 351- and 433-keV levels were not observed in the experimental spectrum. In these calculations the gyromagnetic ratio g_s was chosen to

be 0.6 times the "free" value.[83] This choice produces the branching ratios shown in Table XI and predicts a mixture of 96% M1 + 4% E2 for the 145-keV transition. Prokefev et al.[80] find a mixture of 70% M1 + 30% E2. It was not possible to obtain satisfactory branching ratios and M1, E2 mixing for the 145-keV transition simultaneously.[83] The parameters given in Table XI were employed in the same program used by Erskine[75] in an attempt to re-evaluate the (d,p) spectrum. The calculated (d,p) spectrum was observed to change very little ($<10\%$) when using the new parameters. This confirms the fact that the (d,p) cross sections are less sensitive to the amount of band mixing than the transition probabilities.

In summary, we have seen above that the Nilsson model alone will not explain the experimental spectrum of ^{187}W whereas the inclusion of the Coriolis term (which allows band mixing) seems to improve the theoretical description. Qualitatively, this indicates that although band mixing may be occurring in the states of ^{187}W, this mechanism alone is not sufficient to explain the observed spectrum. The irregularities observed in the parameters which had to be used to fit the data and the discrepancies observed for several of the branching ratios and the mixing ratio of the 145-keV transition indicate that one or both of the following "problems" may exist. (1) ^{187}W is so far from the center of the deformed region that strong deviations from the rotational model occur. (2) Since the Nilsson intrinsic states are not an exact representation of the wave function in the best case, these inaccuracies may be amplified in nuclei which are marginal to the deformed region.

IX. BIBLIOGRAPHY

1. H. J. Lipkin, Lecture notes, Brandeis University Summer Institute in Theoretical Physics, 1959.

2. W. Elsasser, J. de Phys. et Rad. 5, 625 (1934).

3. M. G. Mayer, Phys. Rev. 75, 1969 (1949).

4. M. G. Mayer, Phys. Rev. 78, 16 (1950).

5. O. Haxel, J. H. D. Jensen, and H. E. Suess, Phys. Rev. 75, 1766 (1949).

6. O. Haxel, J. H. D. Jensen, and H. E. Suess, Z. Physik 128, 295 (1950).

7. M. A. Preston, Physics of the Nucleus (Addison-Wesley Publishing Co., Inc., Reading, Mass., 1962).

8. E. U. Condon and G. H. Shortly, Theory of Atomic Spectra (Cambridge University Press, New York, 1935).

9. L. Nordheim, Phys. Rev. 78, 294 (1950); see also M. H. Brennan and A. M. Bernstein, Phys. Rev. 120, 927 (1960).

10. J. P. Elliott and A. M. Lane, Encyclopedia of Physics, ed. S. Flugge, Vol. XXXIX, 241 (Springer-Verlag, Berlin, 1957).

11. O. Nathan and S. G. Nilsson, "Collective Nuclear Motion and the Unified Model," Alpha-, Beta-, and Gamma-Ray Spectroscopy, Chap. X, ed. K. Siegbahn (North-Holland Publishing Company, Amsterdam, 1965).

12. G. Racah, Phys. Rev. 63, 367 (1943).

13. J. Bardeen, L. N. Cooper, and J. R. Schrieffer, Phys. Rev. 108, 1175 (1957).

14. A. Bohr, B. Mottelson, and D. Pines, Phys. Rev. 110, 936 (1958).

15. K. Kumar and M. Baranger, Nucl. Phys. A92, 608 (1967).

16. Rayleigh, Third Baron, The Theory of Sound, Vol. II, Article 364 (Macmillan, London, 1877).

17. H. Goldstein, Classical Mechanics (Addison-Wesley Press, Cambridge, Mass., 1950).

18. M. E. Rose, Elementary Theory of Angular Momentum (John Wiley and Sons, Inc., 1957).

19. A. Bohr, Mat. Fys. Medd. Dan. Vid. Selsk. 26, #14 (1952).

20. A. Bohr and B. Mottelson, Mat. Fys. Medd. Dan. Vid. Selsk. 27, #16 (1953).

21. A. K. Kerman, Nuclear Reactions, Vol. 1, ed. P. M. Endt and M. Demeur (North-Holland Publishing Co., Amsterdam, 1959), p. 427.

22. A. S. Davydov and G. F. Filippov, Nucl. Phys. 8, 237 (1958).

23. S. G. Nilsson, K. Danske Vidensk. Selsk. Mat.-Fys. Medd. 29, #16 (1955).

24. T. D. Newton, Canadian J. Phys. 38, 700 (1960).

25. A. K. Kerman, Mat. Fys. Medd. Dan. Vid. Selsk. 30, #15 (1956).

26. R. T. Brockmeier, S. Wahlborn, E. J. Seppi, and F. Boehm, Nucl. Phys. 63, 102 (1965).

27. R. D. Lawson and J. L. Uretsky, Phys. Rev. 108, 1300 (1957).

28. A. de-Shalit, Phys. Rev. 122, 1530 (1961).

29. K. Adler, A. Bohr, T. Huus, B. Mottelson, and A. Winther, Rev. Mod. Phys. 28, 432 (1956).

30. L. C. Biedenharn and M. E. Rose, Rev. Mod. Phys. 25, 729 (1953).

31. M. Ferentz and N. Rosenzweig, Argonne National Laboratory Report ANL-5324.

32. W. T. Milner (Thesis), Oak Ridge National Laboratory Report ORNL-TM-2121.

33. J. M. Blatt and V. F. Weisskopf, Theoretical Nuclear Physics (John Wiley and Sons, New York, 1952).

34. C. E. Porter and R. G. Thomas, Phys. Rev. 104, 483 (1956).

35. G. A. Bartholomew, "Neutron Capture Gamma Rays," Annual Review of Nuclear Science, Vol. 11, ed. E. Segre (Annual Reviews Inc., Palo Alto, Calif., 1961), p. 259.

36. L. M. Bollinger, "Radiative Transitions from Highly Excited Nuclear States," Nuclear Structure, International Atomic Energy Agency, Vienna, Austria, 1968, p. 317.

37. A. M. Lane and J. E. Lynn, Nucl. Phys. 17, 563 (1960).

38. L. M. Bollinger and G. E. Thomas, Phys. Rev. Letters 18, 1143 (1967).

39. L. M. Bollinger and G. E. Thomas, Phys. Rev. Letters 21, 233 (1968).

40. D. C. Camp, University of California Radiation Laboratory Report UCRL-50156.

41. M. G. Strauss, I. S. Sherman, R. Brenner, S. J. Radnick, R. N. Larsen, and H. M. Mann, Rev. Sci. Instr. 38, 725 (1967).

42. M. G. Strauss, F. R. Lenkszus, and J. J. Eichholz, Bull. Am. Phys. Soc. 14, 531 (1969), to be published.

43. R. D. Evans, The Atomic Nucleus (McGraw-Hill Book Co., Inc., New York, 1955).

44. H. H. Bolotin, M. G. Strauss, and D. A. McClure, to be published.

45. W. C. Davidon, Argonne National Laboratory Report ANL-5990 (Rev. 2).

46. R. G. Roddick and F. J. Lynch, IEEE Trans. Nucl. Sci. NS-11, 399 (1964).

47. A. H. Wapstra, Alpha-, Beta- and Gamma-Ray Spectroscopy, ed. K. Siegbahn, Chap. VIII C, p. 541 (North-Holland Publishing Co., Amsterdam, 1965).

48. H. H. Hopkins, Jr., and B. B. Cunningham, Phys. Rev. 73, 1406 (1948); H. H. Hopkins, Jr., Phys. Rev. 77, 717 (1950).

49. R. A. Ricci and R. Van Lieshout, Nuovo Cimento 4, 1592 (1956); R. A. Ricci, R. K. Girgis, and R. Van Lieshout, Nucl. Phys. 21, 177 (1960).

50. H. H. Bolotin, Bull. Am. Phys. Soc. 8, 524 (1963).

51. Nuclear Data Sheets, compiled by K. Way et al. (Printing and Publishing Office, National Academy of Sciences—National Research Council, Washington 25, D.C.), NRC 60-4-23.

52. J. L. Worcester, W. A. Nierenberg, R. Marrus, and J. C. Hubbs, Bull. Am. Phys. Soc. 2, 383 (1957).

53. J. B. Marion, Nucl. Data A4, 301 (1968).

54. G. Murray, R. L. Graham, and J. S. Geiger, Nucl. Phys. 63, 353 (1965).

55. M. G. Strauss, L. L. Sifter, F. R. Lenkszus, and R. Brenner, IEEE Trans. Nucl. Sci. 15, 518 (1968).

56. A. H. Wapstra, G. J. Nijgh, and R. Van Lieshout, Nuclear Spectroscopy Tables (North-Holland Publishing Company, Amsterdam, 1959).

57. R. F. O'Connell and C. O. Carroll, Nuclear Data A3, 287 (1967).

58. J. Kantele and O. Tannila, Nuclear Data A4, 359 (1968) and pertinent references therein.

59. M. L. Perlman and M. Wolfsberg, Brookhaven National Laboratory Report BNL-485 (T-110), 1958. See also C. M. Lederer, J. M. Hollander, and I. Perlman, Table of Isotopes (John Wiley and Sons, Inc., New York, 1968), 6th edition, p. 575.

60. S. D. Bloom, Nuovo Cimento 32, 1023 (1964).

61. E. L. Church and J. Weneser, Phys. Rev. 103, 1035 (1956).

62. If the spin of the 234.0-keV level were 0^+, it would be expected that the β branch to this state would be considerably weaker than the upper limit of 3.5% obtained from the γ-ray intensity balance into and out of this level. This expectation arises from consideration of the amount of isobaric-spin impurity required to permit this Fermi-type transition to proceed and yet be consistent with isobaric-spin impurity established in this mass region. For example, an isobaric-spin admixture equal to that found in the $0^+ \rightarrow 0^+$ $Ga^{66} \rightarrow Zn^{66}$ beta decay would imply log ft ≈ 8.6 so that the intensity of the β branch to the 234.0-keV state would be $\sim 0.07\%$.

63. S. V. Nilsson, Kgl. Danske Videnskab. Selskab, Mat.-Fys. Medd. 29, #16 (1955).

64. H. H. Bolotin and D. A. McClure, Phys. Rev. 182, 987 (1969).

65. T. Suter, P. Reyes-Suter, W. Scheuer, E. Aasa, and G. Backstrom, Arkiv Fysik 20, 431 (1961).

66. W. R. Pierson and K. Rengan, Phys. Rev. 159, 939 (1967).

67. R. D. Bent, T. W. Bonner, and R. F. Sippel, Phys. Rev. 98, 1237 (1955).

68. G. M. Temmer and N. P. Heydenburg, Phys. Rev. 98, 1308 (1955).

69. G. M. Temmer and N. P. Heydenburg, Phys. Rev. 104, 967 (1956).

70. Nuclear Data Sheets, NRC 60-4-3; NRC 61-2-17 (1961).

71. Nuclear Data Sheets, NRC 6-1-82 (1964).

72. P. H. Stelson and F. K. McGowan, Phys. Rev. 110, 489 (1958) and H. Bichsel, "Passage of Charged Particles through Matter," American Institute of Physics Handbook, ed. by D. E. Gray (McGraw-Hill Book Co., Inc., 1963), p. 8-20.

73. S. A. Moszkowski, Alpha-, Beta-, and Gamma-Ray Spectroscopy, edited by K. Siegbahn (North-Holland Publishing Co., Amsterdam, 1965), Vol. II, p. 863.

74. O. C. Kistner and A. Schwarzschild, Phys. Rev. 154, 1182 (1967).

75. J. R. Erskine, Phys. Rev. 138, B66 (1965) and references therein.

76. A. K. Kerman, Kgl. Danske Videnskab. Selskab, Mat.-Fys. Medd. 30, #15 (1956).

77. R. T. Brockmeier, S. Wahlborn, E. J. Seppi, and F. Boehm, Nucl. Phys. 63, 102 (1965).

78. Nuclear Data, B1-1-84, B1-2-24 (1966).

79. M. J. Martin, J. A. Harvey, and G. G. Slaughter, Bull. Am. Phys. Soc. 11, 336 (1966) and private communication.

80. P. R. Prokefev and L. I. Simonova, Izv. AN SSSR, Ser. fiz. 30, 1210 (1964) [Trans.: Bulletin 30, 1261].

81. Nuclear Data, B1-2-112 (1966).

82. W. M. Doyle and R. Marrus, Nucl. Phys. 49, 449 (1963).

83. M. E. Bunker, private communication (1969).

X. VITA

Donald Allan McClure was born on 18 April 1942 in Omaha, Nebraska. He received his secondary education at Papillion, Nebraska and was graduated valedictorian of his class. He attended Nebraska Wesleyan University in Lincoln, Nebraska, where he was a member of Sigma Pi Sigma, National Physics Society, and Phi Kappa Tau social fraternity.

He was enrolled in the Graduate School of the University of Missouri - Rolla in September of 1964 where he was a member of Kappa Mu Epsilon, National Mathematics Society, and Phi Kappa Phi, National Academic Honor Society. He received the degree Master of Science in Physics in 1966.

Since 1966 he has held an Argonne Universities Association - Argonne National Laboratory Pre-Doctoral Fellowship during which time he completed research in γ-ray spectroscopy and wrote his Ph. D. dissertation.